NOVEL RESISTS FOR NEXT GENERATION LITHOGRAPHY

by

Dongxu Yang

A thesis submitted to

The University of Birmingham

for the degree of

DOCTOR OF PHILOSOPHY

Nanoscale Physics Research Laboratory

School of Physics & Astronomy

The University of Birmingham

November 2015

Abstract

With progress in the semiconductor industry, transistor density on a single computer chip has increased dramatically. This has resulted in a continuous shrinkage of the minimum feature size printed through microlithography technology. Resist, as the pattern recording medium of such printing, has been extensively studied to achieve higher resolution, higher sensitivity and lower line edge roughness. For decades this has been realized through chemical amplification. With the feature size continuously shrinking and the energy of exposure source therefore exceeding the resist ionization threshold, the performance of conventional chemically amplified resists is approaching the limits. Novel high-performance chemically amplified resists or non-chemically amplified resists are urgently needed to meet the requirement of next generation lithography.

In this work a negative tone chemically amplified resist system based on a novel method to control the catalytic chain reaction is presented. The method to control the catalytic chain reaction is demonstrated using two model polymer resists. This method is then applied to a fullerene-based molecular resist system and a combination of good industrial compatibility, high resolution and good sensitivity has been achieved in this resist. Through a chromatographic separation, another chemically amplified molecular resist was also developed with further improved performance. An alternative route to sensitivity improvement other than chemical amplification is then introduced and a family of fullerene-based metal containing materials is presented. Lithographic performance is compared between the

fullerene-metal resists and their control materials without metal. Using an aberration corrected scanning transmission electron microscope, the distribution of metal in the resist film and its behavior during the lithography process is evaluated and discussed.

Acknowledgement

I would like to express my gratitude to my supervisor Dr. Alex P. G. Robinson for introducing me to this novel lithographic material project. I would never have overcome the difficulties or acquired the knowledge and skills to complete this PhD project without his patient supervision and invaluable direction. Moreover, the experience of working in his highly collaborative team provided me with a wide horizon in both academia and industry, which, I believe, will be a great treasure in my future career.

I would like to thank my co-supervisor Prof. Richard. E. Palmer for giving me the opportunity to study in the Nanoscale Physics Research Laboratory (NPRL) and providing me with a high-quality research facility and environment, also for the professional suggestions and directions during the work presentations and publications.

I am especially grateful to my colleague Dr. A. Frommhold for all the training and help in the clean room, also for the EUV and etching experiments. Considerable thanks should be given to Dr. Dongsheng He and Dr. Ziyou Li, for their collaboration on the experiments with the scanning transmission electron microscope (STEM). My thanks go to my colleagues in this project including Ms. Alexandra McClelland and Mr. Alan Brown from Irresistible Materials, as well as Xiang Xue and colleagues from Nano-C, for all their support and contributions.

I would also like to thank our collaborators from other universities and research institutions, including Dr. Mark Rosamond from the University of Leeds, Dr. Johann Osmond from ICFO (Spain), Ms. Xiaoqing Shi and Dr. Stuart Boden from the University of Southampton for all the help and suggestions during the experiments and visits. I am deeply grateful to all the staff and students in NPRL, for creating a positive and active atmosphere throughout my PhD study. I especially would like to acknowledge the China Scholarship Council for the financial support of my study in United Kingdom.

I am grateful to a lot of friends I have met during my four-year PhD life, particularly to Dr. Hao Li, for all the highs and lows we have gone through. The memory of which I have experienced in this country would never be so wonderful without their kind help and support.

Finally I would like to thank my families, who have continuously supported me with love and patience. Especially, thanks to my grandpa and grandma for their care and encouragement, which I will always cherish.

Author's Contribution

All the work presented in this thesis was conducted by the author under the supervision of Dr. Alex Robinson and co-supervision of Prof. Richard Palmer. Considerable support, including training and suggestion was provided by Dr. Andreas Frommhold. A number of collaborators also had contributions to this work. Sample preparation, exposure and imaging in the 50 keV electron beam lithography experiments were done by Ms. Alexandra McClelland and Dr. Johann Osmond. Sample exposure and part of sample imaging work during the 100 keV electron beam lithography experiments were done by Dr. Mark Rosamond. Sample exposure and imaging using the 30 keV helium ion beam microscope were done by Ms. Xiaoqing Shi under the supervision of Dr. Stuart Boden. Scanning transmission electron microscope imaging and energy dispersive X-ray mapping were done by Dr. Dongsheng He under the supervision of Dr. Ziyou Li.

Publication List

1) Frommhold, A., **Yang, D. X.,** McClelland, A., Roth, J., Xue, X., Rosamund, M. C., Linfield, E.H., Robinson, A. P. G., Novel Molecular Resist for EUV and Electron Beam Lithography. *J. Photopolym. Sci. Tec., 28(4),* 537 (2015)

2) Frommhold, A., McClelland, A., **Yang, D. X.,** Palmer, R. E., Roth, J., Ekinci, Y., Rosamund, M. C., Robinson, A. P., Towards 11nm half-pitch resolution for a negative-tone chemically-amplified molecular resist platform for extreme-ultraviolet lithography. *Proc. SPIE, 9425*, 942504 (2015)

3) **Yang, D. X.,** Frommhold, A., Xue, X., Palmer, R. E., Robinson, A. P. G., Chemically amplified phenolic fullerene electron beam resist. *J. Mater. Chem. C, 2(8),* 1505 (2014)

4) Frommhold, A., **Yang, D. X.,** McClelland, A., Xue, X., Ekinci, Y., Palmer, R. E., Robinson, A. P. G., Optimization of fullerene-based negative tone chemically amplified fullerene resist for extreme ultraviolet lithography. *Proc. SPIE,* 9051, 905119 (2014)

5) Frommhold, A., **Yang, D. X.,** McClelland, A., Xue, X., Ekinci, Y., Palmer, R. E., Robinson, A. P., Performance of negative tone chemically amplified fullerene resists in extreme ultraviolet lithography. *J. Micro/Nanolith. MEM., 12(3),* 033010 (2013)

6) Frommhold, A., **Yang, D. X.,** McClelland, A., Xue, X., Palmer, R. E., Robinson, A. P. G., EUV lithography performance of negative-tone chemically amplified fullerene resist. *Proc. SPIE,* 8682, 86820Q (2013)

7) Frommhold, A., **Yang, D. X.,** Manyam, J., Manickam, M., Tarte, E., Preece, J., Palmer, R.E., Robinson, A. P., Chemically amplified fullerene resists, spin-on fullerene hardmasks and high aspect ratio etching. *Nanotechnology (IEEE-NANO) 12th IEEE Conference,* 1 (2012)

8) Manyam, J., Frommhold, A., **Yang, D. X.,** McClelland, A., Manickam, M., Preece, J. A., Palmer, R.E., Robinson, A. P. G., Positive-tone chemically amplified fullerene resist. *Proc. SPIE, 8325,* 83251U (2012)

Acronym List

A

AC-STEM aberration corrected scanning transmission electron microscope

AFM atomic force microscopy

ALIS Atomic Level Imaging Systems

APS aperture plate system

B

BF bright field

Bipy bipyridine

C

CAR chemically amplified resist

CD critical dimension

D

DBU 1,8-diazabicycloundec-7-ene

DCM dichloromethane

DF dark field

DI deionised

DNQ diazonaphthoquinone

DOF depth of focus

DPG digital pattern generator

DPP discharge produced plasmas

DRAM dynamic random access memory

E

EBL electron beam lithography

EDX energy dispersive X-ray (spectroscopy)

EUV extreme ultraviolet

EUVL extreme ultraviolet lithography

EtOAc ethyl acetate

F

FIB focused ion beam

H

HAADF high-angle annular dark-field

HF hydrofluoric (acid)

HIB helium ion beam

HIBL helium ion beam lithography

HIM helium ion microscope

HMMM hexamethoxymethylmelamine

HSQ hydrogen silsesquioxane

HVM high volume manufacturing

I

IBL ion beam lithography

IC integrated circuit

IPA isopropanol

IR infrared

ITRS International Technology Roadmap for Semiconductors

L

LER line edge roughness

LPP laser produced plasmas

LWR line width roughness

M

MALDI matrix-assisted laser desorption/ionization

MAPPER multiple aperture pixel-by-pixel enhancement of resolution

MCB monochlorobenzene

MEMS microelectromechanical systems

MF methanofullerene

MeOH methanol

N

NGL next generation lithography

NMR nuclear magnetic resonance

O

OAI off-axis illumination

OPC optical proximity effect correction

P

PAB post application bake

PAG photo-acid generator

PBOCST poly(4-*tert*-butoxycarbonyloxystyrene)

PCB phenyl-C_{61}-butyrate

PCBM phenyl-C_{61}-butyric acid methyl ester

PDB post-development bake

PEB post exposure bake

PF pyrrolidinofullerene

PGME propylene glycol methyl ether

PHOST poly(4-hydroxystyrene)

PML2 projection maskless lithography

PMMA polymethylmethacrylate

PREVAIL projection reduction exposure with variable axis immersion lenses

PSM phase-shifting mask

R

REBL reflective electron beam lithography

R&D research and development

S

SCALPEL scattering with angular limitation in projection electron-beam lithography

SDD silicon drift detector

SEM scanning electron microscope

SFEG Schottky field emission gun

SHIBL scanning helium ion beam lithography

STEM **s**canning transmission electron microscope

T

TEM transmission electron microscope

TMAH tetramethylammonium hydroxide

$\mathbf{T_g}$ glass transition temperature

U

ULSI ultra-large-scale integration

UV ultra violet

Contents

CHAPTER 1

INTRODUCTION

1.1 Introduction to Microlithography

In pursuit of increased computing power over time and lower operating costs for computing, microelectronic manufacturers never stop trying to make more complex circuits in a smaller device. Since the invention and commercialization of the integrated circuit (IC) in 1960s,[1,2] the semiconductor industry has witnessed a giant leap from struggling to put more than one transistor on a piece of semiconductor, to the commercialization of billion-transistor processors. The striking increase of transistor numbers on a single chip has resulted in faster switching speed and lower power consumption per component as well as lower production cost. The trend of increasing transistor density was first described by Gordon Moore in his 1965 paper,[3] and is known as Moore's Law. Based on the observation that the number of transistors on integrated circuits doubles approximately every other year, Moore's Law not only gave a good prediction of IC technology development, but also provided a roadmap which kept driving the semiconductor industry to constantly improve device performance. For over 45 years Moore's Law has been followed remarkably well. Table 1.1 lists the microprocessor transistor count from Intel,[4] the world's leading semiconductor chip manufacturer. To realize the continuously increasing density, dimensions of the key elements in a microelectronic device have been pushed smaller and smaller. The feature size shrinkage, known as miniaturization, has been continued

from micro scale to nano scale, and is still progressing today (Figure 1.1).[4,5] One of the most important technologies responsible for micro/nano scale fabrication is lithography.

Table 1.1 Intel microprocessor transistor count over time[4]

Microprocessor	Year of Introduction	Transistor Count
Intel 4004	1971	2,300
Intel 8080	1974	4,500
Intel 8086	1978	29,000
Intel 80286	1982	134,000
Intel 80386	1985	275,000
Intel 80486	1989	1,200,000
Pentium	1993	3,100,000
Pentium II	1997	7,500,000
Pentium III	1999	9,500,000
Pentium 4	2000	42,000,000
Itanium	2001	25,000,000
Itanium 2	2003	220,000,000
Core 2 Duo	2006	291,000,000
Core i7 (Quad)	2008	731,000,000
8-Core Itanium Poulson	2012	3,100,000,000

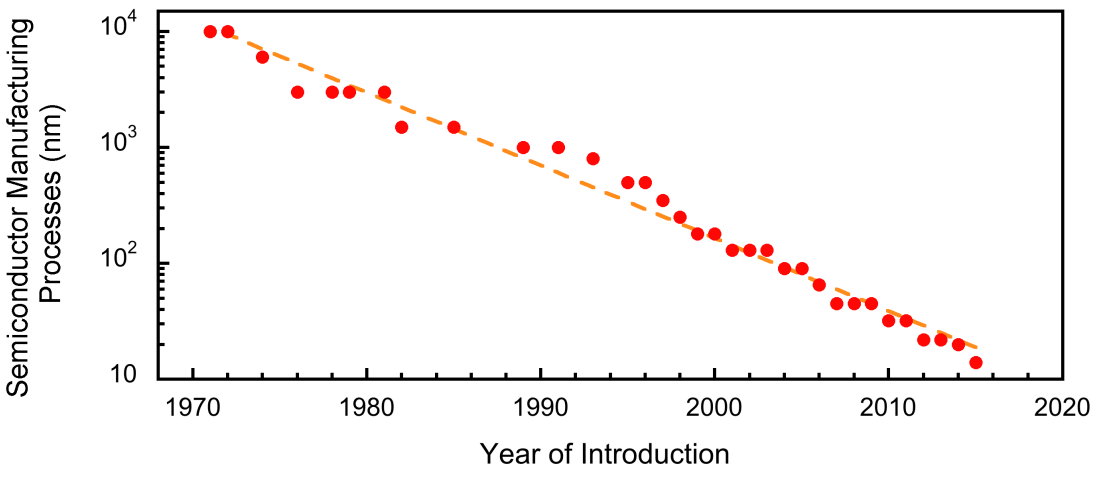

Figure 1.1 Semiconductor manufacturing process size over time

As a process of transferring and recording a pattern from a mask onto a target surface, lithography has been the key technology in the semiconductor industry that enables the miniaturization. Specifically, the particular branch of lithography, which is applied to IC fabrication to print the circuit patterns, is referred to as microlithography. Categorized by different printing mechanisms, lithography can be divided into radiation-based and non-radiation-based. The former utilizes radiation sources such as photons, electrons or ions to trigger a radiation-induced chemical reaction for the pattern formation; whilst the latter patterns with methods other than radiation, such as imprint, scanning probe, and self-assembly, etc.[6]

Among them photolithography has been the most commonly used lithography technique in semiconductor manufacturing. In the process of photolithography, a thin layer of radiation sensitive material, called resist, is coated onto a wafer. Using ultra violet (UV) light and a photomask, a well-defined aerial pattern is generated and projected onto the resist, triggering a chemical reaction in the area of resist that is under exposure. As a result, the solubility of the exposed area in a particular developer is altered whilst the unexposed parts are unchanged. A latent image is thus formed within the resist due to the chemical reaction, and such an image will be further turned into a real pattern by removing the exposed/unexposed area of resist using a developing step. In subsequent processes the patterned and developed resist serves as a mask during etching, doping, etc., which transfers the circuit pattern to the semiconductor substrate. A schematic of a simple photolithography process is shown in Figure 1.2. In actual IC fabrication

this process needs to be repeated many times, patterning multilayer structures to realize an actual device.

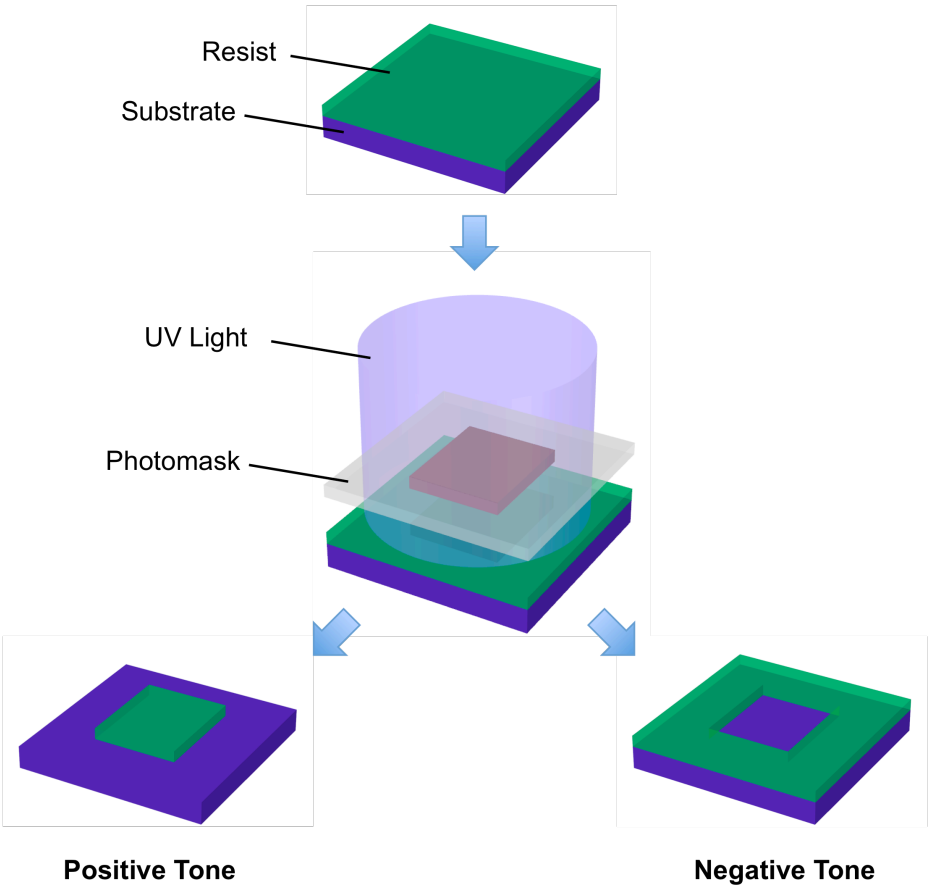

Figure 1.2 Schematic representation of photolithography process

1.2 Lithography Methods and Limitations

Depending on the patterning mechanism, different lithography methods have their own advantages and limitations. The discussion in this thesis will be limited to radiation-based lithography including conventional photolithography, Extreme Ultraviolet Lithography (EUVL), electron beam lithography (EBL) and ion beam

lithography (IBL). The main considerations for lithography technology are resolution, process window, overlay accuracy, throughput, and yield. Both lithography tool and resist material will determine the overall performance. In order to meet the increasingly stringent patterning requirements for next generation lithography (NGL) and continue the miniaturization, a considerable amount of research has been carried out.[6,7]

1.2.1 Photolithography

In modern photolithography, a complex optical system is required to enable projection of clear and small features. In this system the patterns on the mask are usually reduced by four or five times before projection onto the resist material. There is a set of lenses for the projection, demagnification and for aberration corrections.[6] Optical systems are generally constrained by the diffraction limit. The resolution, R, of a lithographic system is the minimum separation between two closely spaced features at which the features can still be resolved in the resist pattern. R can be expressed according to a modified Rayleigh criterion:[8]

$$R = k_1 \frac{\lambda}{NA} \tag{1.1}$$

where k_1 is a factor characterized by resist materials and process conditions, λ is the wavelength of the exposure light, and NA is the numerical aperture of the projection lens, which is defined as

$$NA = n \sin\theta \tag{1.2}$$

where n is the index of refraction of surrounding medium, and θ is the maximum half-angle of diffracted light that can get through the lens. Derived from the

Rayleigh criterion, the process window of a lithography tool can be reflected by the depth of focus (*DOF*),[9] defined as

$$DOF = k_2 \frac{\lambda}{NA^2} \tag{1.3}$$

where k_2 is a experimental constant. The *DOF* is a measure of the range within which the defocus can be tolerated whilst maintaining the image quality. *DOF* values usually determine the requirement of Z positioning accuracy, the upper limit of the resist film thickness, and maximum substrate topography.

From the equation (1.1) the most straightforward way to enhance the resolution is to reduce the radiation wavelength, In fact, past improvements in the patterning resolution have been achieved by pushing the exposure wavelength to smaller values throughout the development of IC photolithography. The earliest exposure light source was based on the mercury arc lamp, initially using the 436 nm g-line and subsequently shifted to the 365 nm i-line. Further evolution was realized by switching to KrF excimer laser source (248 nm), followed by the ArF (193 nm). As the previously proposed 157 nm (F_2 excimer) was ruled out from the roadmap due to a series of technical issues,[10] 193 nm photolithography is still the workhorse in today's IC manufacturing.

Another important resolution enhancement technique employed in the IC production is called immersion lithography. Immersion was originally discovered as a technique to enhance the imaging resolution in the optical microscopes in late 1870s by filling the usual air gap between the final lens and sample with a high refractive index (*n*) fluid. It was first applied to lithography in 1980s and first

introduced into IC industry in mid 2000s.[11,12] Figure 1.3 shows a schematic diagram comparing the conventional "dry" exposure and immersion technique. Replacing the air gap between the lens and wafer with fluid (with refractive index greater than 1.0) enables the light with larger incident angle to reach the resist. This allows a lens with larger *NA* to be adopted, which, following equation (1.1), can push the ultimate resolution further.[13]

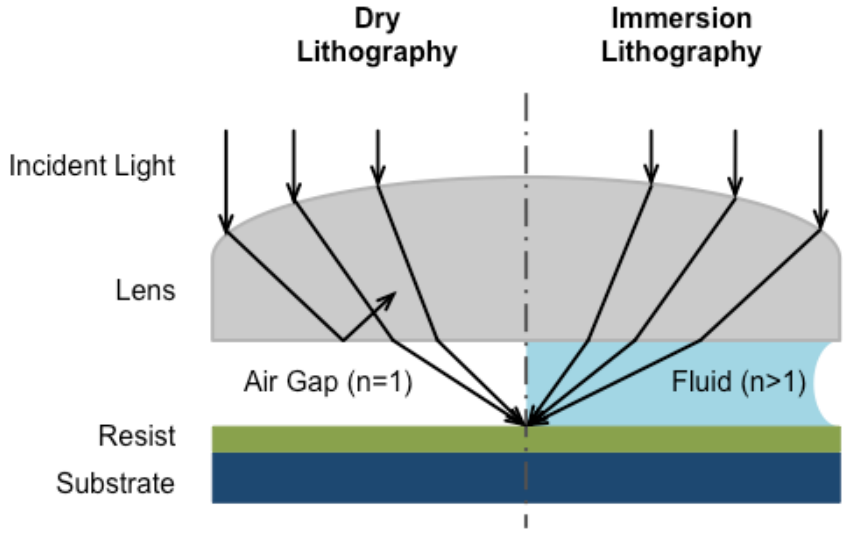

Figure 1.3 Schematic diagram of conventional dry lithography and immersion lithography

In addition, due to the reduced refraction angle at the lens/liquid interface compared with the one at the lens/air interface, the *DOF* at given *NA* can be increased.[13] There are a number of other illumination techniques to mitigate the problems caused by diffraction effects, such as optical proximity effect correction (OPC), in which sub-resolution features are applied on the mask patterns to compensate aerial image degradation;[14] off-axis illumination (OAI), in which the photomask is illuminated obliquely rather than perpendicularly, allowing the zero

order and one of the first order of the diffracted beam to pass the pupil and thus achieving enhanced image contrast for small features;[15,16] and phase-shifting mask (PSM), in which the contrast is improved through modulating the light phase to introduce a constructive or destructive interference.[6,17] However, more recently, considerable improvements in resist material and advanced processing techniques, e.g. multiple patterning[18,19], have been required to maintain progress.

Using the ArF excimer laser source combined with techniques such as off-axis illumination, water immersion and double patterning, the state-of-the-art 193 nm photolithography enables today's 22 nm technology node.[20,21] However, this also pushes the capability of 193 nm lithography to the very limit and any further improvement, especially for multiple patterning, is likely to considerably increase the processing complexity, thus making the yield and cost unacceptable in high-volume manufacturing.

1.2.2 Extreme Ultraviolet Lithography

Extreme Ultraviolet Lithography (EUVL) with an exposure wavelength of 13.5 nm has long been considered as the most promising candidate for NGL. As the proposed next step to extending optical lithography with a much shorter wavelength, EUVL has the potential to obtain higher resolution than the 193 nm lithography without the need for multiple patterning, making this technology cost-effective. Line-space features of 7 nm in hydrogen silsesquioxane (HSQ) resist and 12 nm resolution on chemically amplified resists (CARs) have been achieved using EUV interference lithography.[21,22] Sub-14 nm patterning was also achieved

with an EUV projection lithography tool,[23] which better reflects the final design of an EUV scanner for industrial use.

The EUV light source is normally synchrotron based or plasma based. In a synchrotron source, EUV radiation is generated through radial acceleration of electrons. A synchrotron EUV source has the advantage of high reliability and low contamination. However, the high cost and low power output exclude its application in production scale EUV tools.[24] Plasma based EUV sources use a hot dense plasma to generate EUV radiation with reasonable output. Plasma that meets the required temperature can be excited either by high power laser – known as laser produced plasmas (LPP) – or electrical discharge – known as discharge produced plasmas (DPP).[24] LPP based EUV systems utilizing a tin plasma are presently the best candidate for commercial manufacturing considering the overall performance including throughput, cost and imaging quality, but require extensive contamination control to mitigate plasma debris.

EUV optics in a projection system is significantly different from those in current photolithography systems. Due to the fact that matter, including air, absorbs radiation in the EUV range, the optics in a EUV system have to operate in vacuum and have to be reflective rather than transmissive.[20] This can be realized by employing multilayer reflective mirrors as well as a multilayer photomask. The multilayer structure consists of up to 100 alternating coatings of molybdenum and silicon (Mo/Si) to allow interlayer interference. Figure 1.4 shows a schematic diagram of a typical EUV optics layout in a LPP based EUV system.[20] After the

plasma is created, a collector mirror is used to collect and condense the EUV light. The light beam is then delivered through a series of mirrors to illuminate on the mask and finally projected (with reduced size) onto the wafer. As each one of the mirrors has a theoretical maximum of 72% reflectivity (less than 70% in practice due to defects) and as at least six mirrors are needed in a typical EUV system, only a small portion of radiation from the source actually reaches the wafer, which considerably affects the throughput.[20] Extremely high defect control is required for the mirror manufacturing to minimize power dissipation and image error.[25] In addition, radiation-induced heating and damage to the optical elements, which can shorten the system operation time, is also a concern for developing EUV systems for future mass production.[26] The latest commercial EUV system NXE3300B from ASML has claimed to have a productivity up to 125 wafers per hour with sub-22 nm resolution.[27]

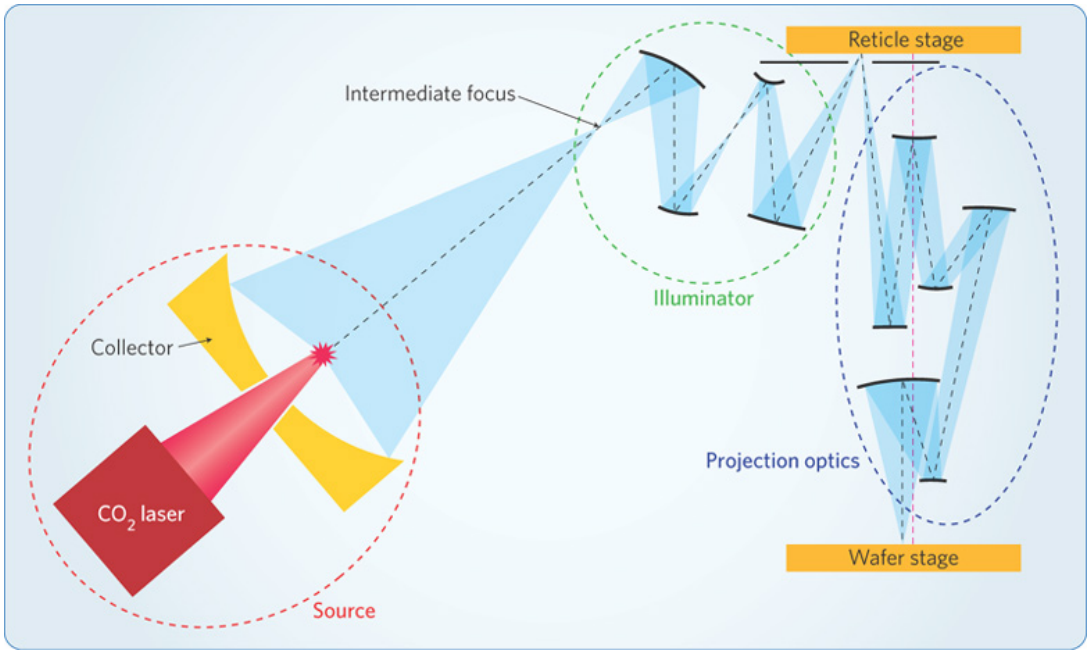

Figure 1.4 Schematic diagram of typical EUV optics in a laser produced plasma (LPP) based EUV system, adopted from reference [20]

1.2.3 Electron Beam Lithography

Electron beam lithography (EBL) is a well-known and mature fabrication technique for nanoscale patterning. Using an accelerated electron beam instead of photons as the exposure source, the diffraction effect is negligible due to the extremely small exposure wavelength. The de Broglie wavelength of an electron accelerated to a typical 25 keV is only 0.008 nm, and the beam can be focused to a couple of nanometers.[28,29]

The first EBL tool was developed in the late 1960's by modifying a scanning electron microscope (SEM).[30] Due to the excellent resolution capability (below 5 nm) and flexibility (ability to form arbitrary patterns through controlling of beam deflection) as well as a good variety of available resist materials, EBL has been widely used in micro/nano scale device fabrication.[29] Nevertheless, the major weakness of EBL is a much lower throughput compared with photolithography, limiting its application to laboratories, research and development (R&D) areas, photomask making, and low volume IC manufacturing.[29,31] As the pattern feature size continues to shrink, the mask cost and cycle time in photolithography has started to increase rapidly due to the complex resolution enhancement techniques.[32] In this context, developing a high-throughput EBL system may be a competitive alternative in the future manufacturing.[32,33] There are two main types of EBL tools, one is direct write and the other is projection.

1.2.3.1 Direct Write Electron Beam Lithography Systems

In a direct write EBL system, an electron beam is controlled to scan across the substrate and "draw" the shapes. The electron source is normally a thermionic or field emission electron gun. The beam can be focused, deflected or blanked by a set of electron optics with electrostatic and electromagnetic lenses and coils. A schematic diagram of a direct write EBL system is shown in Figure 1.5 (a). Two classes of electron beams in direct write systems have been developed – the "Gaussian beam" and the "shaped beam".

In Gaussian beam systems, a finely focused beam is used. The technique is known as Gaussian as this is typically the distribution of electrons in the cross-section of a highly focused electron beam.[34] By scanning across the resist surface in a dot-by-dot fashion, arbitrary and extremely fine patterns can be generated. The simplest and most popular way of scanning is called raster scan, which is similar to the strategy used in an SEM where the whole write field is linearly scanned by the electron beam. The main difference between an SEM and a raster-scan EBL tool is that in the SEM the beam scans every pixel to obtain signals for display, whilst in the EBL the beam is selectively switched on/off by a blanker and only the pixels in pattern areas are exposed during the raster scan.[32,34] Another scanning strategy, which was developed to reduce the writing time, is called vector scan. Instead of linearly scanning across the whole write field, only the pattern areas are addressed in a vector scan system.[35] Figure 1.5 (b) shows the schematic diagrams of these two scanning methods.

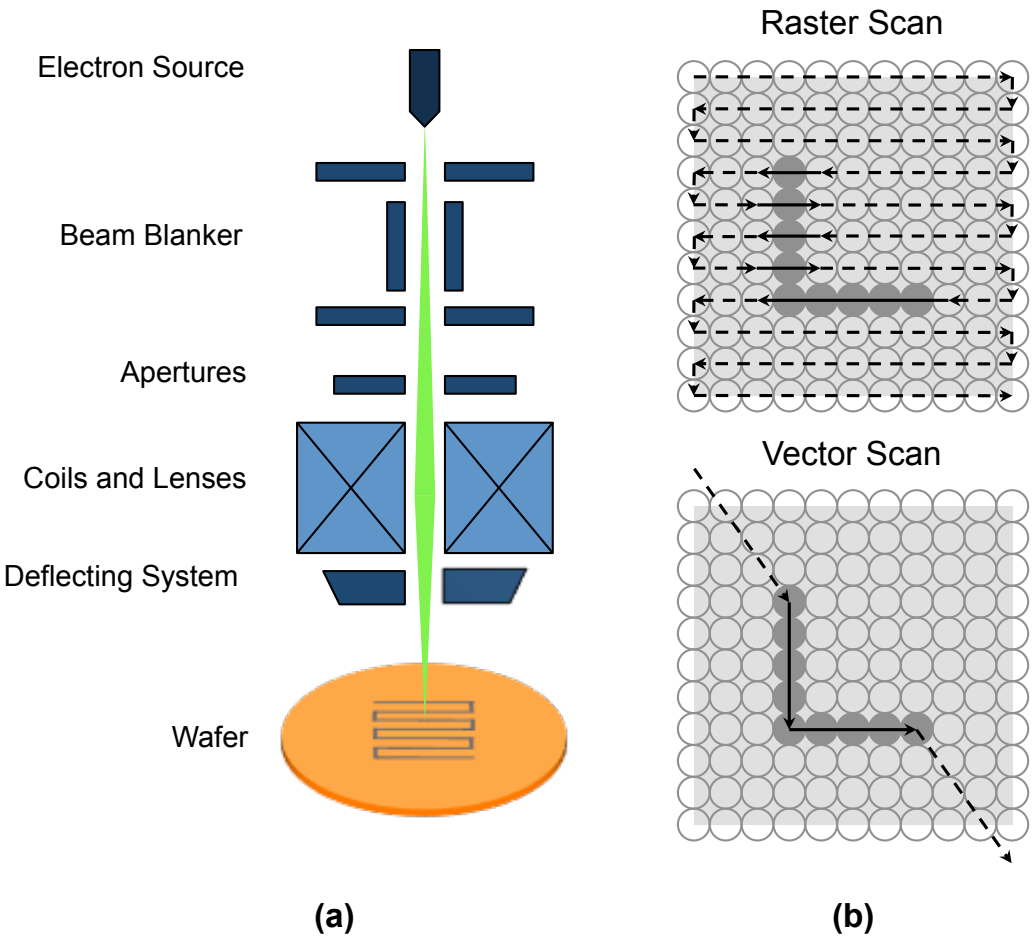

Figure 1.5 Schematic representations of (a) Gaussian beam direct write electron beam lithography system and (b) raster scan and vector scan method

Due to the serial writing nature of the Gaussian beam system, patterns in each write field have to be divided into very small shots. The huge number of shots raises the exposure time beyond the tolerance in industry production where complex patterns are required on a large area. Generally, there is a minimum feature size in a certain pattern, and such a "unit feature" can be much larger than the diameter of a focused Gaussian beam. Thus a shaped beam with various

feature sizes can be designed to considerably reduce the number of exposure shots and, as a result, reduce the exposure time. This is called shaped beam system (Figure 1.6). In this system, a number of variable apertures combined with a set of beam shaping deflectors are placed in the electron column. By controlling the beam path and changing the overlapping condition of the apertures, the size and shape of the electron beam can be varied.[34] The shaped beam system makes it possible to tailor the electron beam to the minimum feature size of a pattern, thus enhancing the throughput for special applications. However, in advanced fabrications such as ultra-large-scale integration (ULSI), where the minimum feature changes frequently and the number of patterns is very large, the throughput capability of the shaped beam direct write system is still too low.[35]

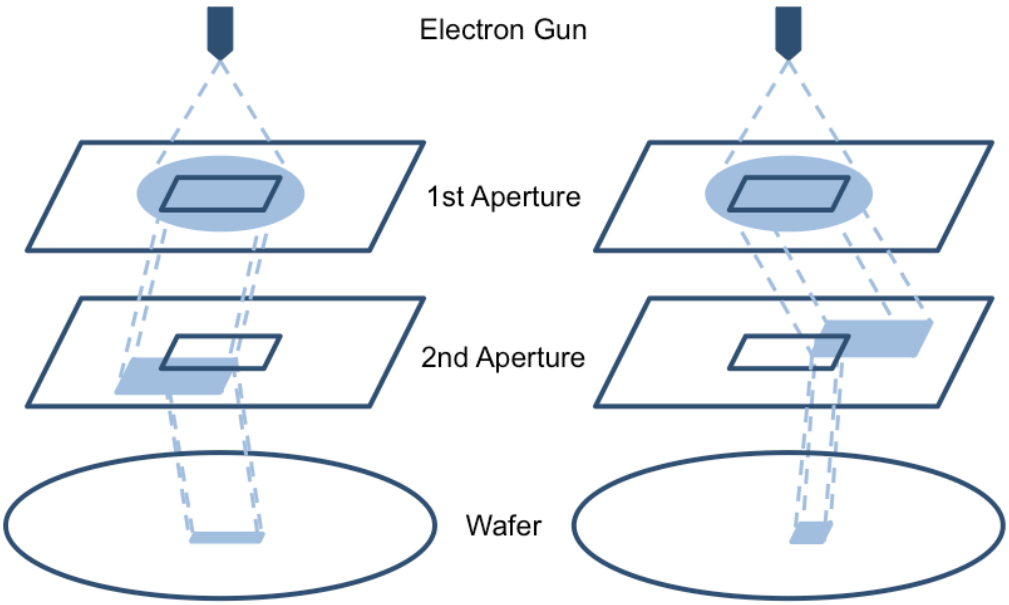

Figure 1.6 Schematic representations of a variable shaped beam system

1.2.3.2 Cell Projection Electron Beam Lithography Systems

In order to address the throughput issue in the direct write EBL systems, a number of projection EBL techniques have been developed. Similar to optical lithography, projection EBL uses an "electron mask" to create an aerial pattern and project it onto the resist. Cell projection, as an extension of the shaped beam direct write, is one of the typical projection EBL methods. Instead of having a beam with simple shapes, a cell projection EBL system has masks with complete features. In IC chip fabrication, a large portion of patterns are repeated structures, especially for memory chip, in which more than 90% of all patterns are periodically arrayed.[35] By utilizing such repetitive units (cells) in the mask and projecting to the wafer, the exposure shots can be considerably reduced in cell projection EBL. However, there are certain drawbacks in conventional cell projection systems. As this system uses a stencil mask, which is a solid membrane with patterns cut through, significant amount of energy is deposited on the stencil when the electrons are absorbed. This will cause mask heating and distortion, which can reduce the resolution as well as the stitching accuracy.[6,36] In addition, the patterns on a stencil mask also have limitation on the amount and size, e.g. an annular structure is difficult to achieve. The resolution of projection EBL systems also limited by the space charge effects due to the mutual repulsion of electrons in the beam. Such effects become more severe with the beam current increasing.[37]

There are some other versions of advanced projection EBL systems being designed, including the scattering with angular limitation in projection electron-beam lithography (SCALPEL) system from Bell Laboratories,[38] and projection

reduction exposure with variable axis immersion lenses (PREVAIL) system from IBM.[39] The main advantage of the SCALPEL system over the cell projection EBL lies in its specially designed scattering mask. Instead of having cutouts on a solid membrane, the scattering mask in the SCALPEL system consists of a much thinner membrane with low atomic number material (e.g. 100 nm of silicon nitride), on which a pattern made of high atomic number material (e.g. gold or tungsten) is placed. When the electron beam pass through, the high atomic number material leads to higher angle scattering compared with the low atomic number membrane, where the scattering is negligible. Then a narrow aperture at the back focal plane of the projection lens blocks most of the scattered electrons and only allows the un-scattered electrons to pass through. As the majority of energy from the blocked electrons is deposited on the aperture rather than on the mask, thermal expansion and distortion of the mask can be effectively reduced. However, the space charging and small field size are the main concerns in this system.[6,36] In the PREVAIL approach, a variable-axis lens system is introduced to shift the electron optical axis curvilinearly. Since the electron beam is deflected to precisely follow the axis, the off axis aberrations can be effectively eliminated. As a result, the write field in the PREVAIL system can potentially be as large as 10 mm × 10 mm, thus simultaneously enhancing the throughput and reducing the stitching errors.

1.2.3.3 Multi-Beam Maskless Lithography

Multi-beam technology has been another active approach to address the throughput issue of direct write EBL. By applying a number of parallel electron

beams instead of a single beam, the throughput can be linearly improved while the excellent resolution and flexibility of the single beam EBL is retained. There are three major maskless EBL programs currently under development: multiple aperture pixel-by-pixel enhancement of resolution (MAPPER) from MAPPER Lithography, projection maskless lithography (PML2) from IMS Nanofabrication and reflective electron beam lithography (REBL) from KLA-Tencor.

The MAPPER system utilizes a massively parallel beam combined with optically controlled switching.[40] A schematic of MAPPER's electron optics is shown in Figure 1.7 (a). A broad electron beam is generated from a single high brightness gun followed by an electrostatic collimator lens. The collimated beam is then split up into up to 13,000 beams by an aperture array and focused before going through a beam blanker array, in which each one of the beamlets can be individually switched on and off. After the beam blanker array the beams are demagnified, deflected and focused in the wafer plane by a projection lens array and a beam deflection array. With these microarrays, each focused beam is able to scan on the wafer over a range of 2 μm, giving an overall exposure field of 26 mm × 33 mm, the same range of the field in an optical stepper. Fast switching is realized by high-speed optical data transport technique used in the telecommunication industry, which means the beamlets are independently controlled by 13,000 light signals. A low acceleration voltage of 5 kV is used in this system to minimize the wafer heating and proximity issue caused by the large multi-beam current above 150 μA.[41] Resolution of 22 nm with a throughput in excess of 10 wafers per hour

(wph) has been reported, and a cluster configuration (10 units per tool) enabling a 100 wph throughput has been proposed.[42,43]

IMS Nanofabrication (Austria) is developing another multi-beam technique known as multi-beam projection.[44] The 50 kV projection maskless lithography (PML2) system was originally designed for the 32 nm node and below.[45] A schematic of PML2's electron optics is shown in Figure 1.7 (b). With electrons generated from a high-brightness electron emitter, PML2 utilizes a programmable aperture plate system (APS) to split the collimated broad beam into thousands of beamlets through an array of 5 μm apertures. Through an electrostatic and magnetic lens system, these electron beams are accelerated to 50 keV and demagnified 200 times before reaching the wafer. Unlike the direct write EBL or MAPPER, where the electron beams scan on the wafer, the PML2 simply projects the parallel electron beams on to a moving wafer stage, which is precisely controlled using a laser interferometer. Each individual beam acts as one pixel in the projection pattern, and each pixel is controlled by the APS. Based on a similar concept to PML2, IMS Nanofabrication is also developing a 50 keV electron Mask Exposure Tool (eMET) for mask writing. A half-pitch resolution of 11 nm has been achieved from the proof-of-concept tool.[46]

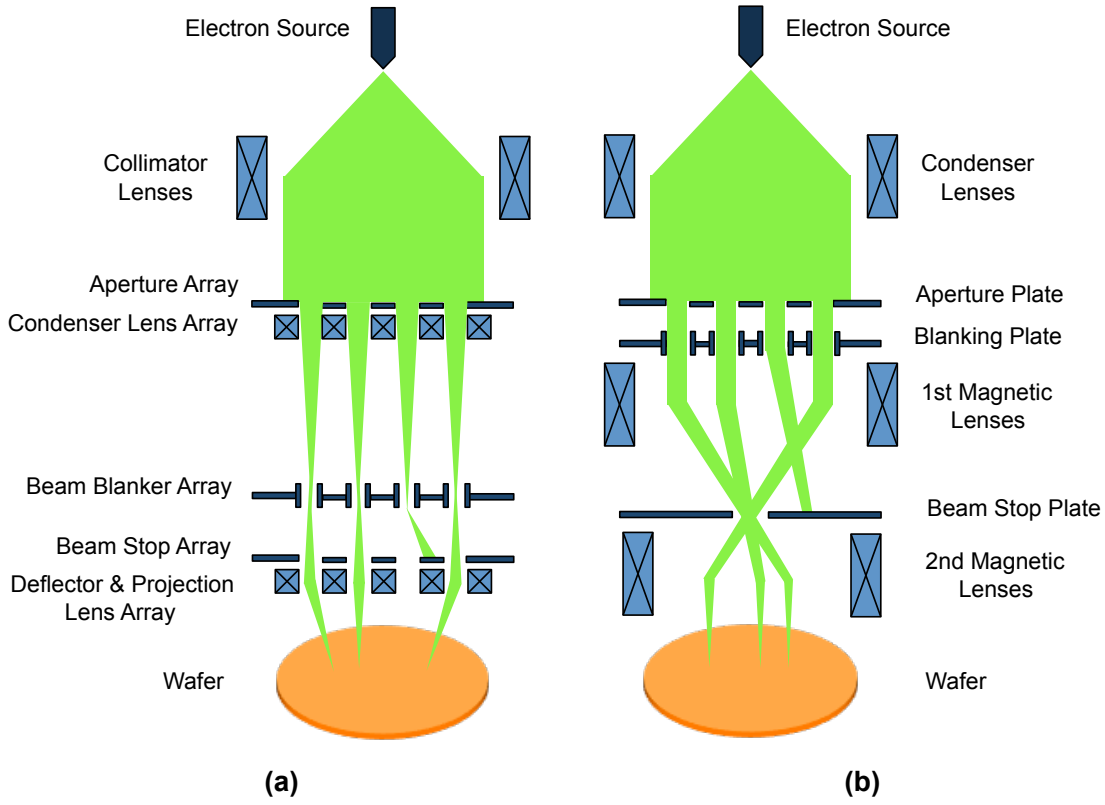

Figure 1.7 Schematic representations of (a) MAPPER lithography system, and (b) projection maskless lithography (PML2) system

The Reflective Electron Beam Lithography (REBL) tool is a novel approach for high throughput maskless lithography.[47,48] The novelty of the REBL design lies in its reflective electron optics combined with a digital pattern generator (DPG). A simplified schematic of REBL's electron optics is shown in Figure 1.8. In the REBL system, electrons are generated from a relatively low brightness source. After generation, the electron beam is bent and guided to the DPG, which is the key to the performance of the REBL system. The DPG is a CMOS ASIC chip with an array of electron mirrors capable of producing over 1 million beamlets. Together with a complex electrostatic microlens array referred to as the DPG lens,

the electrons reaching each mirror can be individually controlled, either reflected or absorbed, through applying different biases.[49] As a result, a pattern is formed with digitally controlled pixels. The electrons reflected from DPG are subsequently reaccelerated to between 50 and 100 keV. Finally the reflected beam with the aerial pattern is demagnified and projected on to the wafer. An unusual rotary wafer stage is used in the REBL system to allow a high throughput with minimized acceleration forces on the wafer. As the pattern formation is almost entirely digital, settling times including analog control of beam deflection and shaping can be eliminated. It has been reported that the REBL system has the potential to provide a solution for high volume manufacturing (HVM) at 16 nm and beyond based on recent simulation and experimental results.[50]

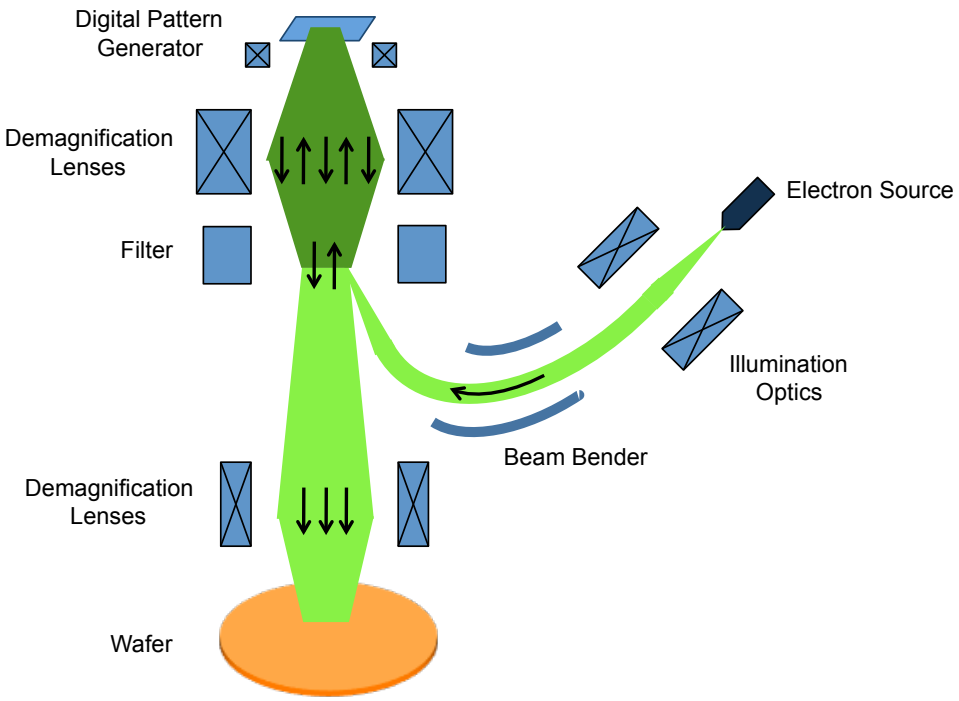

Figure 1.8 Schematic representations of a reflective electron beam lithography (REBL) system

1.2.3.4 Electron-Solid Interactions

Apart from the throughput, which is the main concern in the application of EBL, the ultimate achievable resolution in an EBL tool has also been intensively investigated. Although the diffraction limit is not an issue in EBL and the electron beam can be focused to be an extremely fine probe, the ultimate resolution in the resist pattern never reaches the probe size. This is, to a large extent, due to the fact of electron-solid interactions. After the electrons bombard the resist film, they undergo two types of scattering events, small angle forward scattering and large angle backscattering.[51] The direct results from the scattering are beam broadening and the proximity effect, where the pattern features receive extra dose by the electrons scattered from adjacent features.

Forward scattering usually happens when an electron collides with another electron from an atom in the resist/substrate. Such a collision changes the direction of the incident electron by a small angle, causing a beam broadening effect in the resist film.[52] The effective beam diameter d_f (nm) resulting from the forward scattering is empirically given by the formula:[51]

$$d_f = 0.9(R_t / V_b)^{1.5} \tag{1.4}$$

where R_t is the resist thickness (nm) and V_b is the electron beam voltage (kV). Therefore, forward scattering can be reduced by applying a high-energy beam on a thin resist film. Figure 1.9 shows the relation between forward scattering range parameter (which characterizes the diameter of the incident beam plus an additional radius due to scattering of primary electrons in the resist) and resist thickness at various acceleration voltages.[53] For applications in which a

combination of high resolution and high aspect-ratio is required, a high acceleration voltage is advantageous.

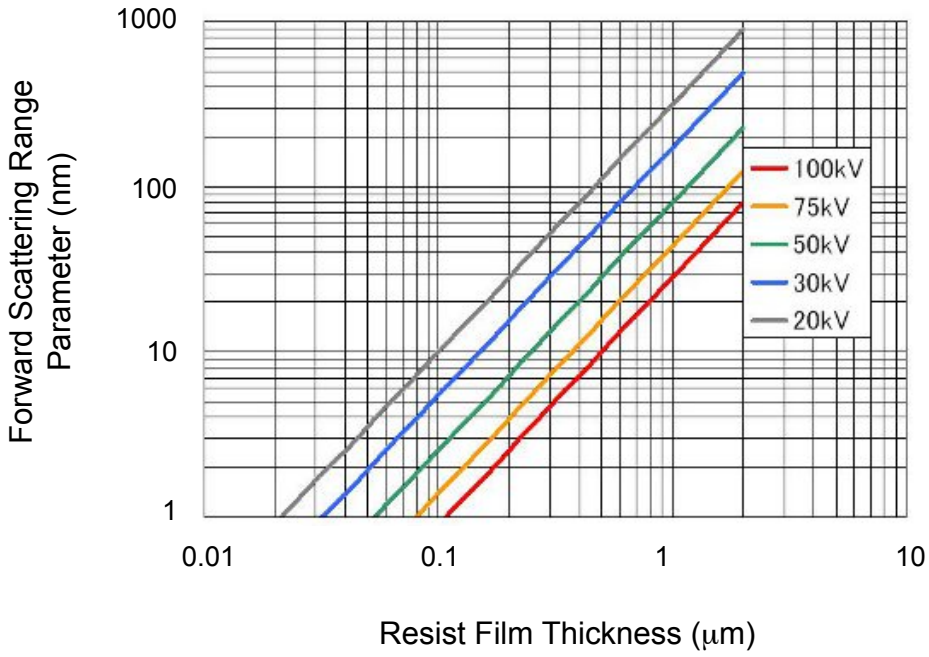

Figure 1.9 Forward scattering range parameter against resist thickness at different electron beam acceleration voltages, adopted from reference [53]

For a typical electron beam with 10 - 100 keV energy, the majority of the primary electrons penetrate into the substrate rather than stopping in the resist film. A fraction of them undergo wide angle backscattering due to elastic collisions with heavy nuclei in the substrate. These electrons may eventually return to the resist film and expose the area far from the incident beam. Backscattering is the main factor contributing to the proximity effect, which limits the minimum attainable feature size and maximum pattern density. Backscattering can range from a few to tens of micrometers depending on the primary electron energy and substrate material.[51] Figure 1.10 demonstrates a distribution of both forward scattering and

backscattering electrons in the resist. Electron beam energies of 30 keV and 100 keV are compared. As the beam energy increases, the forward scattering is suppressed and the backscattering area gets deeper and broader, thus the relative intensity is lower.[53]

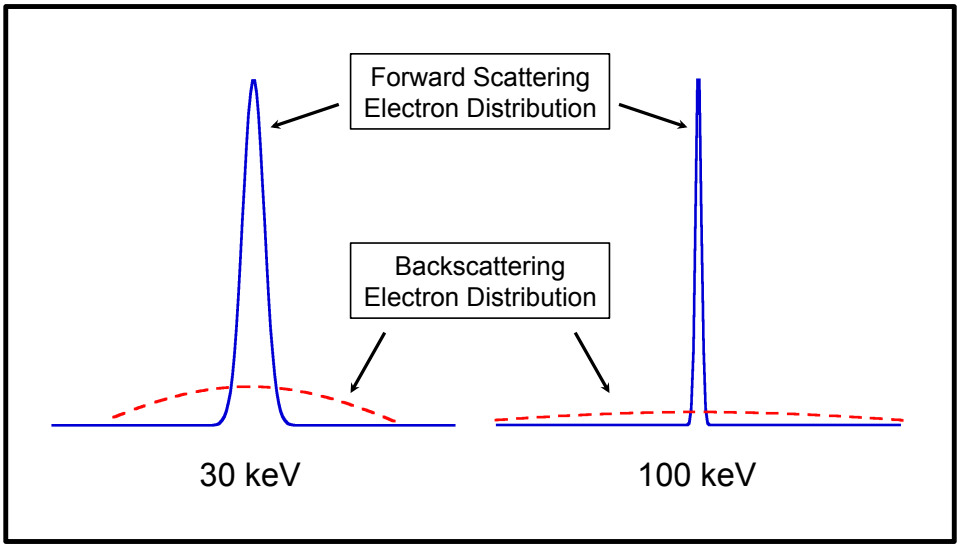

Figure 1.10 Schematic drawing of the forward scattering and backscattering distribution at electron beam energy of 30 keV and 100 keV

As the electrons travel through the resist/substrate, a number of secondary electrons are generated through inelastic scattering, dissipating the energy of the primary electrons. The energy of the secondary electrons is typically 2 to 50 eV. These low-energy electrons are responsible for the majority of the resist exposure, i.e. driving the chemical reactions in the resist material. The path length of the secondary electrons, which is normally in a range of several nanometers before reacting with the resist molecule, also causes additional broadening of the effective beam diameter.[51]

1.2.4 Ion Beam Lithography

Compared with EBL, ion beam lithography (IBL) uses light ions instead of electrons as an exposure source. The ion beam can either be tightly focused to form a scanning probe (direct write) or be collimated and projected onto the sample through a mask. In addition to using ion beam exposure to make material modifications in a sacrificial resist layer, a variety of patterning mechanisms are available in IBL based on the ion-matter interactions, including milling, etching, deposition and implantation.[54] Focused ion beam (FIB) has a number of advantages over electron beam including high energy density, very fine focusing, variable ion species and short penetration depth.[55] Particularly, IBL has advantages in resist exposure due to a much higher secondary electron generation efficiency than in the EBL exposure, and negligible amount of backscattering.[54] Figure 1.11 shows simulation results of secondary electron and backscattered electron/ion distribution upon 30 keV electron beam and 30 keV helium ion beam exposure.[56] A narrower distribution of secondary electrons is observed in helium ion beam radiation as well. As a result, faster exposure and higher feature density (almost no proximity effect) can be potentially achieved. Sub-10 nm resolution has been obtained using gallium ion beam and helium ion beam tools.[56-58] The major limit of IBL on resist lies in the practical film thickness. Due to the short penetration depth and beam widening by the ionization cascade, meeting the resist film thickness requirement (commonly around 60 nm) in semiconductor device fabrication can be difficult in normal IBL.[59,60] Raising the ion beam energy from tens of keV to above 100 keV or even MeV range provides an alternative to achieve features with higher aspect ratio. However, this approach can damage the

structures underneath the resist and also considerably increase the instrument complexity.[60]

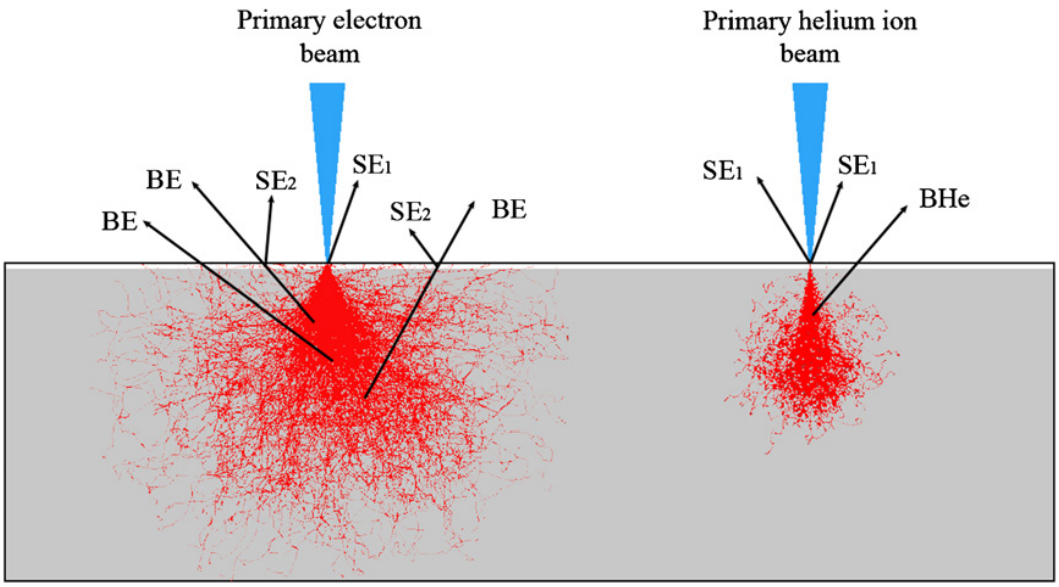

Figure 1.11 Simulation results of secondary electron and backscattered electron/ion distribution in silicon upon 30 keV electron beam (left) and 30 keV helium ion beam (right) exposure, adopted from reference [56]

1.3 Resists

As previously mentioned, a resist is a radiation sensitive material used in lithography to record the aerial image during the exposure. Resist materials are normally organic and, in most cases, polymeric. Together with the exposure tool, the resist determines the eventual lithographic performance. Important resist characteristics in lithography applications include resist tone, sensitivity, contrast, resolution and line edge roughness (LER)/line width roughness (LWR). Depending on the mechanism of pattern formation, resists can be classified as

non-chemically amplified (non-CA) resists or chemically amplified resists (CARs).

1.3.1 Resist Characteristics

Resist Tone

With radiation source exposing the resist layer, various chemical reactions (which will be introduced in next section) can be triggered depending on the resist material. The result of the reactions is a solubility change of the exposed film in specific solvents known as developer. Therefore, a development process can be realized by rinsing the film in a developer solvent to selectively remove the exposed/unexposed areas, forming a resist pattern on the substrate. In this process, there are two possible scenarios that can happen. If the exposed parts of resist film become more soluble in the selected developer while the unexposed areas are insoluble, this resist is called positive tone resist. In this case the exposed areas are removed by the solvent, and the unexposed areas retained. Conversely, if the exposure renders the resist films less soluble in the developer while the unexposed parts are soluble, it is called negative tone resist (Figure 1.2).

For actual applications, both of these two types of resists have their uses. A general comparison of positive and negative tone resist features is presented in Table 1.2.[61] Factors including adhesion to silicon substrate, cost of synthesis, developer availability (aqueous base developers or organic developers), development process window (a range within which variation in development condition can be tolerated) and wet chemical resistance (resistance to the solution

that used to etch the substrate) were compared. The properties of certain resists, especially some advanced novel resist systems, may have properties different from that listed in the table, and the selection of a resist tone depends on the requirement of specific applications such as pattern geometry, resolution, speed, ease of process, cost, etc. [61]

Table 1.2 General comparison of resist properties between positive tone and negative tone resists, adopted from reference [61]

Characteristic	Positive Tone	Negative Tone
Adhesion to Silicon	Fair	Excellent
Relative Cost	More Expensive	Less Expensive
Developer Base	Aqueous	Organic
Development Process Window	Small	Wide
Wet Chemical Resistance	Fair	Excellent

Sensitivity and Contrast

Sensitivity is a measurement of the incident energy that is required to activate a certain extent of chemical response, so as after development, the image in the resist film is as required.[62] This energy is described as the exposure dose, which is usually in mJ/cm^2 in photolithography, and $\mu C/cm^2$ in electron beam lithography. In resist material characterization, the sensitivity of a resist can be obtained by drawing a response curve, which is a plot of remaining film thickness

(often normalized) after development, versus the log of exposure dose (Figure 1.12). In an ideal response curve, there will be a critical dose beyond which the remaining normalized thickness drops to 0 (positive tone resist) or jumps to 1 (negative tone resist) due to the solubility switching. However, in practice, there is a finite slope instead of a step change. Thus, for the positive tone resist, sensitivity is defined as the dose at which the whole exposed film is removed (known as D_0), whilst for the negative tone resist it is the dose where 50% of the film thickness is retained (known as D_{50}), representing the dose above which a useful pattern remains after development.

Contrast reflects the rate change of solubility in a certain developer with respect to the dose increment. The contrast (γ) can be determined by approximating the steeply sloped portion of the response curve with a straight line, to give γ as the slope of the line (Figure 1.12). In the data analysis of a response curve, γ can be expressed as:

$$\gamma = \left| \log_{10}\left(\frac{D_{100}}{D_0} \right) \right|^{-1} \tag{1.5}$$

with D_0 and D_{100} shown in Figure 1.12. A higher contrast resist usually has a more vertical sidewall profile as well as broader process window (the extent of variation in process conditions that can be tolerated to remain an acceptable feature size), both of which contribute to a potentially higher resolution.[63,64] Response curves are not only dependent on the resist material, but may also vary with different development processes, post application bake (PAB) and post exposure bake (PEB) conditions.[65]

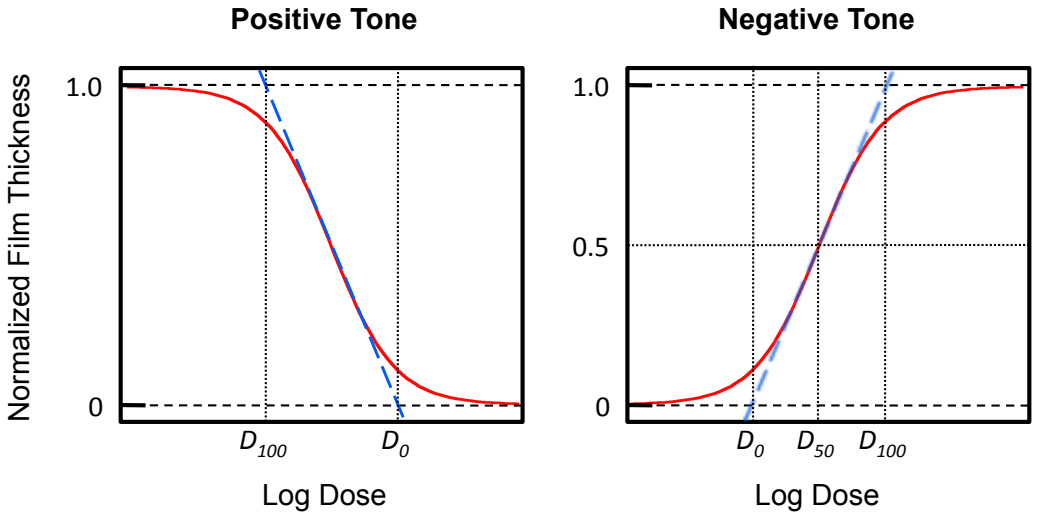

Figure 1.12 Typical response curve for positive tone (left) and negative tone (right) resist.

Resolution

The resolution of a resist is often evaluated by patterning line-and-space features with various ratios (dense or sparse lines). Line width and pitch size are the most common measurements to represent the resolution capability. As schematically shown in Figure 1.13, pitch is the width of one period of a periodic line-and-space pattern. In the high-resolution dense case, one feature may receive some extra exposure from adjacent features due to the proximity effect, which not only changes the actual dose, but also reduces the sharpness of the edges of the energy deposition profile. As a result, the line width of dense lines is normally bigger than that of an isolated line in same conditions, and the capability of dense patterning of a resist is thus evaluated by the smallest achievable pitch size or half-pitch size rather than just line width.

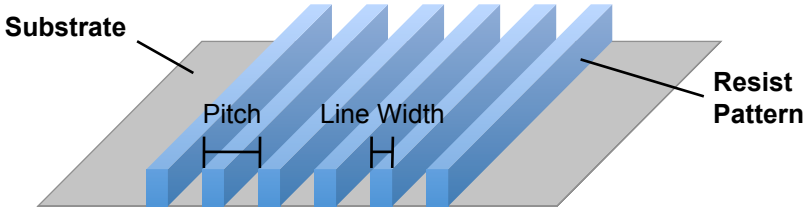

Figure 1.13 Schematic illustration of pitch and line width in a periodic line-and-space resist pattern

Line edge/width roughness

Line edge roughness (LER) is described as the fluctuation along the edge of a line feature; Line width roughness (LWR) is the deviation of the line width due to fluctuations in the edges of both sides. These two parameters are measured as three standard deviation (3σ) values. In the case of uncorrelated edges (when the left and right edges of a line vary independently), the relation between LWR and LER is given as:[66]

$$LWR \approx \sqrt{2} LER \tag{1.6}$$

In IC manufacturing, significant degradation of electrical characteristics can be induced by high LWR.[67,68] There are various factors that may bring about LER or LWR. From the aspect of exposure system, any statistical fluctuation of the number of incident photons or electrons (shot noise) can cause a rough edge or variation in feature size. From the resist material itself, the LER can be affected by factors like molecular weight and molecule distribution,[69,70] molecular structure,[71] and inhomogeneous reaction at the feature boundaries.[72] Furthermore, in most chemically amplified resists, LER is determined in a large part by the acid diffusion, and, at high resolutions, the inhomogeneous mixing of resist components .[73]

1.3.2 Resist Materials

As mentioned above, resists can be categorized into non-chemically amplified (non-CA) resists or chemically amplified resists (CARs). The term "non-chemically amplified (non-CA)" refers to the resist systems in which a single reaction is triggered by one photon or electron. Non-CA resists usually have a relatively low sensitivity. In CAR systems a catalytic chain reaction is introduced to realize a number of reactions initialized by one photon or electron. As a result, the sensitivity of the resists can be greatly enhanced. A great many CARs have been developed with various imaging mechanisms. CARs for microlithography have been well reviewed by Ito. H in 2005,[64] and the typical CAR systems introduced in this section are selected and discussed on the basis of this review article. Some other novel materials developed more recently are introduced in Chapter 4.

1.3.2.1 Non-Chemically Amplified Resists

In the early IC productions utilizing g-line and i-line lithography, a non-CA resist system was employed. This positive tone resist consists of an aqueous base soluble novolac resin and a lipophilic, photoactive dissolution inhibitor diazonaphthoquinone (DNQ) (Figure 1.14). The novolac resin undergoes an azo coupling reaction with the DNQ molecules, increasing the molecular weight and hence inhibiting the solubility of the resist in aqueous alkaline solutions.[74,75] Upon UV light irradiation, the photoactive DNQ is converted to an indene carboxylic acid which serves as a dissolution promoter and renders the resist readily soluble in aqueous alkaline solutions.[74,75] Therefore a positive tone relief

pattern is formed. Despite an impressive sub-0.5 μm resolution achieved in the i-line photolithography,[76] DNQ/novolac resist was found unsuitable in the subsequent deep UV technology. This is due to the low sensitivity and strong absorption (which limits the penetration of light through the resists film) of this material in deep UV range.[64]

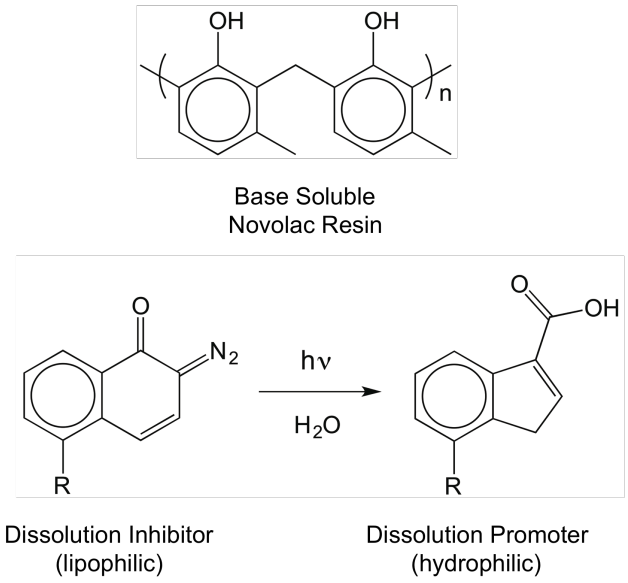

Figure 1.14 Structures and mechanism of diazonaphthoquinone/novolac resist

There are another two well-known non-CA resists, polymethylmethacrylate (PMMA) and hydrogen silsesquioxane (HSQ), both of which are mainly used in EBL. As a positive tone resist, PMMA is one of the first resists developed for EBL. Upon electron beam irradiation, the PMMA polymer will undergo main chain scission, which reduces the molecular weight in the exposed area, thus increasing the solubility in certain developers. In the case of HSQ resist, the electron beam radiation will lead to a cross-linking reaction between the

monomers and thus the exposed area becomes insoluble in developer, forming a negative tone pattern. Both PMMA and HSQ have excellent resolution (sub-5 nm) and superior LER.[29,77] However, their poor sensitivity together with the low throughput of EBL excludes them from most of the industry applications.

1.3.2.2 Chemically Amplified Resists

Taking the quantum yield into consideration, typically several photons or electrons are required to activate one molecule in the non-CA resists, which limits the sensitivity.[64] To meet sensitivity requirements in the lithography technologies with shorter exposure wavelength, a new mechanism is necessary. The concept of chemical amplification was devised in 1982 by Ito, Willson and Frechet,[78] in which a catalytic chemical reaction is activated upon radiation via a photo sensitive compound, leading to orders of magnitude sensitivity enhancement. CARs have dominated the photolithography industrial application subsequently. The photoactive component in CARs is typically a photo-acid generator (PAG). Upon irradiation, the PAG decomposes, releasing a strong acid. The base resist resin is also changed to incorporate a chemical moiety that will react catalytically with the acid to form the pattern (Figure 1.15).[64]

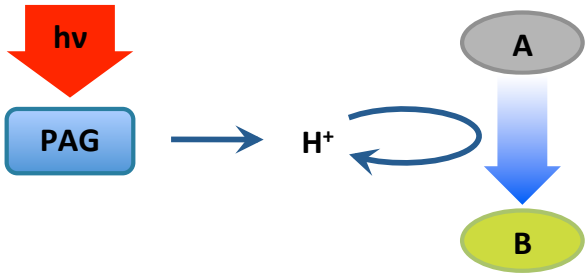

Figure 1.15 Schematic representation of chemical amplification process

A great many PAGs have been developed for CARs and the mechanisms of acid generation have been extensively investigated. Among them, onium salts such as triarylsulfonium antimonates have been heavily used in CAR formulations due to their high photosensitivity, high thermal stability, and the strong acid generated with excellent quantum yield (Figure 1.16).[64,79]

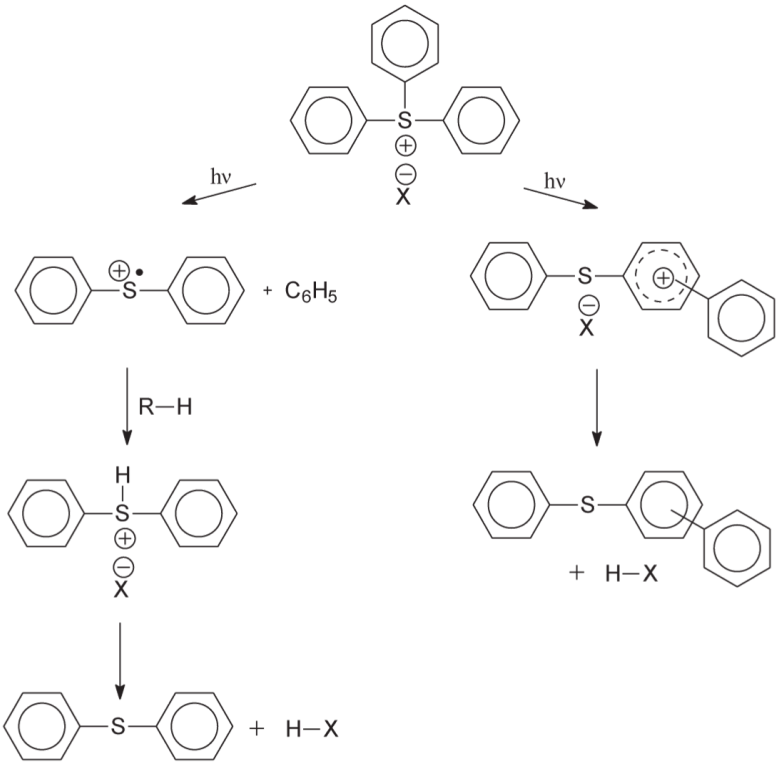

Figure 1.16 Chemical structures and photolysis mechanism of triphenylsulfonium salts, adopted from reference [64]

Based on the acid-catalysed chain reaction, many pattern formation mechanisms have been investigated, including deprotection, catalytic main chain scission, rearrangement and polymerization/depolymerization, etc.[64] Deprotection was among the very first categories of chemical amplification to be realised, via an

acid-catalysed cleavage of a hydrophobic protecting group to expose a hydrophilic functional group. A typical example of CAR based on this mechanism is IBM's *t*BOC resist, which was also the first CAR utilised in dynamic random access memory (DRAM) manufacturing with 248 nm deep UV lithography.[80] This is a two-component positive tone resist consisting of poly(4-*tert*-butoxycarbonyloxystyrene) (PBOCST) and onium salt PAG, triphenylsulfonium trifluoromethanesulfonate. The deprotection reaction of this resist is shown in Figure 1.17.

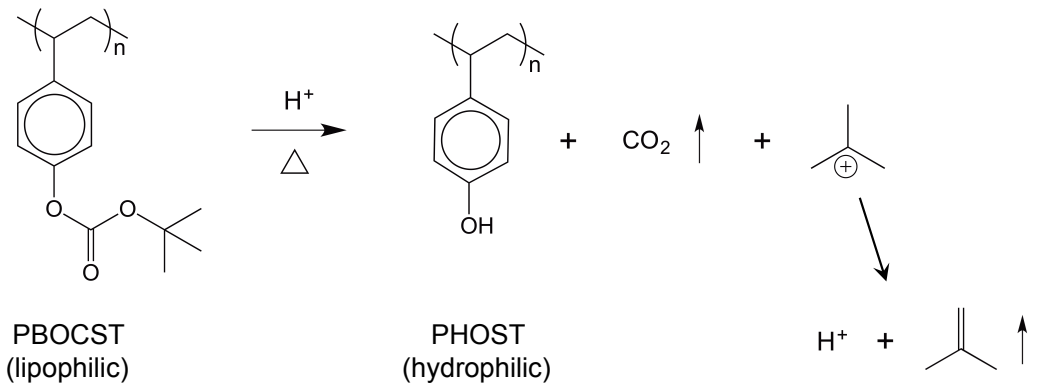

Figure 1.17 Acid-catalyzed deprotection of the poly(4-*tert*-butoxycarbonyloxystyrene) resist

The phenolic hydroxyl group is blocked in the PBOCST with an acid-labile *tert*-butoxycarbonyl (*t*BOC) group, making the polymer hydrophobic. After the generation of photo-acid under exposure, the *t*BOC protection group can react with the acid, finally releasing isobutene and carbon dioxide, with a proton regenerated. The PBOCST is subsequently converted into a hydrophilic poly(4-hydroxystyrene) (PHOST), which is soluble in aqueous developers. As the acid is

regenerated rather than consumed after the deprotection, the reaction is catalytic with a chain length of ~1000 under normal process conditions.[64] The temperature required to activate the acid-catalysed reaction is around 100°C, whilst the *t*BOC group is thermally stable up to 190°C without acid. Therefore, a post-exposure bake (PEB) at approximately 100°C is necessary before development.[64] Due to the excellent lithographic performance, most of the subsequently developed advanced positive tone CARs are based on the acid-catalysed deprotection. Typical examples are hydroxystyrene type APEX resist, hydroxystyrene/methacrylate type ESCAP resist and acrylate type resists.[74]

Negative tone CARs can be achieved by using the photo-acid to catalyze the reactions that either convert the material polarity, or increase the molecular weight by crosslinking to provide the solubility change. The PBOCST resist, as an example of polarity change, can also be turned into a negative tone resist by using a non-polar organic developer such as anisole, which dissolves the PBOCST readily rather than PHOST.[64] Generally, resists that have dual-tone behavior (such as PBOCST) allow for development in both aqueous base developer (known as positive tone development) and solvent-based developer (known as negative tone development). In former process, the exposed resist is removed and a positive tone image is formed; whilst in latter process, the unexposed resist is removed, forming a negative tone image.[81]

SU-8 (MicroChem) is a successful negative tone CAR based on crosslinking of epoxy resins. In this type of resist, negative tone patterning is realized via an acid-

initiated, cationically catalyzed ring-opening polymerization, resulting in an increase in molecular weight and thus reducing the solubility (Figure 1.18).[64,74] SU-8 resist is capable of patterning structures in very thick films (>50 μm) with large aspect ratio. In addition, this resist also shows a high sensitivity, high thermal stability and compatibility with electroplating, which make it an ideal material for applications in microelectromechanical systems (MEMS).[82]

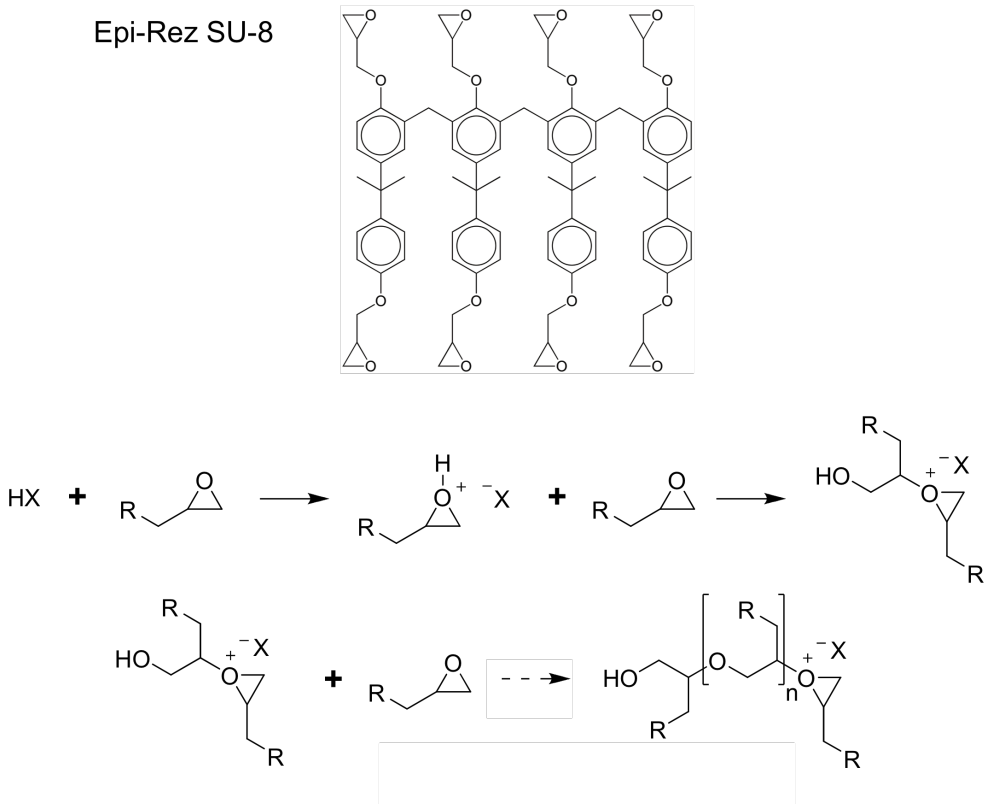

Figure 1.18 Chemical structure of SU-8 resist (top) and mechanisms for acid catalyzed cross-linking of epoxy resists (bottom)

Epoxy based polymers generally have advantages of excellent adhesion, high mechanical strength, good sensitivity, low outgassing and low cost.[83] However, such crosslinking based CARs often have swelling issues which can limit their high-resolution capability. This is due to the penetration of solvent into the crosslinked network. As a result, the patterned structures can be enlarged and/or distorted. In the case of line patterns, bridging and wobbling can be observed.[64] There are several possible ways to reduce the swelling in the crosslinking CARs including using materials with lower molecular weight and designing a base-developable polymer.[64,83]

1.3.3 Limitations and Challenges

In the semiconductor industry, the requirements of throughput, minimum feature size and pattern quality lead to the pursuit of resists with high sensitivity, high resolution and low LWR simultaneously. The technological challenges and requirements are summarized annually by the International Technology Roadmap for Semiconductors (ITRS).[84] In terms of resist requirements, a target of 20 nm dynamic random access memory (DRAM) half-pitch and 14 nm Flash half-pitch, with a low frequency LWR (3σ) less than 1.6 nm has been specified by ITRS for the coming year 2016. The resist sensitivity requirement is also dependent on the power of available sources, so as to maintain throughput.[84]

The difficulty in simultaneously improving the sensitivity, resolution and LWR lies in a trade-off relationship among these three factors, known as RLS trade-off.[72] This trade-off relationship states that, by varying process conditions, two

of the parameters may be improved only at the expense of the third performance parameter. Taking the RLS trade-off relation into consideration, an overall evaluation of the lithographic performance of a resist, known as Z factor, can be given as[85]

$$Z = (resolution)^3 \times (LER)^2 \times (sensitivity) \tag{1.7}$$

Z factor is a material-related constant reflecting the intrinsic property of a particular resist (note that LER is specified instead of LWR. For uncorrelated edges the relation between LER and LWR was introduced in Section 1.3.1). Improving the resist design (e.g. modifying the material or formulation) can reduce the Z factor. However, the RLS trade-off relation still remains, albeit at a lower level. Due to the catalytic nature of CARs, the RLS trade-off has been the most challenging problem in the development of the resist technology. The factors contributing to the trade-off relation in CARs have been intensively studied and efforts on both material design and process conditions have been made to improve the overall resist performance.[72,86]

One of the main factors causing the RLS trade-off in the CARs, which has been noted since the very beginning of RLS study, is photo-acid diffusion.[72] The extent of acid diffusion, measured as diffusion length, is dependent on various factors including the polymer type,[87,88] molecular size of PAG,[88] PEB temperature and duration,[89] etc. In acid-catalyzed CARs, a certain level of acid diffusion is required to provide sufficient sensitivity. This is due to the fact that at low exposure dose the initial distribution of photo-acids is relatively sparse thus the acids need to migrate and fill the volume in between to achieve a sufficient

number of reactions.[72] In addition, the acid diffusion process can also smoothen the feature roughness induced by the shot noise and molecular distribution statistics, therefore reducing the LER.[88] However, acid diffusion inevitably brings about a resolution blur as the photo-acids migrate from the defined exposed area into the unexposed regions. As a result, the feature size of the resist pattern after development is larger than the designed pattern. Figure 1.19 (a) shows a schematic of acid diffusion induced resolution blur in the case of a positive tone resist. As the intermediate region between exposed and unexposed area contains a mixture of soluble and insoluble molecules in a stochastic manner, additional LER can also be introduced.[86] Moreover, resists with large acid diffusion length showed smaller exposure latitude due to a low chemical contrast.[88] As a result, improving the RLS trade-off by suppressing acid diffusion without sacrificing sensitivity is of particular importance.

A successful method to reduce unwanted acid diffusion is the addition of a base compound (quencher) into the resist formulation. As shown in Figure 1.19 (b), the uniformly distributed base molecules can effectively neutralize the small amount of acid diffused into the unexposed region, thus increasing the chemical contrast and suppressing the resolution blur.[90] In areas with a lot of acid the quencher still neutralized some acid but sufficient is left to expose the resist via the catalytic process. Base quenchers have been widely used in advanced CARs to improve the environmental stability, resolution, exposure latitude and LER.[91,92] However, adding base quenchers can also reduce the sensitivity and change the dissolution property.[93]

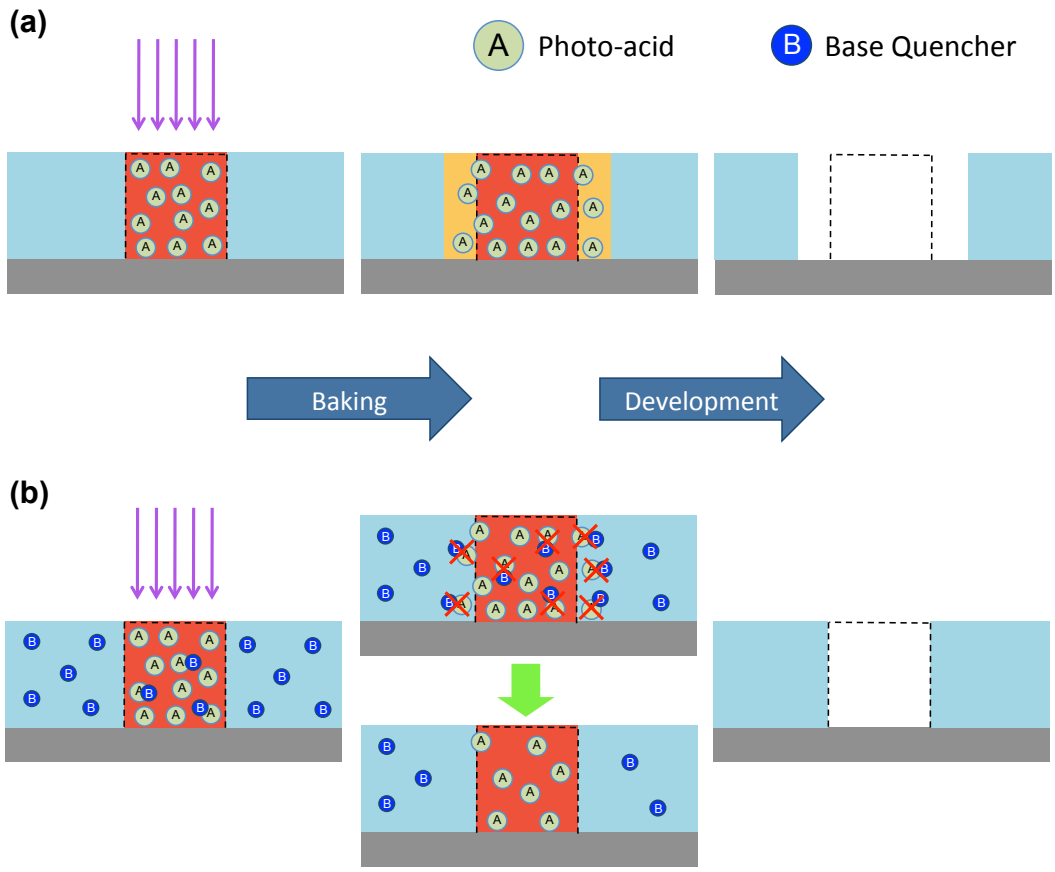

Figure 1.19 Schematic representations of (a) acid diffusion induced resolution blur in a positive tone resist and (b) diffusion suppression by base quenchers

A similar approach to suppress acid diffusion is using a polymer-bound PAG in which the anion of the photo-acid is covalently bonded to the polymer. The diffusion is therefore reduced due to a stronger interaction between protons and the bulky anions compared to those with small anions.[94]

Apart from acid diffusion control, utilizing resist materials with lower molecular weight is believed to be another approach to improve the RLS trade-off. As the

required feature dimension and roughness becomes comparable to the size of the resist polymers, improvement in resolution and LER becomes limited by the resist molecules. Therefore, using smaller polymers or molecular resists provides the potential for higher resolution and lower LER, which can push the Z factor to smaller values. A number of molecular resist materials, including calixarene, triphenylene and fullerene derivatives, have been developed and demonstrated to have excellent lithographic performance.[95]

Exploring new approaches to improve RLS trade-off and developing novel resists for NGL is the main focus of this thesis. A new method to control the acid catalytic chain reaction in negative tone CAR system was demonstrated using a model polymeric resist, which is presented in Chapter 3. In Chapter 4 a series of high-performance molecular CAR systems base on this method are presented. Chapter 5 presents a novel approach to enhance the sensitivity through introducing a metal complex into the resist material, which also enables an arbitrary patterning of metal-containing carbon nanostructures. Finally a brief summary and future work outlook is given in Chapter 6.

References

1. Morton Jr., D. L., Gabriel, J., Electronics: the life story of a technology. Westport, CT: *Greenwood Press,* 74 (2004)
2. Kilby, J. S., Miniaturized electronic circuits. U.S. Patent 3,138,743 (1964)
3. Moore, G. E., Cramming more components onto integrated circuits, *Electronics 38(8),* 114 (1965)
4. a) Intel® Microprocessor Transistor Count Chart, Available from: http://www.intel.com (accessed 05/08/2015); b) Transistor Count, Available from: http://www.wikipedia.org (accessed 05/08/2015)
5. Ferain, I., Colinge, C. A., Colinge, J. P., Multigate transistors as the future of classical metal-oxide-semiconductor field-effect transistors. *Nature*, *479,* 7373, 310 (2011)
6. Harriott, L. R., Limits of lithography. *Proc IEEE*, *89*(3), 366 (2001)
7. Brainard, R. L., Barclay, G. G., Anderson, E. H., Ocola, L. E., Resists for next generation lithography. *Microelectron. Eng.*, *61*, 707 (2002)
8. Levinson, H. J., Arnold, W. H., in Handbook of microlithography, micromachining, and microfabricaiton, Rai-Choudhury, P., editor. Bellingham, WA: *SPIE Press, Vol.1,* 28 (1997)
9. Levinson, H. J., Arnold, W. H., in Handbook of microlithography, micromachining, and microfabricaiton, Rai-Choudhury, P., editor. Bellingham, WA: *SPIE Press, Vol.1,* 57 (1997)
10. Bates, A. K., Rothschild, M., Bloomstein, T. M., Fedynyshyn, T. H., Kunz, R. R., Liberman, V., Switkes, M., Review of technology for 157-nm lithography. *IBM J. Res. Dev.*, *45*, 605 (2001)
11. Lin, B. J., The future of subhalf-micrometer optical lithography. *Microelectron. Eng., 6(1)*, 31 (1987)
12. Smith, B. W., Kang, H., Bourov, A., Cropanese, F., Fan, Y., Water immersion optical lithography for 45-nm node. *Proc. SPIE, 5040,* 679 (2003)
13. Mack, C. A., Field guide to optical lithography. Bellingham, Washington, USA: *SPIE Press, Vol. 6* (2006)

14. Nakae, A., Kamon, K., Hanawa, T., Moriizumi, K., Nakao, S., Precision improvement in optical proximity correction by optimizing second illumination source shape. *Jpn. J. Appl. Phys., 35(12B),* 6395 (1996)
15. Kamon, K., Miyamoto, T., Myoi, Y., Nagata, H., Tanaka, M., Horie, K., Photolithography system using annular illumination. *Jpn. J. Appl. Phys., 30(11S),* 3021 (1991)
16. Levinson, H. J., Arnold, W. H., in Handbook of microlithography, micromachining, and microfabricaiton, Rai-Choudhury, P., editor. Bellingham, WA: *SPIE Press, Vol.1,* 71 (1997)
17. Levenson, M. D., Viswanathan, N. S., Simpson, R. A., Improving resolution in photolithography with a phase-shifting mask. *IEEE Trans. Electron. Dev., 29(12),* 1828 (1982)
18. Dai, H., Bencher, C., Chen, Y., Woo, H., Ngai, C., Xu, X., 45nm and 32nm half-pitch patterning with 193nm dry lithography and double patterning. *Proc. SPIE, 6924,* 692421 (2008)
19. Bencher, C., Chen, Y., Dai, H., Montgomery, W., Huli, L., 22nm half-pitch patterning by CVD spacer self alignment double patterning (SADP). *Proc. SPIE, 6924,* 69244E (2008)
20. Wagner, C., Harned, N, EUV lithography: Lithography gets extreme. *Nat. Photonics, 4(1),* 24 (2010)
21. Mojarad, N., Hojeij, M., Wang, L., Gobrecht, J., Ekinci, Y., Single-digit-resolution nanopatterning with extreme ultraviolet light for the 2.5 nm technology node and beyond. *Nanoscale, 7(9),* 4031 (2015)
22. Buitrago, E., Yildirim, O., Verspaget, C., Tsugama, N., Hoefnagels, R., Rispens, G., Ekinci, Y., Evaluation of EUV resist performance using interference lithography. *Proc. SPIE, 9422,* 94221S (2015)
23. Hori, M., Naruoka, T., Nakagawa, H., Fujisawa, T., Kimoto, T., Shiratani, M., Nagai, T., Ayothi, R., Hishiro, Y., Hoshiko, K., Kimura, T., Novel EUV resist development for sub-14nm half pitch. *Proc. SPIE, 9422,* 94220P (2015)
24. Smith, B. W., Suzuki, K., Microlithography: science and technology. 2nd ed., Boca Raton: *CRC press, Vol. 126,* 399 (2007)

25. Ito, T., Okazaki, S., Pushing the limits of lithography. *Nature, 406(6799),* 1027 (2000)
26. Barkusky, F., Bayer, A., Döring, S., Grossmann, P., Mann, K., Damage threshold measurements on EUV optics using focused radiation from a table-top laser produced plasma source. *Opt. Express, 18(5),* 4346 (2010)
27. Peeters, R., Lok, S., Mallman, J., van Noordenburg, M., Harned, N., Kuerz, P., Lowisch, M., van Setten, E., Schiffelers, G., Pirati, A., Stoeldraijer, J., Brandt, D., Farrar, N., Fomenkov, I., Boom, H., Meiling, H., Kool, R., EUV lithography: NXE platform performance overview. *Proc. SPIE, 9048,* 940481J (2014)
28. McCord, M. A., Rooks, M. J., in Handbook of microlithography, micromachining, and microfabricaiton, Rai-Choudhury, P., editor. Bellingham, WA: *SPIE Press, Vol.1,* 156 (1997)
29. Pimpin, A., Srituravanich, W., Review on micro-and nanolithography techniques and their applications. *Engineering Journal, 16(1),* 37 (2011)
30. McCord, M. A., Rooks, M. J., in Handbook of microlithography, micromachining, and microfabricaiton, Rai-Choudhury, P., editor. Bellingham, WA: *SPIE Press, Vol.1,* 142 (1997)
31. Altissimo, M., E-beam lithography for micro-/nanofabrication. *Biomicrofluidics, 4(2),* 026503 (2010)
32. Pain, L., Tedesco, S., Constancias, C., Direct write lithography: the global solution for R&D and manufacturing. *C. R. Phys., 7(8),* 910 (2006)
33. Henry, D., Gemmink, J. W., Pain, L., Postnikov, S. V., Status and future of maskless lithography. *Microelectron. Eng., 83(4),* 951 (2006)
34. Robinson, A. P. G., Novel resists for nanolithography. PhD Thesis, School of Physics and Astronomy, University of Birmingham, 18 (1999), Available from: https://inis.iaea.org (accessed 15/08/2015)
35. Okazaki, S., High resolution optical lithography or high throughput electron beam lithography: The technical struggle from the micro to the nano-fabrication evolution. *Microelectron. Eng.,* 133, 23 (2015)

36. Tseng, A. A., Chen, K., Chen, C. D., Ma, K. J., Electron beam lithography in nanoscale fabrication: recent development. *IEEE T. Electron. Pack., 26(2),* 141 (2003)
37. Harriott, L. R., Berger, S. D., Liddle, J. A., Watson, G. P., Mkrtchyan, M. M., Space charge effects in projection charged particle lithography systems. *J. Vac. Sci. Technol. B, 13(6),* 2404 (1995)
38. Berger, S. D., Gibson, J. M., New approach to projection electron lithography with demonstrated 0.1 micron linewidth. *Appl. Phys. Lett., 57,* 153 (1990)
39. Pfeiffer, H. C., Advanced e-beam systems for manufacturing. *Proc. SPIE, 1671,* 100 (1992)
40. Kuiper, V., Kampherbeek, B. J., Wieland, M. J., Boer, G., de Berge, G. F. ten, Boers, J., Jager, R., Peut, T. van de, Peijster, J. J. M., Slot, E., Steenbrink, S. W. H. K., Teepen, T. F., Veen, A. H. V. van, Mapper: high throughput maskless lithography. *Mask and Lithography Conference (EMLC), 2009 25th European*, 1 VDE (2009), Available from: http://ieeexplore.ieee.org (Accessed 16/08/2015)
41. Slot, E., Wieland, M. J., De Boer, G., Kruit, P., Ten Berge, G. F., Houkes, A. M. C., Jager, R., Peut, T. van de, Peijster, J. J. M., Steenbrink, S. W. H. K., Teepen, T. F., Veen, A. H. V. van, Kampherbeek, B. J., MAPPER: high throughput maskless lithography. *Proc. SPIE, 6921,* 69211P (2008)
42. Wu, B., Next-generation lithography for 22 and 16 nm technology nodes and beyond. *Science China Information Sciences, 54(5),* 959 (2011)
43. Wieland, M. J., De Boer, G., Ten Berge, G. F., Van Kervinck, M., Jager, R., Peijster, J. J. M., Slot, E., Steenbrink, S. W. H. K., Teepen, T. F., Kampherbeek, B. J. MAPPER: high-throughput maskless lithography. *Proc. SPIE, 7637,* 76370F (2010)
44. Loeschner, H., Stengl, G., Buschbeck, H., Chalupka, A., Lammer, G., Platzgummer, E., et al., Large-field particle beam optics for projection and proximity printing and for maskless lithography. *J. Micro-nanolith. MEM. 2(1),* 34 (2003)

45. Klein, C., Platzgummer, E., Loeschner, H., Gross, G., Dolezel, P., Tmej, M., et al., Projection maskless lithography (PML2): proof-of-concept setup and first experimental results. *Proc. SPIE, 6921,* 69211O (2008)
46. Klein, C., Loeschner, H., Platzgummer, E., 50 keV electron multibeam mask writer for the 11nm HP node: first results of the proof of concept tool (eMET POC). *Proc. SPIE, 8323,* 83230G (2012)
47. Freed, R., Sun, J., Brodie, A., Petric, P., McCord, M., Ronse, K., et al., Demonstration of lithography patterns using reflective e-beam direct write. *Proc. SPIE, 7970,* 79701T (2011)
48. Petric, P., Bevis, C., McCord, M., Carroll, A., Brodie, A., Ummethala, U., et al., New advances with REBL for maskless high-throughput EBDW lithography. *Proc. SPIE, 7970,* 797018 (2011)
49. Carroll, A., Grella, L., Murray, K., McCord, M. A., Petric, P., Tong, W. M., et al., The REBL DPG: recent innovations and remaining challenges. *Proc. SPIE, 9049,* 904917 (2014)
50. Freed, R., Gubiotti, T., Sun, J., Kidwingira, F., Yang, J., Ummethala, U., et al., Reflective electron-beam lithography: progress toward high-throughput production capability. *Proc. SPIE, 8323,* 83230H (2012)
51. McCord, M. A., Rooks, M. J., in Handbook of microlithography, micromachining, and microfabricaiton, Rai-Choudhury, P., editor. Bellingham, WA: *SPIE Press, Vol.1,* 157 (1997)
52. van de Kraats, A., Murali, R., Proximity effect in e-beam lithography. *Atlanta, Georgia: Nanotechnology Research Center, Georgia Institute of Technoogy* (2005), Available from: http://nanolithography.gatech.edu (Accessed 20/08/2015)
53. a) Wu, C. S., Chen, C., Makiuchi, Y., High-energy electron beam lithography for nanoscale fabrication. *INTECH Open Access Publisher* (2010), Available from: http://cdn.intechopen.com (Accessed 20/08/2015); b) Rooks, M., Belic, N., Kratschmer, E., Viswanathan, R., Experimental optimization of the electron-beam proximity effect forward scattering parameter. *J. Vac. Sci. Technol. B, 23(6),* 2769 (2005)

54. Joshi-Imre, A., Bauerdick, S., Direct-Write Ion Beam Lithography. *Journal of Nanotechnology, 2014* (2014)
55. Kim, C. S., Ahn, S. H., Jang, D. Y., Review: developments in micro/nanoscale fabrication by focused ion beams. *Vacuum, 86(8),* 1014 (2012)
56. Postek, M. T., Vladár, A., Archie, C., Ming, B., Review of current progress in nanometrology with the helium ion microscope. *Meas. Sci. Technol., 22(2),* 024004 (2011)
57. Bruchhaus, L., Bauerdick, S., Peto, L., Barth, U., Rudzinski, A., Mussmann, J., et al., High resolution and high density ion beam lithography employing HSQ resist. *Microelectron. Eng.,* 97, 48 (2012)
58. Sidorkin, V., van Veldhoven, E., van der Drift, E., Alkemade, P., Salemink, H., Maas, D. Sub-10-nm nanolithography with a scanning helium beam. *J. Vac. Sci. Technol. B, 27(4),* L18 (2009)
59. Baglin, J. E. E., Ion beam nanoscale fabrication and lithography—a review. *Appl. Surf. Sci., 258(9),* 4103 (2012)
60. Gierak, J., Focused ion beam technology and ultimate applications. *Semicon. Sci. Tech., 24(4),* 043001 (2009)
61. Madou, M. J., Fundamentals of microfabrication: the science of miniaturization. 2nd ed., Boca Raton: *CRC press* (2002)
62. Moss, S. J., Ledwith, A., The chemistry of the semiconductor industry. Glasgow: *Blackie,* 180 (1987)
63. McCord, M. A., Rooks, M. J., in Handbook of microlithography, micromachining, and microfabricaiton, Rai-Choudhury, P., editor. Bellingham, WA: *SPIE Press, Vol.1,* 202 (1997)
64. Ito, H., Chemical amplification resists for microlithography. *Adv. Polym. Sci., 172,* 37 (2005)
65. Campbell, S. A., The science and engineering of microelectronic fabrication. New York: *Oxford University Press* (1996)
66. Constantoudis, V., Patsis, G. P., Gogolides, E., Photoresist line-edge roughness analysis using scaling concepts. *J. Micro-nanolith. MEM., 3(3),* 429 (2004)

67. Chandhok, M., Datta, S., Lionberger, D., Vesecky, S., Impact of line-width roughness on Intel's 65-nm process devices. *Proc. SPIE, 6519,* 65191A (2007)
68. Ban, Y., Sundareswaran, S., Panda, R., Pan, D. Z., Electrical impact of line-edge roughness on sub-45nm node standard cell. *Proc. SPIE, 7275,* 727518 (2009)
69. Patsis, G. P., Gogolides, E., Van Werden, K., Effects of photoreist polymer molecular weight and acid diffution on line-edge roughness. *Jpn. J. Appl. Phys. 44(8),* 6341 (2005)
70. Yoshimura, T., Shiraishi, H., Yamamoto, J., Okazaki, S., Nano edge roungness in polymer resist patterns. *Appl. Phys. Lett., 63,* 764 (1993)
71. Fedynyshyn, T. H., Astolfi, D. K., Goodman, R. B., Cann, S., Roberts, J., Contribution of resist polymer to material roughness. *J. Vac. Sci. Technol. B, 26(6),* 2281 (2008)
72. Gallatin, G. M., Resist blur and line edge roughness. *Proc. SPIE, 5754,* 38 (2005)
73. Thackeray, J. W., Materials challenges for sub-20-nm lithography. *J. Micro-nanolith. MEM., 10(3),* 033009 (2011)
74. Lawson, R. A., Molecular resists for advanced lithography-design, synthesis, characterization, and simulation. Doctoral dissertation, Georgia Institute of Technology, 14 (2011), Available from: https://smartech.gatech.edu (Accessed 22/08/2015)
75. Roy, D., Basu, P. K., Raghunathan, P., Eswaran, S. V., DNQ-novolac photoresists revisited: 1H and 13C NMR evidence for a novel photoreaction mechanism. *Magn. Reson. Chem., 41(2),* 84 (2003)
76. Dammel, R., Diazonaphthoquinone-based resists. Bellingham, WA: *SPIE Press, Vol. 11* (1993)
77. Yasin, S., Hasko, D. G., Ahmed, H., Fabrication of <5 nm width lines in poly (methylmethacrylate) resist using a water : isopropyl alcohol developer and ultrasonically-assisted development. *Appl. Phys. Lett., 78(18),* 2760 (2001)
78. Ito, H., Willson, C. G., Frechet, J. H., New UV resists with negative or positive tone. In 1982 Symposium on VLSI Technology. *Digest of Technical*

Papers 86 (1982), Available from: https://www.infona.pl (Accessed 25/08/2015)

79. Crivello, J. V., The discovery and development of onium salt cationic photoinitiators. *J. Polym. Sci. Pol. Chem., 37(23),* 4241 (2000)
80. Ito, H., Chemical amplification resists: History and development within IBM. *IBM J. Res. Dev.*, *41(1),* 69 (1997)
81. Mack, C., Fundamental principles of optical lithography: the science of microfabrication. West Sussex: *John Wiley & Sons,* 472 (2008)
82. Lorenz, H., Despont, M., Fahrni, N., LaBianca, N., Renaud, P., Vettiger, P., SU-8: a low-cost negative resist for MEMS. *J. Micromech. Microeng., 7(3),* 121 (1997)
83. Shaw, J. M., Gelorme, J. D., LaBianca, N. C., Conley, W. E., Holmes, S. J., Negative photoresists for optical lithography. *IBM J. Res. Dev.*, *41(1.2),* 81 (1997)
84. International Technology Roadmap for Semiconductors, 2012 Edition, Available from: http://www.itrs.net (Accessed 30/08/2015)
85. Wallow, T., Higgins, C., Brainard, R., Petrillo, K., Montgomery, W., Koay, C. S., et al., Evaluation of EUV resist materials for use at the 32 nm half-pitch node. *Proc. SPIE, 6921,* 69211F (2008)
86. Itani, T., Kozawa, T., Resist materials and processes for extreme ultraviolet lithography. *Jpn. J. Appl. Phys., 52(1R),* 010002 (2013)
87. Postnikov, S. V., et al., Study of resolution limits due to intrinsic bias in chemically amplified photoresists. *J. Vac. Sci. Technol. B, 17(6),* 3335 (1999)
88. Van Steenwinckel, D., Lammers, J. H., Koehler, T., Brainard, R. L., Trefonas, P., Resist effects at small pitches. *J. Vac. Sci. Technol. B, 24(1),* 316 (2006)
89. Yoshimura, T., Nakayama, Y., Okazaki, S., Acid-diffusion effect on nanofabrication in chemical amplification resist. *J. Vac. Sci. Technol. B, 10(6),* 2615 (1992)
90. Hinsberg, W. D., et al., Effect of resist components on image spreading during postexposure bake of chemically amplified resists. *Proc. SPIE, 3999,* 148 (2000)

91. Kawai, Y., Otaka, A., Tanaka, A., Matsuda, T., The effect of an organic base in chemically amplified resist on patterning characteristics using KrF lithography. *Jpn. J. Appl. Phys., 33(12S),* 7023 (1994)
92. Brainard, R. L., Cobb, J., Cutler, C. A. Current status of EUV photoresists. *J. Photopolym. Sci. Tec., 16(3),* 401 (2003)
93. Pawloski, A. R., Christian, Nealey, P. F. The multifunctional role of base quenchers in chemically amplified photoresists. *Chem. Mater., 14(10),* 4192 (2002)
94. Lawson, R. A., Molecular resists for advanced lithography-design, synthesis, characterization, and simulation. Doctoral dissertation, Georgia Institute of Technology, 29 (2011), Available from: https://smartech.gatech.edu (Accessed 05/09/2015)
95. Manyam, J., Novel Resist Materials for Next Generation Lithography, PhD thesis, School of Physics and Astronomy, University of Birmingham, 26 (2010), Available from: http://etheses.bham.ac.uk (Accessed 08/09/2015)

CHAPTER 2

EXPERIMENTAL TECHNIQUES

A number of experimental techniques were used in resist preparation, processing and characterization to obtain the results presented in Chapter 3, 4 and 5. This chapter first summarizes the exposure tools used in this study, including a scanning electron microscope (SEM) based exposure system, two high-energy EBL systems and a scanning helium ion beam lithography (SHIBL) tool, followed by the details of the resist preparation and processing. Finally, the methods of resist characterization, including the sensitivity, resolution and LER/LWR measurements, are introduced.

2.1 Exposure Tools

2.1.1 Scanning Electron Microscope with Beam Controller

As mentioned in the previous chapter, a modified SEM can be a suitable tool for direct write EBL. This is done through externally controlling the scan coils and beam blanker of the SEM using a beam controller. Figure 2.1 shows a schematic diagram of an SEM. The electron beam is generated from an electron gun at the top of the SEM column. The electrons can be extracted through thermionic emission or field emission. The former occurs by heating the cathode to provide sufficient thermal energy for emission, whilst the latter applies a strong electric field on a sharp tip to produce a large potential gradient. Field emission guns have

been widely utilized in advanced SEMs due to their high brightness, small source size and low energy spread compared with the thermionic electron sources.[1] The electron beam generated from the tip is then collimated and focused by a series of apertures and condenser lenses. A set of deflection coils is placed above the final objective lens to perform the beam scanning across the sample. A number of specialized detectors are placed at different positions to collect various signals including secondary electrons, backscattered electrons, X-ray photons, etc. The electron beam energy in a typical SEM ranges from 0.2 keV to 40 keV, with a beam spot size down to sub-nanometer range, in the latest tools.

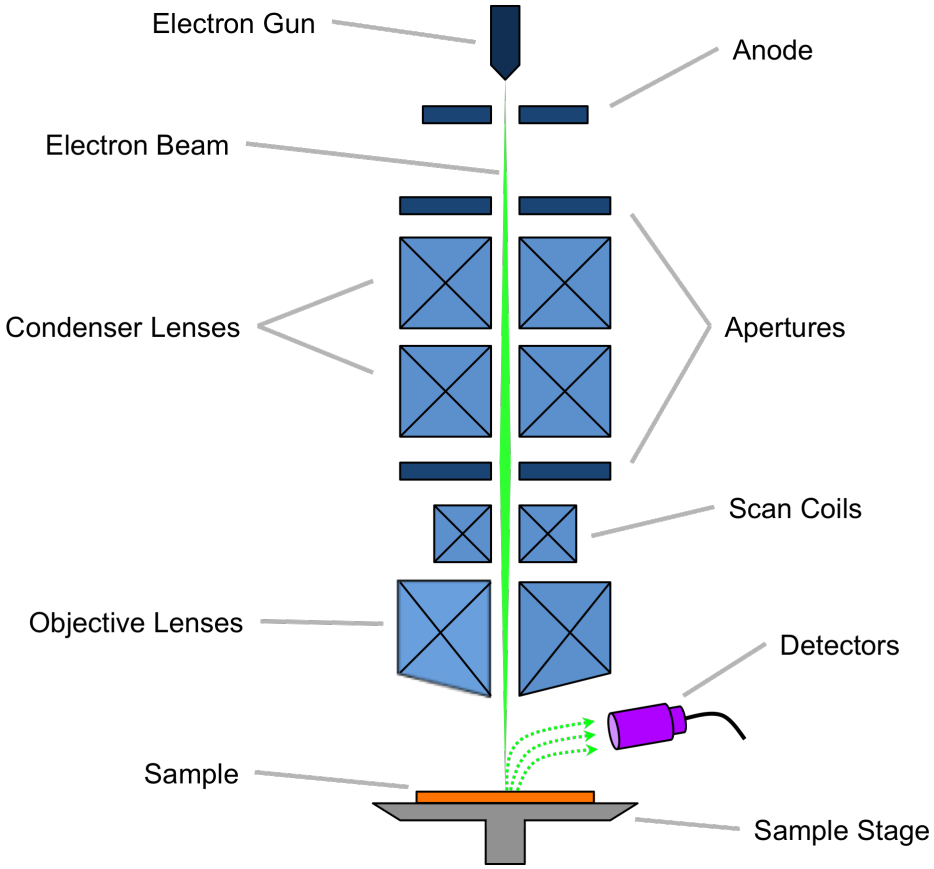

Figure 2.1 Schematic diagram of a scanning electron microscope

An XL30 SFEG SEM (FEI) at the University of Birmingham was employed in this study for both exposing and imaging of the resist samples. The Schottky field emission gun (SFEG) in this SEM is able to generate an electron beam with a beam current from 1 pA to 25 nA and a beam energy from 0.2 keV to 30 keV. An ELPHY Plus beam controller from Raith GmbH is attached to the SEM to control the electron beam for lithography. By taking remote control of the beam deflection and blanking, arbitrary patterns can be exposed in a raster scan mode. The dose of exposure is defined as

$$D_A = (I_e \times \tau)/\Delta l^2 \tag{2.1}$$

$$D_L = (I_e \times \tau)/\Delta l \tag{2.2}$$

where D_A and D_L are the area dose and line dose, respectively; I_e is the beam current; τ is the dwell time; and Δl is the step size.

2.1.2 High Resolution Electron Beam Lithography Systems

Two high-resolution EBL tools from our collaborators were used to further evaluate the resolution capability of the resist materials. One is the CABL 9510C (Crestec) EBL system at Fundacio Institut de Ciencies Fotoniques (ICFO, Spain) operating at 50 kV and another is a JBX 6300FS (JOEL) EBL system at the University of Leeds (UK) operating at 100 kV.

The CABL 9510C EBL system uses a SFEG source (ZrO/W) with acceleration voltage up to 50 kV. A point beam with 2 nm in diameter and sub-10 nm resolution capability has been reported. Flexible writing methods are available in this system, including vector/raster scan, axial symmetrical, field size modulation,

etc. It is equipped with a laser interferometer stage as well as a thermal controller to ensure high stitching/overlay accuracy and stability.[2] The JBX 6300FS is a vector scan EBL system. It also utilizes a SFEG as the electron source and provides a selectable acceleration voltage of 25 kV, 50 kV or 100 kV with very stable current over the range 30 pA to 20 nA. Sub-8 nm feature sizes have been demonstrated using this tool. The writing area of this system can be as large as 150 × 150 mm. An auto-loader is provided for continuous operation of up to 10 sample cassettes.[3]

2.1.3 Helium Ion Microscope

An ORION PLUS helium ion microscope (Carl Zeiss) at the University of Southampton (UK) was used in this study to evaluate the resolution and dose properties of the resist materials and compare with the EBL results. With an ALIS (Atomic Level Imaging Systems) helium ion source and an electrostatic ion column, a helium ion beam with high brightness and small probe size is generated and rastered across the sample. The probe size can be sub-0.75 nm at the acceleration voltage of 30 kV. The helium ion microscope can be used for both sample exposure and imaging.

2.2 Sample Preparation and Processing

Preparation of resist samples starts from silicon substrate cutting and cleaning, followed by resist film coating. Then the samples go through an exposure and development process with various conditions. All the steps of sample preparation

and processing, apart from substrate cutting, were carried out in clean room environment. Some resist samples were also deposited on copper grids for use in STEM characterization, which will be detailed in the experimental section in Chapter 5.

2.2.1 Substrate Preparation

Unless otherwise specified, the substrates in this study were diced from 4-inch, n-type, <100> oriented silicon wafers, using a DAD321 automatic dicing saw (Disco). With a dicing blade mounted on a high-frequency spindle, this dicing machine can precisely control the chip size and cutting depth. Typically the wafers are cut into 18 × 18 mm chips for resist deposition. Several substrate-cleaning methods were used for different resist materials. The majority of silicon substrates went through a simple acetone/isopropanol (IPA) clean, in which the silicon chips were ultrasonicated for 10 minutes in acetone followed by another 10 minutes in IPA. For some of resist samples, an additional fullerene-based thin underlayer was coated onto the silicon chip to enhance the resist adhesion. This underlayer is thermally curable at 260 °C. In the case of underlayer coating, prior to underlayer deposition the chips underwent 10 minutes immersion in piranha solution, a 1:1 (by volume) mixture of sulfuric acid (95-97%) with hydrogen peroxide (30%), followed by one minute immersion in a weak hydrofluoric (HF) acid solution (0.1-1%). Silicon chips were rinsed with deionised (DI) water (from Purite Neptune, 18.2 MΩ.cm) and dried with a nitrogen blow after each cleaning step. The underlayer was then deposited onto the cleaned silicon chips through

spin coating followed by 260 °C baking for 5 minutes to form ~ 20 nm insoluble (crosslinked) underlayer.

2.2.2 Resist Processing

Both CARs and non-CARs were investigated in this work. For the CARs, each of the compounds was stored separately in a fridge at 5 °C, and mixed immediately prior to use. A number of organic casting solvents were used in this study including chloroform, anisole, propylene glycol methyl ether (PGME) and ethyl lactate.

Resists were deposited onto the substrates through spin coating using a P-6708D spin coater (SCS). By adjusting the resist concentration and spin speed, resist film thickness can be controlled. Typically, a three-step spinning recipe is employed, including a slow spin (around 500 rpm, 5 s) for resist solution dispersion, followed by a medium spin (1000-3000 rpm, 1-2 min) for film formation and drying, and finally, a fast spin step (>3000 rpm, 10 s) to ensure no flowback of excess solution at the edge bead or sample corners.

A post application bake (PAB) on a hotplate was applied after spin coating to further evaporate the residual solvent trapped in the film and enhance the mechanical strength. The typical PAB condition in this work was 70 °C for 5 minutes. The exposure of resist samples was normally undertaken immediately after the PAB process. Otherwise the samples were stored in a vacuum desiccator and exposed within 24 hours. For most of the CAR samples, a post exposure bake

(PEB) process was needed after the exposure to activate the catalytic reaction, whilst for non-CA samples there was no PEB step. The PEB temperature used in this work varied from 90 °C up to 160°C, for a typical duration of 1 minute. In the subsequent development step, several different organic developers were used including monochlorobenzene (MCB), a mixture of MCB and IPA, cyclohexanone, 2-heptanone and n-butyl acetate (nBA). Resists were dipped in the developer for 20 seconds to 60 seconds and rinsed in IPA before drying with a nitrogen blow.

2.3 Resist Characterization

Resist characterization is based on sensitivity, contrast, resolution and LER (LWR). As introduced in Chapter 1, the sensitivity and contrast is evaluated by measuring the resist film thickness as a function of exposure dose. The resolution and LER (LWR) are normally evaluated by analyzing the SEM images of the lithographic patterns. In the study of the metal containing resists (presented in Chapter 5), imaging and analysis at atomic level resolution were undertaken using an aberration corrected scanning transmission electron microscope (AC-STEM).

2.3.1 Measurement and Analysis Tools

Thickness Measurements

A Dektak^3 ST (Veeco Instrument) surface profiler was used for the film thickness measurements. The profiler uses a contact diamond-tipped stylus to scan on the sample surface and obtains a one-dimensional topography. As a contact force of 1

mg to 10 mg is applied during the scanning, only the films with certain level of rigidity can be measured without being damaged by the stylus. A high vertical resolution down to sub-5 nm can be achieved. In this work the surface profiler was mainly used for measuring the resist film thickness in sample preparation, and the remaining thickness after development in the sensitivity tests.

Resist Pattern Imaging

The XL30 SFEG SEM was used for the majority of resist pattern imaging work. During imaging, a high-resolution mode (with a secondary electron detector) or an ultra-high resolution mode (with a through lens detector) can be selected. An acceleration voltage of 5 kV was typically used here. Profile images of the resist patterns can be obtained by using a tilt sample holder (45° fixed) combined with tilted SEM stage (0° to 45° adjustable). Several resist patterns from the JBX 6300FS EBL system were imaged using an LEO 1530 Gemini SEM (ZEISS) at the University of Leeds immediately after development (to avoid degradation during transportation). For the samples exposed by the ORION PLUS helium ion microscope, the same tool was used for some of the imaging. The energy of the helium ion beam was 30 keV for both patterning and imaging.

Material Characterization using AC-STEM

A JEOL 2100F Scanning Transmission Electron Microscope (STEM) located at the University of Birmingham was used for the characterization of the metal containing fullerene resists. STEM is a type of transmission electron microscope (TEM) with a focused beam scanned over the sample. Equipped with an

aberration corrector, this 200 kV STEM is capable of sub-angstrom resolution. A high-angle annular dark-field (HAADF) detector below the sample captures the high angle, incoherently scattered electrons. As this signal is highly sensitive to the atomic number of the sample material, the HAADF STEM image can provide information of the element and quantity of atoms through the Z-contrast variation. In addition to HAADF image (or DF image for short), a bright field (BF) image is simultaneously taken by collecting the signal from the main beam. A Bruker XFlash 4030 Silicon Drift Detector (SDD) is positioned in the STEM column, enabling a high-resolution energy dispersive X-ray (EDX) mapping for selected sample areas. This, combined with the HADDF images, provides further information of the element type and distribution.

2.3.2 Resist Characterization Methods

2.3.2.1 Compound Characterizations

The chemicals used in this study are from several different suppliers, which will be specified in the Method Sections in the three following chapters. The material synthesis and chemical characterizations during synthesis are not within the scope of this thesis. However, a chromatography method was used after synthesis to separate one early version of fullerene based resist material. Chromatography is a technique for separation of mixed compound. In a typical column chromatography, the mixed compound is placed at one end of a column and a flow of liquid is applied to dissolve the mixture and carry it towards the other end. As various constituents of the mixture travel at different speed, the compounds can be separated.[4] There is another type of planar chromatography in which the

separation takes place on a plane. In this study a column chromatography method was used to separate a fullerene based material. The detail will be presented in Chapter 4.

2.3.2.2 Sensitivity and Contrast

For electron beam sensitivity and contrast evaluation, a set of well-separated squares was patterned in a relatively thick resist layer (typically 30-40 nm) with an increasing electron dose across the array. The size of the square in the pattern was 50 × 50 μm for CARs and 30 × 30 μm for non-CARs. Samples were developed and the film thickness of each square after development was measured using the surface profiler. The film thicknesses were normalized by taking the highest thickness in each case as being equal to 1. For the helium ion beam sensitivity and contrast evaluation, smaller rectangle patterns were used and the thickness was measured by atomic force microscopy (AFM).

The measured film thickness was plotted as a function of dose in the software Kaleidagraph (Synergy Software) and a damped least squares method (Levenberg–Marquardt algorithm) was used to fit a sigmoidal function to the data:[5]

$$y = \frac{1}{(1 + Ax^{-B})} \tag{2.1}$$

As introduced in Chapter 1, the sensitivity for a positive tone resist is the dose required to fully clear the film (D_0), whilst the sensitivity for a negative tone resist, defined as the dose at which 50% of the film is retained (D_{50}), can be derived from the response curve fit as:

$$D_{50} = A^{\frac{1}{B}} \tag{2.2}$$

and contrast, γ, was derived from the fit as:

$$\gamma = \frac{\ln(10)}{4} B \tag{2.3}$$

2.3.2.3 Resolution and Line Edge/Width Roughness

The resist resolution and LER/LWR were evaluated from periodical line-space patterns with varying pitch size. The resist films for resist resolution and LER/LWR measurements were relatively thin (typically 20-30 nm unless otherwise stated) to avoid pattern collapse. Top-down SEM images were analyzed using SuMMIT, an off-line analysis software package from EUV Technology Corporation, for critical dimension (CD) and LER/LWR processing. Figure 2.2 shows the interface of this software. SuMMIT provides a number of user-settable algorisms and parameters in the calibration and filtering, edge detection and LER calculation etc. In this work, SEM images with magnification of 300,000× were typically used for the analysis, giving a pixel size of 1.087 nm. The line edge was determined based on the intensity of the line profile. Several filtering processes were enabled to eliminate SEM noise by performing a high frequency cutoff. The same filtering and edge detection parameters were used throughout. Although the LER/LWR data with and without filtering are both shown in the analysis output, the values presented in this thesis are all filtered values.

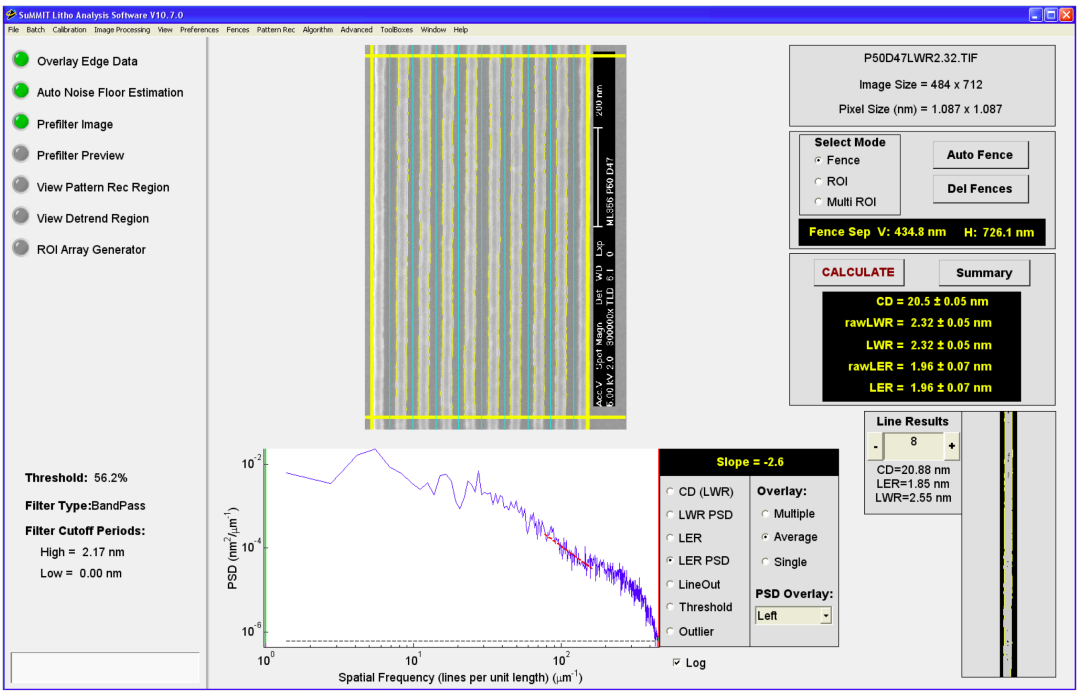

Figure 2.2 Screen capture of the interface of the SuMMIT image analysis software

References

1. McCord, M. A., Rooks, M. J., in Handbook of microlithography, micromachining, and microfabricaiton, Rai-Choudhury, P., editor. Bellingham, WA: *SPIE Press, Vol.1,* 147 (1997)
2. X-Y-Z TYPE EB lithography system CABL-9000C series, Available from: http://www.crestec8.co.jp (Accessed 20/09/2015)
3. JBX-6300FS Electron Beam Lithography System, Available from: http://www.jeolusa.com (Accessed 20/09/2015)
4. Snyder, L. R., Kirkland, J. J., Dolan, J. W., Introduction to modern liquid chromatography. New Jersey: *John Wiley & Sons, 3* (2011)
5. Mack, C.A., Legband, D.A., Jug, S., Data analysis for photolithography. *Microelectron. Eng., 46,* 65 (1999)

CHAPTER 3

POLY(4-HYDROXYSTYRENE) BASED NEGATIVE TONE CHEMICALLY AMPLIFIED RESISTS

3.1 Introduction

With the continuous development of chemically amplified resists (CARs) with stringent resolution requirements, controlling the resolution blur, which is usually caused by acid diffusion, has attracted increasing focus. As introduced in Chapter 1, adding base quenchers can efficiently suppress the acid diffusion. However, this is normally at the cost of reduced resist sensitivity. In addition, for those CARs that are not based on acid catalyzed chain reactions, such as the epoxy resists based on cationic polymerization, base quenchers have limited effect on the resolution enhancement.[1] In this chapter a novel way to control the resolution blur in negative tone CAR systems is presented using the model resist polymer, poly(4-hydroxystyrene) (PHOST) and its protected version, poly(4-*tert*-butoxycarbonyloxystyrene) (PBOCST), as shown in Figure 3.1.

PHOST type polymers have been intensively used as a matrix resist polymer in a variety of experimental and simulation studies due to a number of advantages including good coating properties, solubility in aqueous base developers, high proton generation efficiency, etc.[2-4] Negative tone crosslinkable resists

containing PHOST, PAG and a variety of crosslinkers have been also developed.[2,5,6] Two typical crosslinker systems were used in this study, one was hexamethoxymethylmelamine (HMMM) crosslinker and the other an epoxy novolac crosslinker, CL12-01 (Figure 3.1).

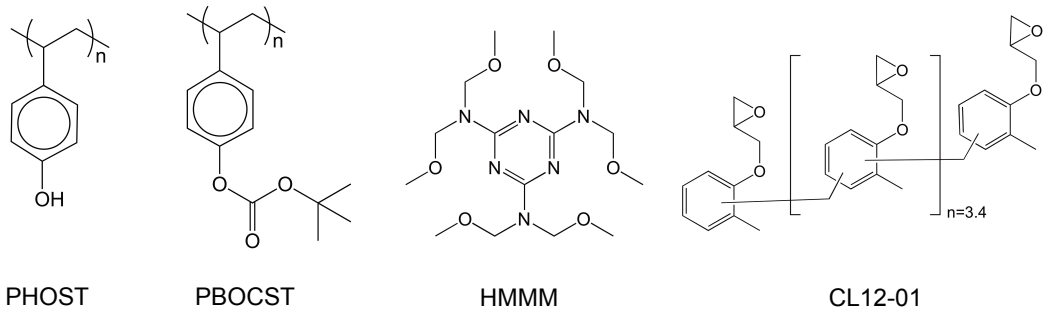

Figure 3.1 Chemical structures of (left to right) poly(4-hydroxystyrene) (PHOST), poly(4-*tert*-butoxycarbonyloxystyrene) (PBOCST), hexamethoxymethylmelamine (HMMM) crosslinker and poly[(phenyl glycidyl ether)-co-formaldehyde] (CL12-01, M_n = 1270)

In the HMMM system, an ether linkage is formed between the hydroxyl group of the PHOST and the HMMM at the presence of photo acid (Figure 3.2 (a)). A PEB temperature at around 110 °C is required to activate the acid catalyzed reaction.[7,8] In the case of PHOST with epoxy crosslinkers, both epoxide homopolymerization and epoxide-alcohol crosslinking (Figure 3.2 (b)) occur with the reaction rate depending on the compound ratio, type of polymer and PAG, temperature, etc.[9,10]

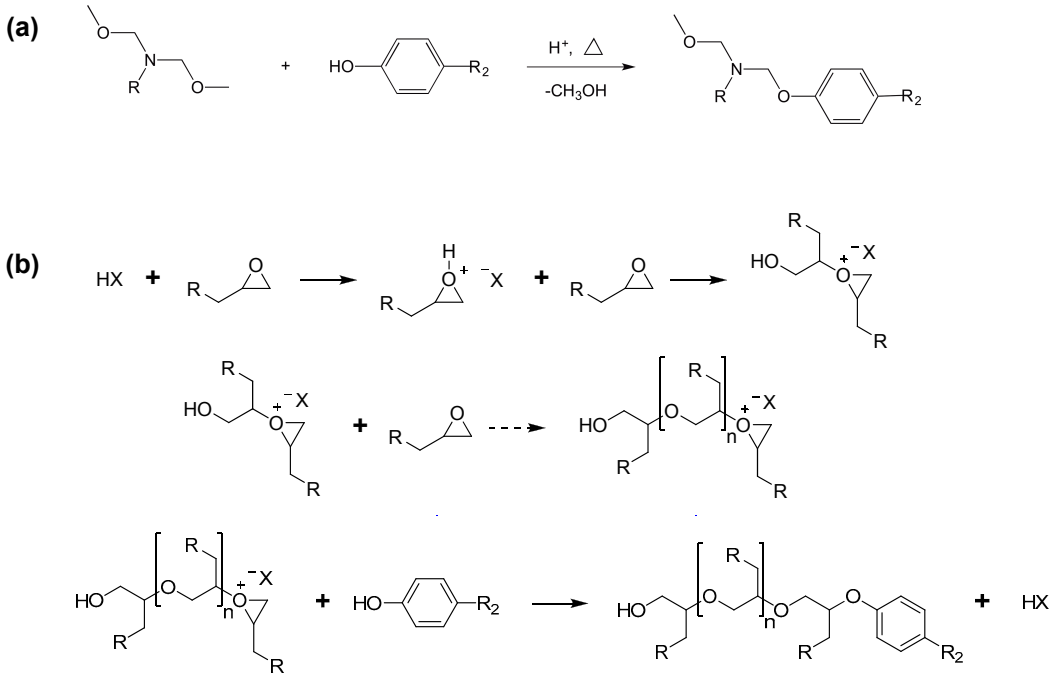

Figure 3.2 (a) mechanism for the acid catalyzed crosslinking between HMMM and phenol; (b) mechanisms of acid catalyzed epoxy homopolymerization and epoxide-alcohol crosslinking

A *tert*-butoxycarbonyl (*t*BOC) protected version, PBOCST, was used in place of the PHOST in the novel variant. Although conventionally being considered as a positive tone resist, PBOCST has been demonstrated here to be a good negative tone crosslinkable resist with lithographic performance exceeding that of PHOST at certain PEB conditions. As the hydroxyl site is blocked by the acid-labile *t*BOC group, a two-step reaction upon exposure is proposed: the PBOCST is deprotected catalytically to create PHOST, then the hydroxyl group in the PHOST reacts with the crosslinkers. This two-step reaction might give better control of the catalytic chain length and provide sharper chemical contrast, which contributes to high resolution. As the reaction in each of the steps has different activation energy, the overall reaction can be controlled by adjusting the PEB conditions.

3.2 Methods

The PHOST and PBOCST polymers (2500 backbone MW.) were synthesized at the Department of Chemistry, University of Warwick. The HMMM crosslinker was purchased from Sigma Aldrich, and CL12-01 crosslinker, poly[(phenyl glycidyl ether)-co-formaldehyde], was purchased from Huntsman Advanced Materials. The PAG used in this study was triphenylsulfonium hexafluoroantimonate from Midori Kagaku Co. The compounds were dissolved and mixed in propylene glycol methyl ether (PGME). Silicon chips with acetone/IPA clean were used as the substrate. A PAB was applied after spin coating. The PAB condition was 70 °C / 1 min for HMMM crosslinker and 70 °C / 5 min for CL12-01 crosslinker, respectively. The resists were exposed using a 20 keV (for sensitivity measurement) and 30 keV (for high-resolution evaluation) electron beam. Various PEB conditions were used in this study. The developer used in this study was a mixture of monochlorobenzene (MCB) and IPA [1:1]. Samples underwent a dip development for 20 s followed by a rinse in IPA for several seconds, and dried with a nitrogen blow.

3.3 Results and Discussion

The lithographic performance of PHOST and PBOCST polymers was evaluated for both the HMMM and epoxy crosslinker systems. First the sensitivity was measured at various PEB temperatures to demonstrate the crosslinking between the PBOCST and crosslinkers. As the activation temperature for the deprotection reaction of PBOCST is ~100 °C, the different behavior between PHOST and

PBOCST around this PEB temperature reflects the effect of the two-step reaction. Then fine line-and-space features were patterned on both materials to evaluate the resolution improvement through the two-step reaction.

3.3.1 HMMM Crosslinker

3.3.1.1 Sensitivity Evaluation

The sensitivity of the three-component resist system with HMMM crosslinker at 20 keV was evaluated. The resist formula was 5:5:1 weight ratio of PHOST/PBOCST, crosslinker and PAG, respectively. This ratio was reported to give an improved sensitivity in the PHOST/HMMM system at high PEB temperature.[7] Various PEB temperatures were applied from no PEB (room temperature of 20 °C) to 140 °C PEB. The response curves and sensitivity values extracted from fitting are shown in Figure 3.3 and Table 3.1, respectively. For the PHOST, exposed patterns started showing up from 90 °C PEB with sensitivity of 51.6 μC/cm^2. Considerable improvement of resist sensitivity was obtained by increasing the PEB temperature to above 120 °C, which corresponds with previous studies reporting an enhancement of crosslinking between PHOST and HMMM with increasing PEB temperature.[11] A layer of residual film was observed at the un-exposed area at 140 °C PEB, possibly due to thermal crosslinking. On the other hand, the PBOCST was not patternable until receiving 120 °C PEB, which gave a sensitivity of 17.3 μC/cm^2. Further increase of the baking temperature to 140 °C improved the sensitivity to 7.8 μC/cm^2.

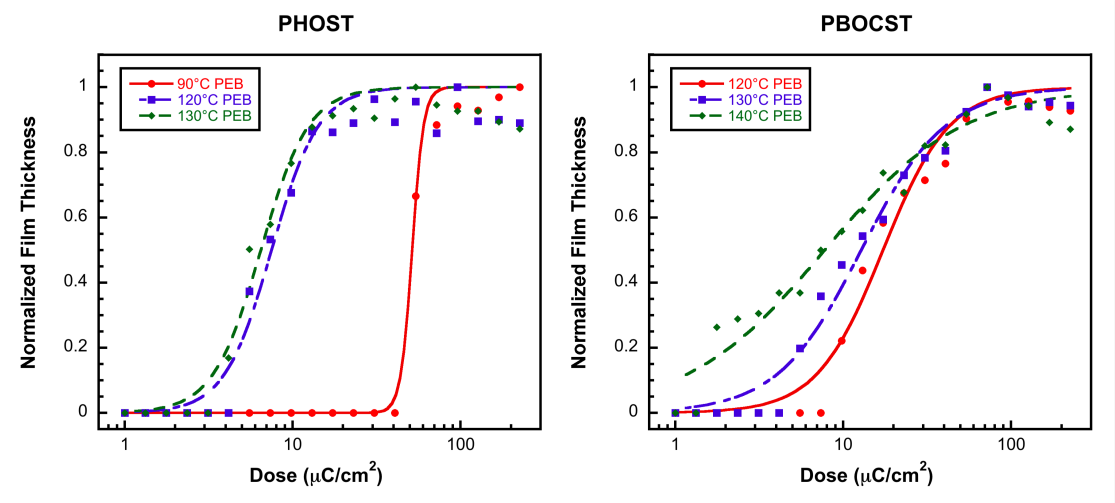

Figure 3.3 Response curves of PHOST (left) and PBOCST (right) with HMMM crosslinker. Various PEB temperatures from no PEB (room temperature of 20 °C) to 140 °C were used for both materials. The PEB duration was 1 minute.

Table 3.1 Sensitivity values for the resist formulate with 5:5:1 compound ratio of PBOCST/PHOST, HMMM crosslinker, and triphenylsulfonium hexafluoroantimonate photo-acid generator, respectively. The PEB duration was 1 minute.

	No PEB	90 °C PEB	120 °C PEB	130 °C PEB	140 °C PEB
PHOST	No Pattern	51.6	7.5	6.5	-
PBOCST	No Pattern	No Pattern	17.3	12.8	7.8

($\mu C/cm^2$)

Since there is no hydroxyl group available in the PBOCST for the expected crosslinking reaction with the HMMM,[7] a two-step reaction consisting of deprotection and subsequent crosslinking is proposed. As an approximate 100 °C PEB temperature is required for the effective deprotection of PBOCST in the presence of acid,[12] there might be insufficient amount of OH groups provided for

the subsequent crosslinking without PEB or with 90 °C PEB. The increase of the baking temperature drove the sensitivity of PBOCST closer to the PHOST resist. However, the sensitivity of PBOCST did not reach the same value of PHOST at any of the tested temperatures, which is hypothesized to be a result of reduced catalytic chain length in the two-step reaction.[13]

As mentioned in Chapter 1, the two-compound resist based on deprotection, consisting of PBOCST and a PAG, can also be converted into a negative tone resist by selecting a proper non-polar organic developer that dissolves the PBOCST readily rather than the deprotected PHOST. However, this possibility can be eliminated since the developer used in this study, MCB and IPA [1:1], is a developer for both PHOST and PBOCST. To confirm this, an additional rinsing test was done. The same PBOCST sample with 130 °C PEB (which had already undergone MCB:IPA development, IPA rinse and nitrogen drying) was chosen and an additional two-minute rinse in aqueous tetramethylammonium hydroxide (TMAH) solution (concentration of 2.5% by weight) after the MCB:IPA development was applied. Figure 3.4 (a) shows the response curves of the sample before and after TMAH rinse. Figure 3.4 (b) shows change in film thickness after the TMAH rinse at various doses. With more than 80% of the resist film retained, this result indicates that the patterned structures were mostly formed by crosslinking rather than polarity change. The exposed film actually showed considerable swelling instead of film loss at low-dose region (<5 $\mu C/cm^2$). It is known that the "loosely" crosslinked network with low molecular weight material trapped at lower doses contributes significantly to the swelling, especially when

using aggressive developers.[14] In the case of PBOCST resist, upon 130 °C PEB, there might be significant amount of deprotected and uncrosslinked material trapped in the network at low doses, which tends to have stronger interaction with the TMAH than MCB:IPA, resulting in the swelling.

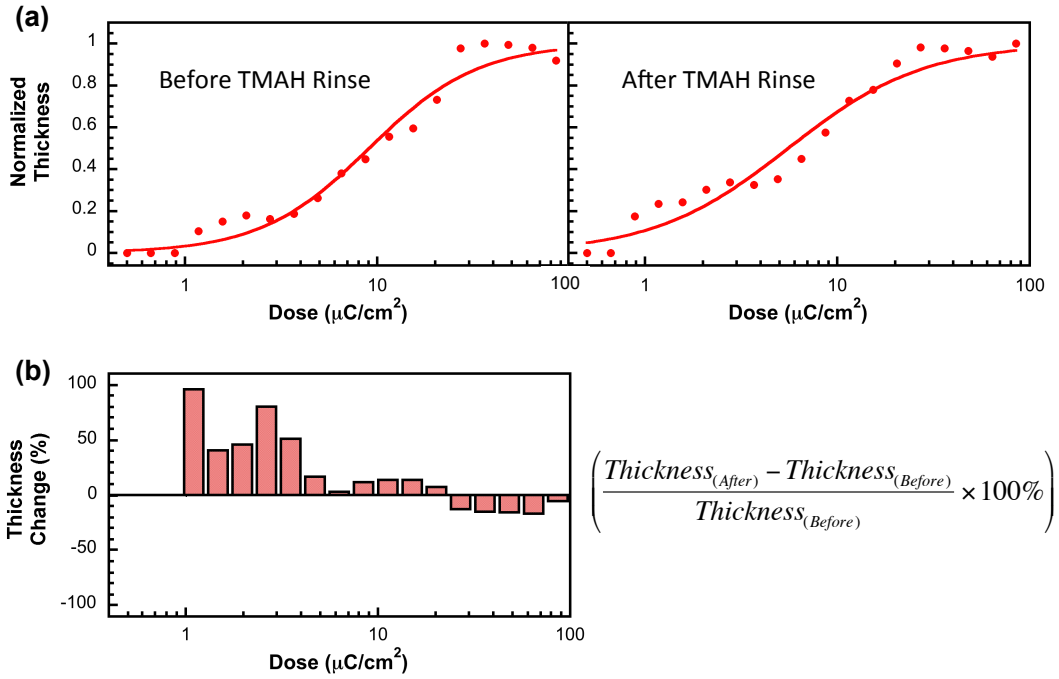

Figure 3.4 (a) Response curves of PBOCST with HMMM crosslinker before (left) and after (right) a post-development rinse in a 2.5% TMAH solution for 2 minutes; (b) The change of film thickness after the TMAH rinse

3.3.1.2 Resolution Evaluation

With a 30 keV electron beam, fine patterns were used to evaluate the resolution and acid diffusion in the resists. The same resist formulation was used, and the PEB condition was 130 °C/1 min. Rectangles of 2 μm width were patterned with a

dose matrix from 10 μC/cm^2 to 320 μC/cm^2. Although considerable diffusion was observed in both materials, the PBOCST resist (Figure 3.5 (b)) had a better control of the CD compared with the PHOST resist (Figure 3.5 (a)). The capability of diffusion control of PBOCST might be due to the shortened catalytic chain length resulting from the two-step reaction, which suppresses the undesired crosslinking at the pattern edges where acid level is low, whilst having less effect in areas with excess acid.

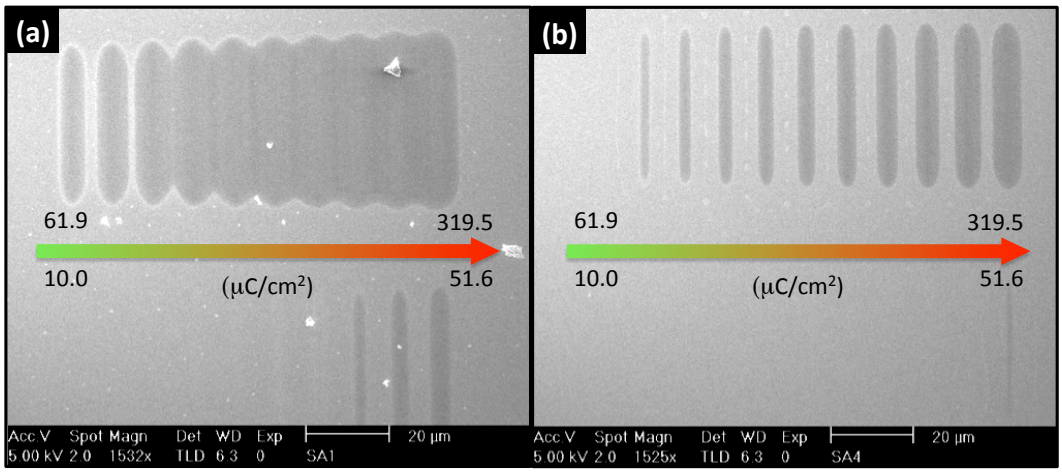

Figure 3.5 SEM images of (a) PHOST and (b) PBOCST resists (5:5:1 compound ratio of PHOST/ PBOCST, HMMM and photo-acid generator, respectively) after 30 keV electron beam exposure. 40 μm × 2 μm rectangles with a dose matrix from 10.0 μC/cm^2 to 319.5 μC/cm^2 were patterned.

For higher resolution patterns, an increased ratio of the hydroxyl group is favored.[7] A ratio consisting of six parts of PBOCST/PHOST, one part of HMMM and one part of PAG has been used with same process conditions. Line patterns with pitch size of 400 nm, 200 nm, 100 nm and 50 nm were used to

evaluate the resolution capability of the two resists. Again the PBOCST shows better diffusion control than the PHOST resist (Figure 3.6 (a) and (b)). None of the tested pitch sizes were resolved in PHOST resist. In contrast, line-and-space patterns with 200 nm and 100 nm pitch were resolved in PBOCST, albeit with high LER as shown in Figure 3.6 (c) and (d), respectively.

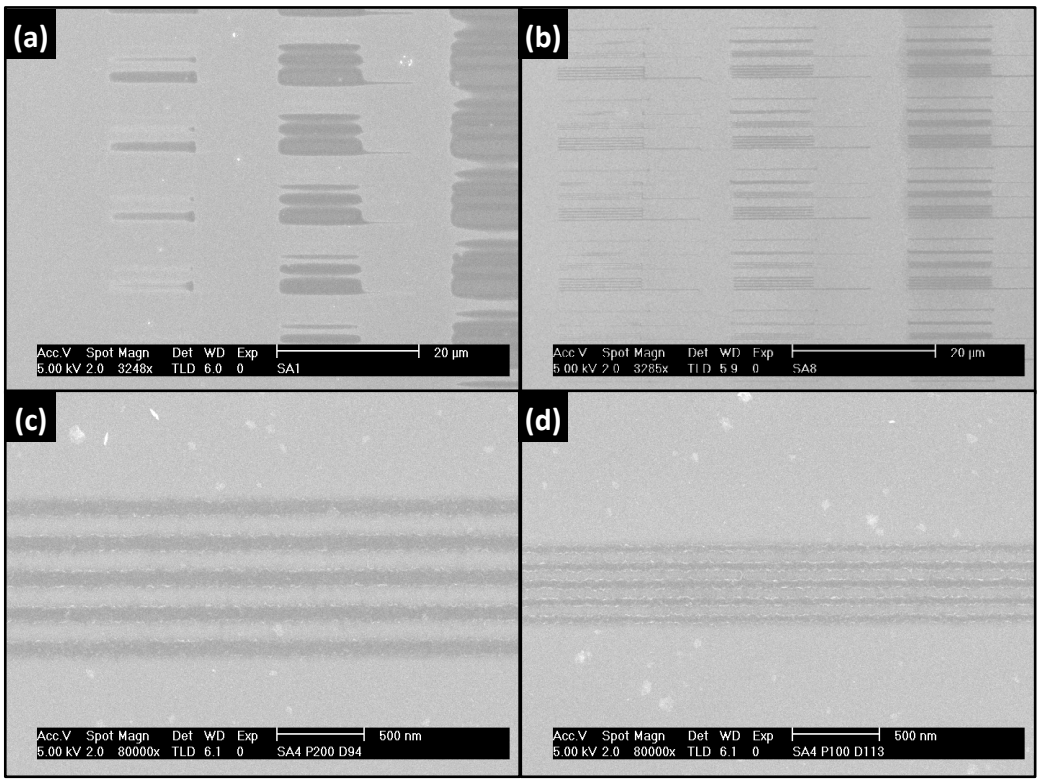

Figure 3.6 SEM images of (a) PHOST and (b) PBOCST resists (6:1:1 compound ratio of PHOST/ PBOCST, HMMM and photo-acid generator, respectively) after 30 keV electron beam exposure. Sparse and dense features of 200 nm, 100 nm, 50 nm and single pixel lines were patterned with various doses; (c) 200 nm pitch lines from (b) with a dose of 94 $\mu C/cm^2$; (d) 100 nm pitch lines from (b) with a dose of 113 $\mu C/cm^2$.

3.3.2 Epoxy Crosslinker

3.3.2.1 Sensitivity Evaluation

The three-component resist system with CL12-01 as crosslinker was formulated to give a ratio of one part PBOCST/PHOST, two parts crosslinker and one part PAG by weight. Due to the additional epoxide homopolymerization reaction, the dependence of resist sensitivity on PEB temperature was different from the resists with HMMM crosslinker. To investigate the role of PBOCST/PHOST in the crosslinking, another control test, in which the PBOCST/PHOST was replaced by same amount of epoxy crosslinker CL12-01 (i.e. three parts of CL12-01 and one part of PAG), has been done for comparison. The response curves of the three resists are shown in Figure 3.7 (a) - (c). The sensitivity values were extracted from fitting (shown in Table 3.2) and plotted against the PEB temperature (shown in Figure 3.7 (d)).

Both of the PBOCST and PHOST resists were patterned even without PEB, and with similar sensitivity. As the sensitivity increased with the PEB temperature, the PHOST reached 7.4 $\mu C/cm^2$ at 130 °C while PBOCST reached 9.6 $\mu C/cm^2$ at 160 °C. Some residual film was observed at the un-exposed area of PHOST at 160 °C PEB, possibly due to thermal crosslinking. In contrast, the reference resist with just epoxy and PAG had a higher sensitivity without PEB and was ~6 $\mu C/cm^2$ at all PEB temperatures.

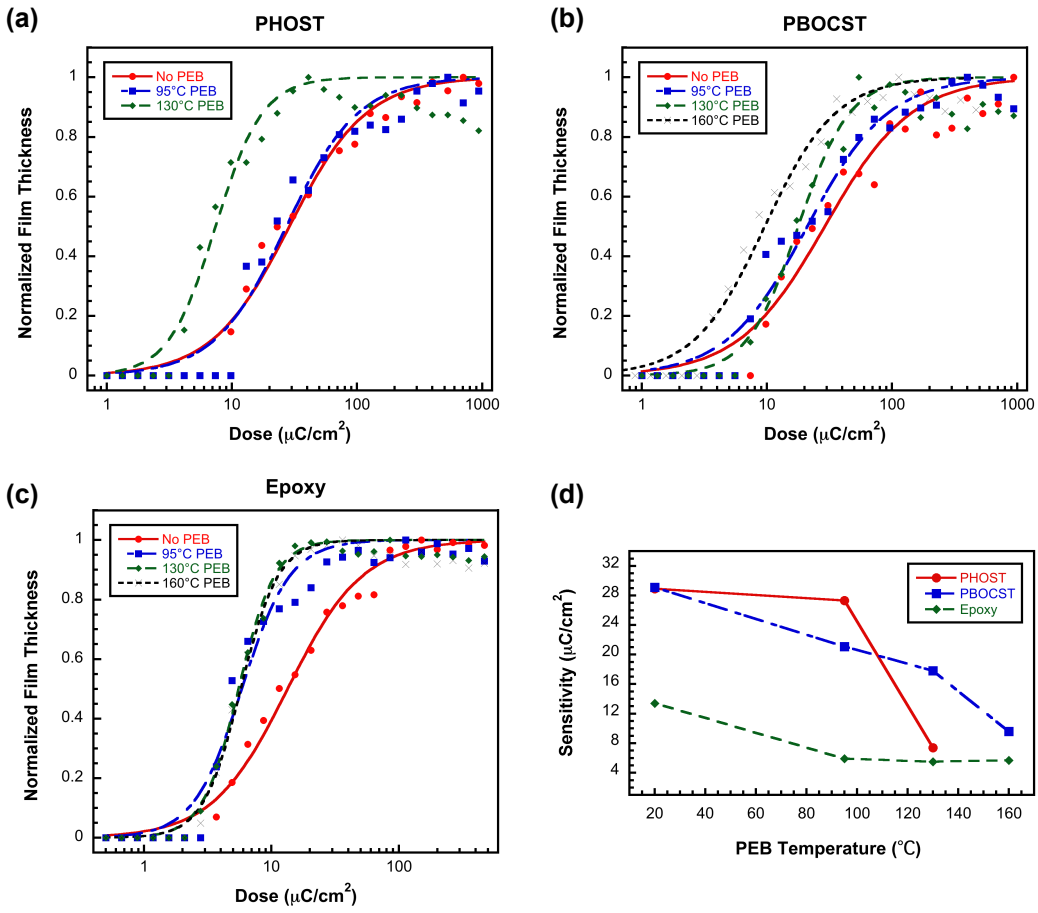

Figure 3.7 Response curves of (a) PHOST resist with epoxy novolac crosslinker; (b) PBOCST resist with epoxy novolac crosslinker; and (c) control group of epoxy novolac crosslinker only. Various PEB temperatures were used. (d) Sensitivity of the three resists against PEB temperatures. The PEB duration was 1 minute.

Table 3.2 Sensitivity values for the resist formulate with 1:2:1 compound ratio of PBOCST/PHOST, CL12-01, and triphenylsulfonium hexafluoroantimonate photo-acid generator, respectively. The PEB duration was 1 minute.

	No PEB	95 °C PEB	130 °C PEB	160 °C PEB
PHOST	28.9	27.3	7.4	-
PBOCST	29.1	21.1	17.8	9.6
Epoxy	13.4	5.9	5.5	5.7

($\mu C/cm^2$)

Clearly, the introduction of PBOCST/PHOST into the epoxy-PAG system reduced the resist sensitivity, which may be caused by an increased glass transition temperature (T_g) and reduced crosslinking density.[9,15] Due to the complexity of crosslinking reactions in the PHOST/epoxy resist system as described in Section 3.1, the exact reaction at various PEB temperatures is difficult to evaluate solely from the lithographic performance. However, PBOCST tends to need a higher PEB temperature to reach similar sensitivity level as PHOST, which might also indicate an extra deprotection step needed prior to crosslinking. Unexpectedly, the sensitivity of PHOST at 95 °C PEB was lower than the PBOCST. The result was repeatable. It is not clear why the sensitivity is reversed in this case.

3.3.2.2 Resolution Evaluation

The resolution capability of PBOCST and PHOST resist with CL12-01 was evaluated using a 30 keV electron beam. 95 °C PEB was applied to both materials. Periodical single-pixel lines were patterned. Figure 3.8 shows SEM images of 60 nm pitch dense lines of the two materials with various doses (according to the sensitivity values presented in last section). The CD was measured and plotted against the line dose (Figure 3.9). Despite some wobbling and collapse of the lines, the PBOCST resist has smaller CD and wider exposure latitude compared with the PHOST resist. The smallest feature size in the 60 nm pitch line pattern was 20.4 nm for the PHOST and 15.9 nm for the PBOCST, respectively. At high doses the PHOST started showing microbridgings, which made the edge detection and CD measurement difficult. Therefore, the CD values for PHOST at dose 191

pC/cm and 216 pC/cm are not shown. The situation became worse in the patterns with smaller pitch of 50 nm in Figure 3.10 and the CD values were not measured due to the pattern collapse and bridging.

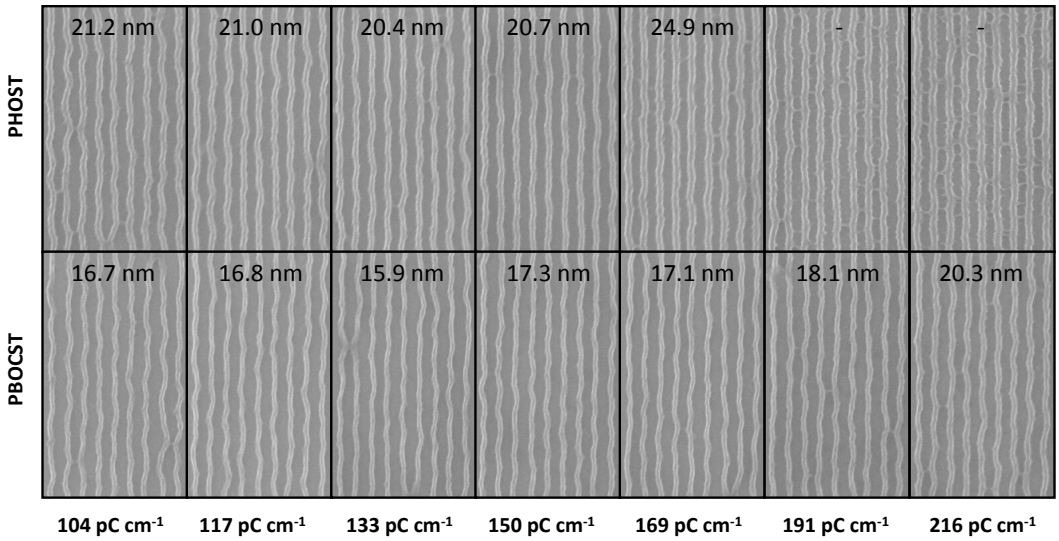

Figure 3.8 SEM images of electron beam exposed 60 nm pitch lines in PHOST (top) and PBOCST (bottom) resists (1:2:1 compound ratio of PHOST/PBOCST, CL12-01 and photo-acid generator, respectively) with various doses. 30 keV electron beam was used for patterning. The critical dimension (CD) values are shown in the individual images.

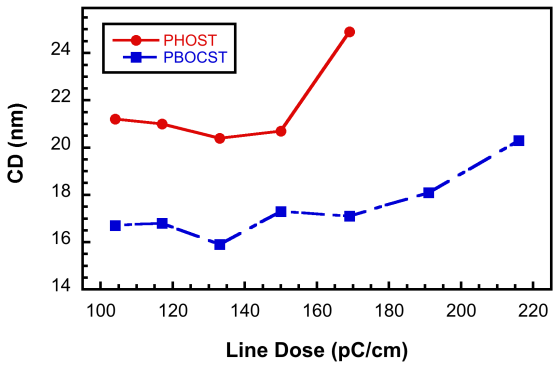

Figure 3.9 The critical dimension (CD) values of 60 nm pitch line patterns measured from Figure 3.8 against line dose.

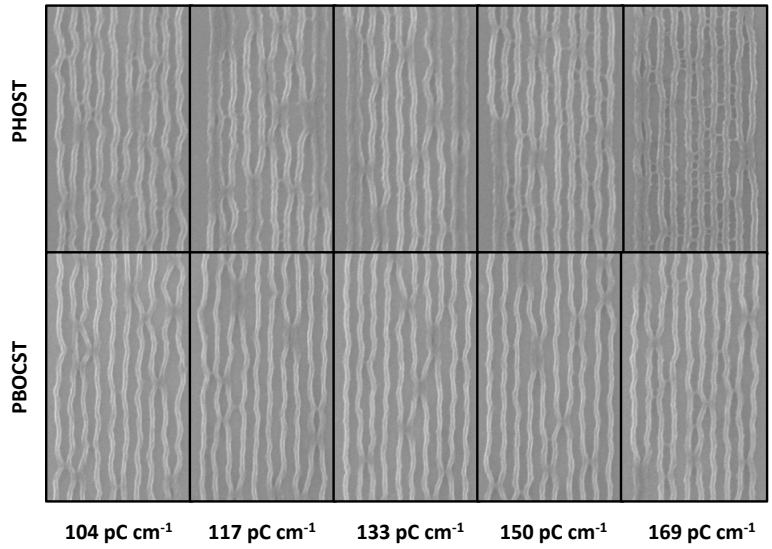

Figure 3.10 SEM images of electron beam exposed 50 nm pitch lines patterned in PHOST (top row) PBOCST (bottom row) resists (1:2:1 compound ratio of PHOST/ PBOCST, CL12-01 and photo-acid generator, respectively) with various doses. 30 keV electron beam was used for patterning.

3.3.2.3 Defocusing Response

The CD broadening of the PBOCST and PHOST resists upon defocusing the electron beam during exposure was evaluated. Compared with the focused beam, the defocused beam has a broader energy profile and lower imaging contrast, resulting in a broadening of resist feature size as well as a larger LER (Figure 3.11). Thus the extent of feature size broadening caused by the beam defocus reflects the resist capability of CD control and exposure latitude.

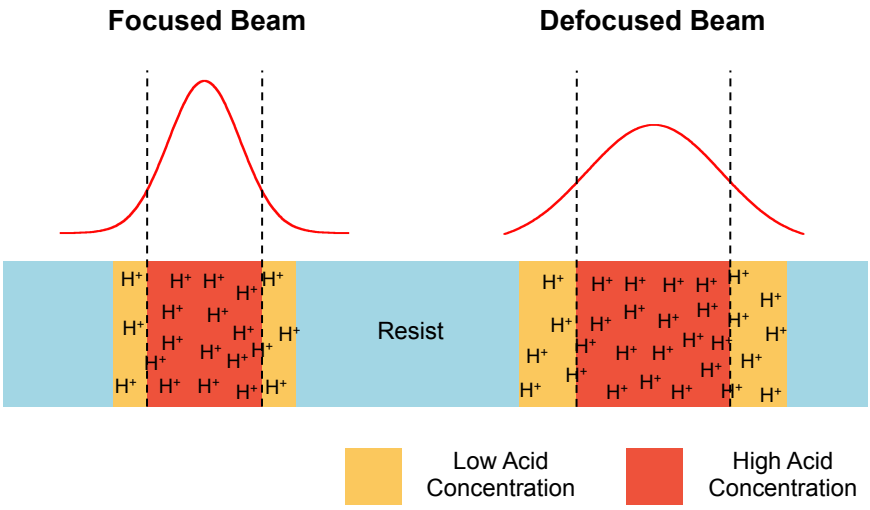

Figure 3.11 Schematic illustration of electron beam profile and corresponding photo-acid concentration in the resist for focused (left) and defocused (right) beams.

Using a 30 keV electron beam, isolated single pixel lines were patterned with various doses. Defocus of the electron beam was done by vertically shifting the focal point from 0 up to 20 μm.[16] The measured CD values against defocus level are plotted in Figure 3.12 (a). In general, the CDs of PBOCST were smaller than the PHOST, which again reveals a higher resolution capability. The data were then fitted linearly at each dose and the slope reflects the extent of CD broadening with beam defocus. The values of the slopes at different doses are shown in Figure 3.12 (b). For line doses from 156 to 490 pC/cm, the fitted rate of CD broadening of the PBOCST is lower than PHOST. The value in PBOCST exceeds the PHOST at the highest dose of 651 pC/cm. However, due to the considerable level of uncertainty indicated by the error bar range (from fitting) in Figure 3.12 (b), the trend seems unclear. Further investigations such as increasing the data points and non-linear fitting methods may be necessary.

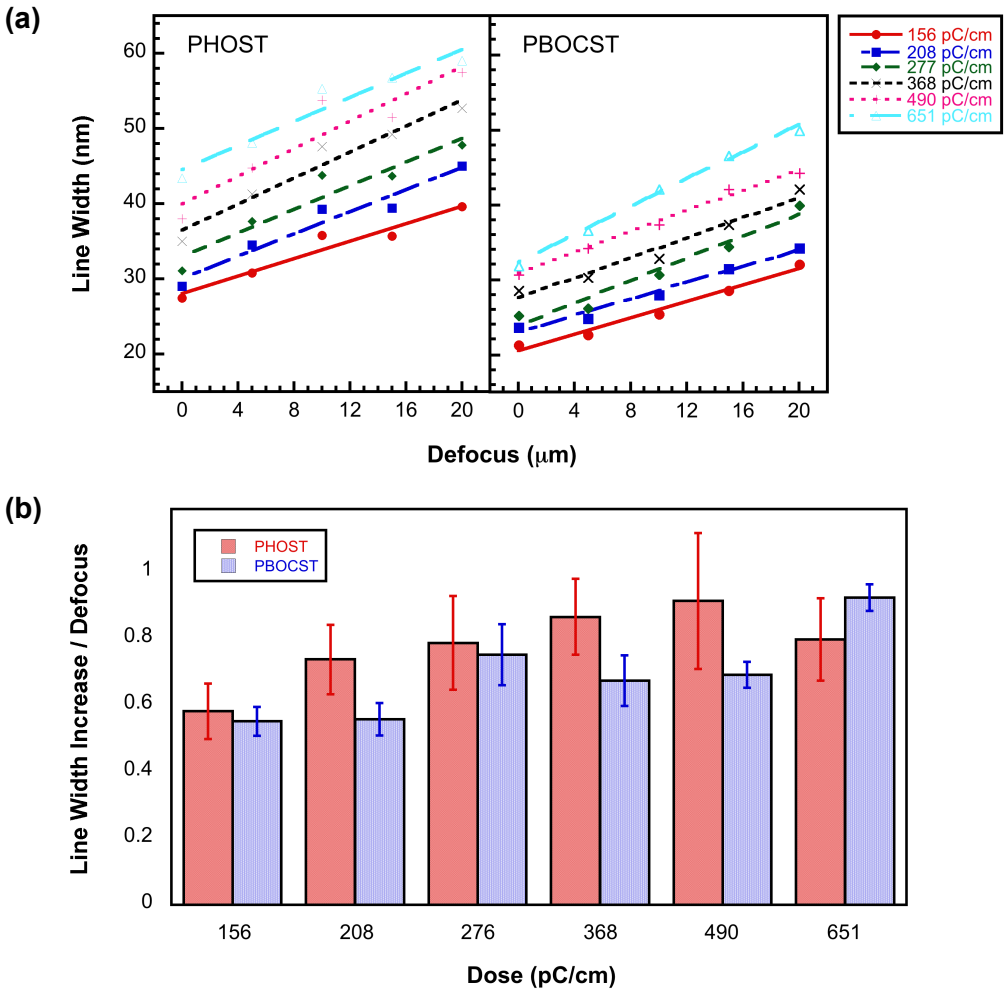

Figure 3.12 (a) The line width variation of the PHOST (left) and PBOCST (right) resists against the defocus level; (b) The fitting values of the slopes in (a) against various doses. Error range from fitting is also shown.

3.4 Conclusions and Future Work

Two model resist polymers, poly(4-hydroxystyrene) (PHOST) and poly(4-tert-butoxycarbonyloxystyrene) (PBOCST), were investigated by mixing the polymer with a crosslinker and a photo-acid generator to form a three-compound negative tone resist. Two types of crosslinkers were tested: hexamethoxymethylmelamine

(HMMM) and an epoxy novolac resin, CL12-01. The HMMM crosslinker system showed considerable acid diffusion and relatively poor resolution (100 nm pitch). The sensitivity of PHOST and PBOCST resist in this system revealed that the crosslinking mechanism of the PBOCST resist might be a two-step reaction including acid-catalyzed deprotection followed by crosslinking. In the resolution test with electron beam exposure, the PBOCST resist showed better diffusion control compared with the PHOST resist. In the epoxy crosslinker system, better resolution down to 60 nm pitch was achieved. The reaction in this system is more complex as there are two possible crosslinking schemes and the mechanism is still unclear. However, the sensitivity change of the PBOCST resist with various PEB temperatures also showed evidence of a similar two-step reaction. Again, higher resolution and improved exposure latitude was observed in the PBOCST resist.

Through demonstrating the feasibility of reactions between PBOCST and crosslinkers, this work presents a novel way to control the catalytic chain reaction by introducing functional group protected materials into crosslinking negative tone resist systems. Based on this work, a family of chemically amplified molecular resists has been developed, which is presented in Chapter 4. It is proposed that the improved CD control comes from the incorporation of a two-step reaction that shortens the catalytic reaction chain length and increases the chemical contrast. Some preliminary comparison between PHOST and PBOCST has been investigated to demonstrate this proposed mechanism from the lithography point of view. However, the exact reaction mechanism is still unclear.

To further investigate the chemistry of the crosslinking, two aspects of future work are suggested:

First, a more systematic comparison of the lithographic performance between PHOST and PBOCST resist is necessary. Due to a limit in the amount of material from the supplier, the PHOST and PBOCST were mixed in a couple of weight ratios and tested in a limited number of PEB conditions in this study. In future work, molecular weight and number of functional groups will need to be taken into consideration due to the molecular weight difference between PBOCST and PHOST. The molecular weight and functional group consideration was taken into account in the following work presented in Chapter 4. More variation in PEB conditions including finer temperature steps and different durations may be applied. In addition, various base polymers and protection groups may be tested and compared as well. Secondly, some other characterization techniques such as infrared (IR) spectroscopy and nuclear magnetic resonance (NMR) spectroscopy may be useful to understand the crosslinking chemistry by tracking the functional groups before, during and after the crosslinking reaction.

References

1. Manyam, J., Novel Resist Materials for Next Generation Lithography, PhD thesis, School of Physics and Astronomy, University of Birmingham, 76 (2010), Available from: http://etheses.bham.ac.uk (Accessed 22/09/2015)
2. Lee, S. M., Frechet, J. M., Willson, C. G., Photocrosslinking of Poly (4-hydroxystyrene) via Electrophilic Aromatic Substitution: Use of Polyfunctional Benzylic Alcohols in the Design of Chemically Amplified Resist Materials with Tunable Sensitivities. *Macromolecules, 27(18),* 5154 (1994)
3. Kozawa, T., Tagawa, S., Side Wall Degradation of Chemically Amplified Resists Based on Poly (4-hydroxystyrene) for Extreme Ultraviolet Lithography. *Jpn. J. Appl. Phys., 47(10R),* 7822 (2008)
4. Lee, C. T., Wang, M., Gonsalves, K. E., Yueh, W., Roberts, J. M., Younkin, T. R., Henderson, C. L., Effect of PAG and matrix structure on PAG acid generation behavior under UV and high-energy radiation exposure. *Proc. SPIE, 6923,* 69232F (2008)
5. Reichmanis, E., Novembre, A. E., Lithographic resist materials chemistry. *Annu. Rev. Mater. Sci, 23(1),* 11 (1993)
6. Argitis, P., et al., Aqueous base developable epoxy resist for high sensitivity electron beam lithography. *Microelectron. Eng., 53(1),* 453 (2000)
7. Thackeray, J. W., Orsula, G. W., Canistro, D., Mcllnay, S. E., DUV ANR photoresists: Resist design considerations. *J. Photopolym. Sci. Tec., 3(3),* 401 (1990)
8. Thackeray, J. W., Orsula, G. W., Rajaratnam, M. M., Sinta, R. F., Herr, D. J., Pavelchek, E. K., Dissolution inhibition mechanism of ANR photoresists: crosslinking vs. -OH site consumption. *Proc. SPIE, 1466,* 39 (1991)
9. Lawson, R. A., Chun, J. S., Neisser, M., Tolbert, L. M., Henderson, C. L., Methods of controlling cross-linking in negative-tone resists. *Proc. SPIE, 9051,* 90510Q (2014)

10. Lawson, R. A., Chun, J. S., Neisser, M., Tolbert, L. M., Henderson, C. L. Positive tone cross-linked resists based on photoacid inhibition of cross linking. *Proc. SPIE, 9051,* 90510E (2014)
11. Lin, Q., Katnani, A. D., Willson, C. G., Effects of crosslinking agent on lithographic performance of negative-tone resists based on poly (p-hydroxystyrene). *Proc. SPIE, 3049,* 974 (1997)
12. Ito, H., Chemical amplification resists for microlithography. *Adv. Polym. Sci., 172,* 53 (2005)
13. McKean, D. R., Schaedeli, U., MacDonald, S. A., Acid photogeneration from sulfonium salts in solid polymer matrices. *J. Polym. Sci. Pol. Chem., 27(12),* 3927 (1989)
14. Olynick, D. L., Ashby, P. D., Lewis, M. D., Jen, T., Lu, H., Liddle, J. A., Chao, W., The link between nanoscale feature development in a negative resist and the Hansen solubility sphere. *J. Polym. Sci. Pol. Phys., 47(21),* 2091 (2009)
15. Chatzichristidi, M., Raptis, I., Diakoumakos, C. D., Glezos, N., Argitis, P., Sanopoulou, M., Strippable aqueous base developable negative photoresist for high aspect ratio micromachining. *Microelectron. Eng., 61,* 729 (2002)
16. Manyam, J., Manickam, M., Preece, J. A., Palmer, R. E., Robinson, A. P., Characterization of the effects of base additives on a fullerene chemically amplified resist. *Proc. SPIE, 7639,* 76391N (2010)

CHAPTER 4

HIGH RESOLUTION CHEMICALLY AMPLIFIED MOLECULAR RESISTS FOR ELECTRON BEAM LITHOGRAPHY

4.1 Introduction

With EBL attracting increasing interest for potential volume production, the importance of developing a high-performance electron beam resist has recently risen. Due to the low throughput of EBL, even for newly developed multi-beam tools, the sensitivity of the electron beam resist is one of the most important factors. According to the ITRS, the sensitivity requirements of electron beam resists have been set to be 50-60 $\mu C/cm^2$ for high voltage electron beam (50-100 keV) and 30-60 $\mu C/cm^2$ for low voltage electron beam (1-5 keV) based on shot noise considerations.[1] Therefore, improving the sensitivity while maintaining high resolution and low LER/LWR is a primary target in developing new electron beam resists.

Among currently available electron beam resists, positive tone resists have been most commonly used for sub-20 nm resolution. A typical example is PMMA, which has shown sub-10 nm resolution using 30 keV electrons with low temperature development (4 °C),[2] and sub-5 nm resolution using 80 keV electrons with ultrasonically assisted development.[3] However, the electron beam

sensitivity of PMMA is relatively low (typically 500 μC/cm^2).[4] Another well-known resist, ZEP (Nippon Zeon) has a similar resolution to PMMA with an improved sensitivity. Dense features with 40 nm half-pitch were achieved using 5 keV electrons with a low dose of 2.6 μC/cm^2.[5] Higher resolution features with 12 nm half-pitch were obtained at 25 keV with a much higher dose of 300 μC/cm^2.[6]

The scenario is worse for negative tone resists – with fast resists typically having poor resolution whilst high-resolution resists have low sensitivity. SU-8 (MicroChem) and AZnLOF 2020 (AZ Electronic Materials) are two commercial negative tone resists with excellent sensitivity (sub-10 μC/cm^2 for SU-8 at 50 keV and sub-30 μC/cm^2 for AZnLOF 2020 at 100 keV). However, the smallest dense features reported for SU-8 and AZnLOF 2020 were 70 nm half-pitch and 50 nm half-pitch, respectively.[7-9] In contrast, hydrogen silsesquioxane (HSQ) has been reported to achieve sub-5 nm half-pitch dense lines with 10 keV electron beam, which is amongst the best resolution of any other resist to date.[10] However, patterning with HSQ requires an extremely high dose (line dose of 5000 pC/cm at 10 keV; area dose above 2500 μC/cm^2 at 100 keV).[10,11]

Recently a number of newly developed negative tone resists have shown an improved combination of sensitivity and resolution. An epoxy based crosslinking CAR, referred to as 2-Ep, has shown 25 nm half-pitch resolution with 38 μC/cm^2 sensitivity at 100 keV.[8] A number of novel non-CA resists have also shown promising performance, such as an organic copolymer, MAPDST–MMA (20 nm semi-dense features and 2.06 μC/cm^2 sensitivity at 20 keV)[12] and an inorganic

metal oxide resist (12 nm half-pitch resolution with medium sensitivity at 30 keV).[13]

In this work a new family of high-performance negative tone CARs has been designed by applying the "two-step" concept (introduced in Chapter 3) to a molecular resist. CAR materials based on small molecules rather than traditional large polymers have been reported to show potential for higher resolution and lower LER/LWR.[4,14] Depending on the resist material type and characterization, this work can be divided into three parts. First, a family of phenol-based fullerene resists, IM-MFPT, was developed, which showed good industrial compatibility (developable in appropriate solvents), high resolution (18 nm half-pitch) and good sensitivity (sub-50 $\mu C/cm^2$). In the second stage, the mixed fullerene compounds were purified by chromatography and an evaluation of the lithographic performance of the various components was undertaken. Finally, based on these results a non-fullerene based resist named IM-xMT, was developed with improved sensitivity and resolution capability.

A study on the extreme ultraviolet (EUV) performance of these resists has been carried out simultaneously with EBL work (by Dr. Andreas Frommhold of the University of Birmingham). Therefore some of the resist formulations and experimental conditions were also optimized according to the EUV results.

4.2 Methods

The fullerene derivatives were synthesized at Nano-C (USA) and shipped to the University of Birmingham, UK. The crosslinkers were purchased from Sigma Aldrich (UK) and Huntsman Advanced Materials (USA). The PAG used in this study was triphenylsulfonium hexafluoroantimonate from Midori Kagaku Co. (Japan). There were also two nucleophilic additives, triphenylsulfonium nonaflate and triphenylsulfonium tosylate, which were purchased from Sigma Aldrich and Midori Kagaku Co., respectively. The compounds were dissolved and mixed in propylene glycol methyl ether (PGME) or ethyl lactate. Silicon chips with an acetone/IPA clean were used as the substrate unless otherwise specified. The post-application bake (PAB) condition was 75 °C / 5 min and the post-exposure bake condition was 90 °C / 2 min unless otherwise specified.

For the samples exposed by the XL30 SFEG SEM (20 kV and 30 kV) at the University of Birmingham (UK), the sample preparation, exposure and development was carried out at the same place. For the samples exposed by the CABL 9510C EBL system (50 kV) at Fundacio Institut de Ciencies Fotoniques (ICFO, Spain), the formulated resist solution was shipped to Spain for spin coating, exposure and development. For the samples exposed by the JBX 6300FS EBL system (100 kV) at the University of Leeds (UK), the samples were spin coated in Birmingham, and then taken to Leeds for exposure and development.

4.3 Results and Discussion

4.3.1 Fullerene Based Resist I

A family of fullerene based CARs consisting of a methanofullerene derivative, epoxy crosslinker, CL12-01 (Huntsman Advanced Materials), and PAG, is presented (Figure 4.1).[4] Three fullerene derivatives were synthesized, including a phenolic methanofullerene, MFP-03, a tBOC protected phenolic fullerene, MFPT-02, and another longer side chain version, MFPT-08. The corresponding three-compound CARs containing MFP-03, MFPT-02 and MFPT-08 are named as IM-MFP-03, IM-MFPT-02 and IM-MFPT-08, respectively. Apart from the targeted fullerene compounds, other synthesis impurities were identified in later studies, which will be discussed in sections 4.3.2 and 4.3.3.

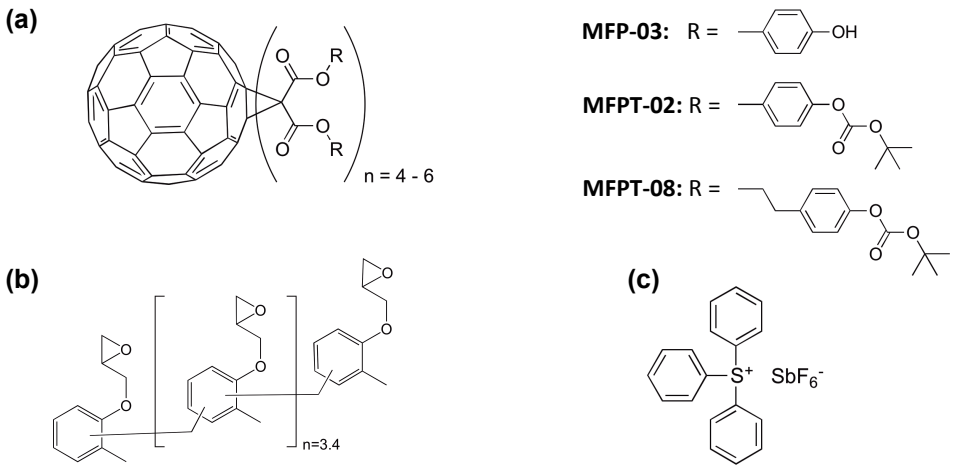

Figure 4.1 Chemical structures of (a) MFP-03: a phenolic malonate C_{60}; MFPT-02: a tert-butoxycarbonyl (tBOC) protected phenolic malonate C_{60}; and MFPT-08: a tBOC protected propyl phenolic malonate C_{60}, (b) epoxy crosslinker CL12-01: poly[(phenyl glycidyl ether)-co-formaldehyde] (M_n = 1270), and (c) triphenylsulfonium hexafluoroantimonate photoacid generator, adopted from reference [4]

4.3.1.1 Varying the Fullerene Derivative

First, the sensitivity and contrast of the fullerene resists at 20 keV were evaluated. The resist formula (dissolved in PGME) was 1:2:1 weight ratio of fullerene derivative, CL12-01 and PAG, respectively. The compound ratio was optimized through a linear regression analysis of data generated in the EUV resist project. The samples were exposed and developed for 20 seconds in MCB:IPA [1:1]. The response curve of the three resists and sensitivity/contrast values extracted from fitting are shown in Figure 4.2 and Table 4.1, respectively. A comparison between the values from IM-MFP-03 and IM-MFPT-02 shows that the protection of the phenol group in the fullerene derivative causes a reduced sensitivity but an improved contrast. However, the propyl chain version, MFPT-08 has a significantly higher sensitivity over the short chain version, MFPT-02. The sensitivity enhancement of MFPT-08 might be due to the higher flexibility of the long propyl side chain, which may help to reduce steric hindrance and enhance the extent of crosslinking.[15,16]

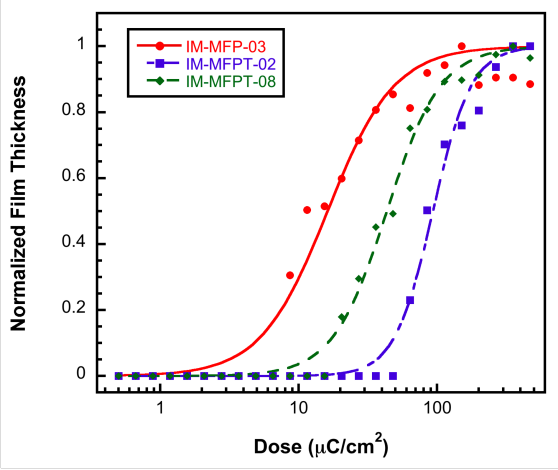

Figure 4.2 Response curves of IM-MFP-03, IM-MFPT-02 and IM-MFPT-08. Samples were developed in MCB-IPA [1:1]

Table 4.1 Sensitivity and contrast values for the IM-MFP-03, IM-MFPT-02 and IM-MFPT-08 at 20 keV. Samples were developed in MCB-IPA [1:1]

	IM-MFP-03	IM-MFPT-02	IM-MFPT-08
Sensitivity	32 μC/cm^2	93 μC/cm^2	43 μC/cm^2
Contrast	1.0	1.8	1.3

The resolution of the resists was evaluated through patterning of single pixel lines at various pitches using 30 keV electron beam. Isolated lines and dense lines at 50 nm pitch were pattered on the IM-MFP-03, IM-MFPT-02 and IM-MFPT-08 with various doses. SEM images of the patterns are shown in Figure 4.3. IM-MFP-03 required the lowest dose of the three resists (200 pC/cm). However, the lines had high roughness and showed considerable bridging in the dense patterns. Significant residuals were observed in the unexposed areas, which might be due to impurities in the resist or undesired crosslinking. The IM-MFPT-02 sample had relatively smoother lines with a clear background. However, the required dose was very high (over 1000 pC/cm) and the dense features were prone to collapse. IM-MFPT-08 demonstrated the best combination of dose and resolution. Sub-14 nm sparse line and ~20 nm lines on a 50 nm pitch were achieved with line doses of 350 pC/cm and 240 pC/cm, respectively. Thus, MFPT-08 based fullerene derivatives were used in most of the subsequent electron beam and EUV tests.

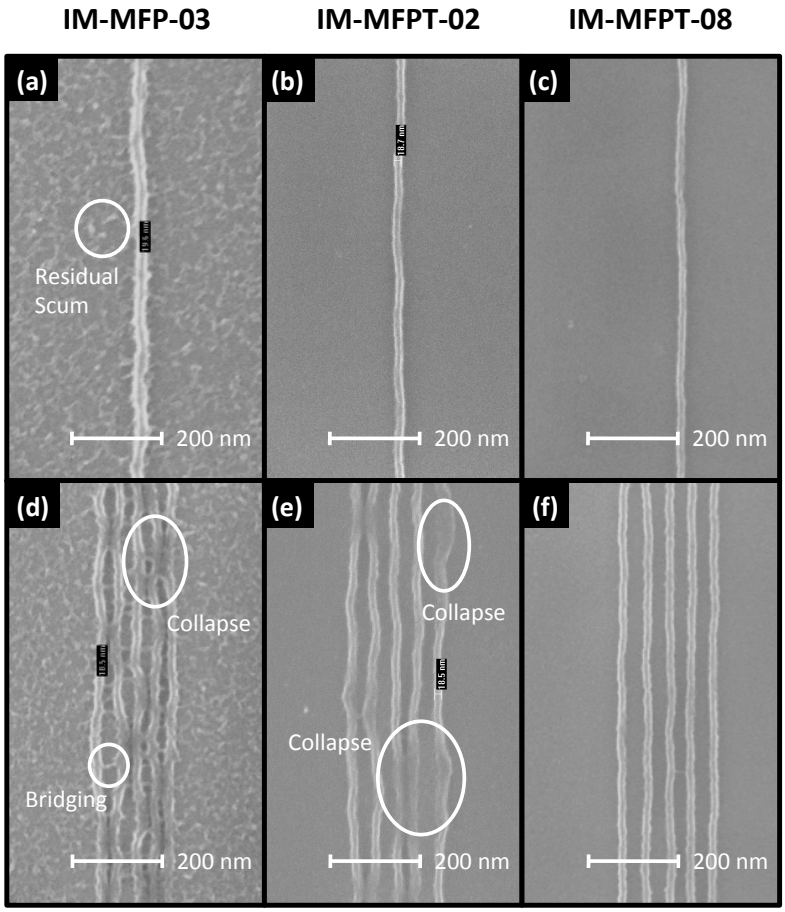

Figure 4.3 SEM images of sparse features and dense features at 50 nm pitch on IM-MFP-03, IM-MFPT-02 and IM-MFPT-08. Doses for sparse features are: (a) 200 pC/cm, (b) 1670 pC/cm and (c) 350 pC/cm. Doses for dense features are: (d) 200 pC/cm, (e) 1520 pC/cm and (f) 240 pC/cm

4.3.1.2 Developers and Development Conditions

In the IC industry, non-halogenated developers are usually preferred, due to considerations of environmental contamination, and worker safety. Apart from the MCB-IPA developer (halogenated), several industrial acceptable non-halogenated developers, including cyclohexanone, 2-heptanone and n-butyl acetate (nBA), were tested with IM-MFPT-08. The resist sensitivity at 20 keV with the three developers was measured and compared with the MCB-IPA developer. The

response curves and sensitivity/contrast values extracted from fitting are shown in Figure 4.4 and Table 4.2, respectively. No significant sensitivity or contrast variation was observed in the four developers.

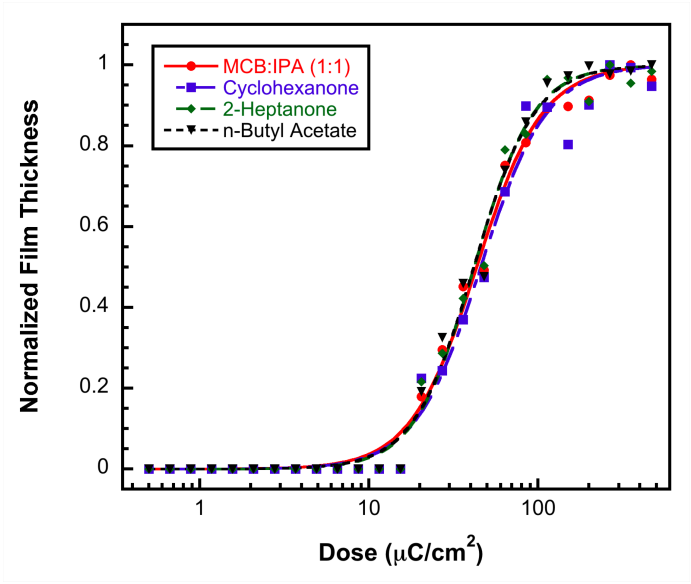

Figure 4.4 Response curves of IM- MFPT-08 resist at 20 keV, developed in MCB-IPA [1:1], cyclohexanone, 2-heptanone, and n-butyl acetate

Table 4.2 Sensitivity and contrast values for the IM-MFPT-08 resist developed in MCB-IPA [1:1], cyclohexanone, 2-heptanone, and n-butyl acetate

	MCB-IPA [1:1]	Cyclohexanone	2-Heptanone	n-Butyl Acetate
Sensitivity	43 μC/cm²	46 μC/cm²	42 μC/cm²	42 μC/cm²
Contrast	1.3	1.3	1.4	1.4

The resolution of IM-MFPT-08 with various developers was evaluated using 30 keV electron beam. Resist films with thickness of 30 nm were prepared. Isolated lines and dense lines on a 50 nm pitch were exposed and developed in MCB-IPA, cyclohexanone, 2-heptanone and nBA. The SEM images of the patterns, and the measured CD and LWR are shown in Figure 4.5 and Table 4.3, respectively.

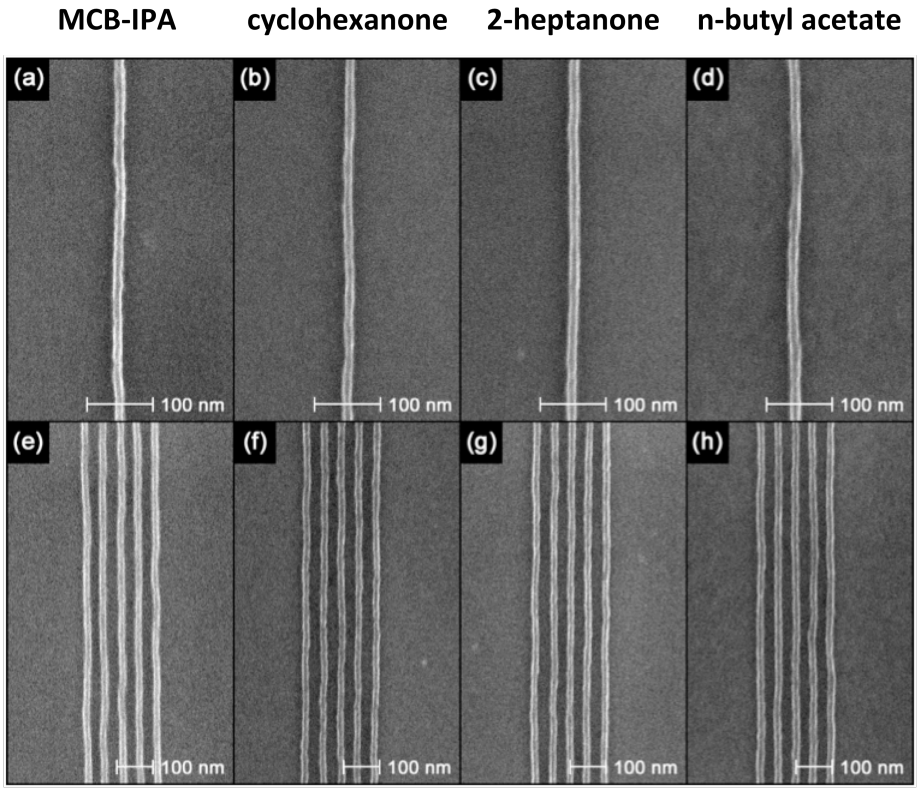

Figure 4.5 SEM images of patterns in IM-MFPT-08 developed with (from left to right) MCB–IPA [1:1], cyclohexanone, 2-heptanone, or n-butyl acetate. The doses for isolated features are: (a) 350 pC/cm, (b) 260 pC/cm, (c) 350 pC/cm, and (d) 350 pC/cm. The doses for dense features are: (e) 240 pC/cm, (f) 260 pC/cm, (g) 290 pC/cm, and (h) 350 pC/cm. Adopted from reference [4]

Table 4.3 Line width and line width roughness (LWR) values for the IM-MFPT-08 resist developed in MCB-IPA [1:1], cyclohexanone, 2-heptanone, and n-butyl acetate, adopted from reference [4]

Developer	Isolated line Linewidth (nm)	Isolated line LWR 3σ (nm)	Dense lines Linewidth (nm)	Dense lines LWR 3σ (nm)
MCB-IPA [1:1]	13.9	2.6	18.3 ± 0.1	3.8 ± 0.1
Cyclohexanone	13.6	3.5	17.0 ± 0.1	4.1 ± 0.2
2-Heptanone	14.6	2.6	17.1 ± 0.1	4.0 ± 0.1
n-Butyl Acetate	14.4	3.8	18.3 ± 0.1	5.1 ± 0.4

All of the fine features were clearly resolved with line doses between 240 and 350 pC/cm. Sub-15 nm isolated features and sub-20 nm lines on a 50 nm pitch were achieved with low LWR. The variation in the values of line width and LWR for the four samples was within 2 nm, demonstrating reasonably good compatibility with industrial friendly organic developers. Among the four samples, the one developed in cyclohexanone gave the best resolution with a relatively large LWR. A solubility test revealed that the fullerene compound was soluble in all the four developers at concentrations in excess of 100 g/L; whilst the solubility of the crosslinker, CL12-01, was ~80 g/L in MCB-IPA [1:1], >100 g/L in cyclohexanone, ~50 g/L in 2-heptanone and ~30 g/L in nBA. The higher solubility of epoxy crosslinker in cyclohexanone might be responsible for the higher resolution and reduced pattern quality of the cyclohexanone sample as reported elsewhere.[17]

In addition to room temperature immersion development, another two frequently used techniques, hot development[18,19] and ultra-sonic assisted development,[19] were also investigated. Single pixel lines were patterned on the IM-MFPT-08 and developed in cyclohexanone. A developer temperature of 40 °C was used in the hot developer test. No significant improvement in line quality was achieved. Moreover, considerable post development residues were observed in the unexposed areas. The same pattern was exposed on another sample followed by a 30-second ultra-sonic assisted development (room temperature). Again, no significant improvement was observed.

4.3.1.3 Post-exposure Baking Conditions

Similar to the PBOCST study (Chapter 2), the sensitivity of IM-MFPT-08 resist with different PEB conditions was evaluated. Various PEB temperatures from room temperature of 20 °C (no PEB) to 150 °C were applied with duration of 2 minutes. The response curves are shown in Figure 4.6 (a) and the fitted sensitivity as a function of PEB temperature is plotted in Figure 4.6 (b). In contrast with the PBOCST results, no sensitivity trend was observed with increasing PEB temperature. The reason for this relationship is still under investigation but we speculate a more complex interaction between the fullerene derivative and the epoxy crosslinker.

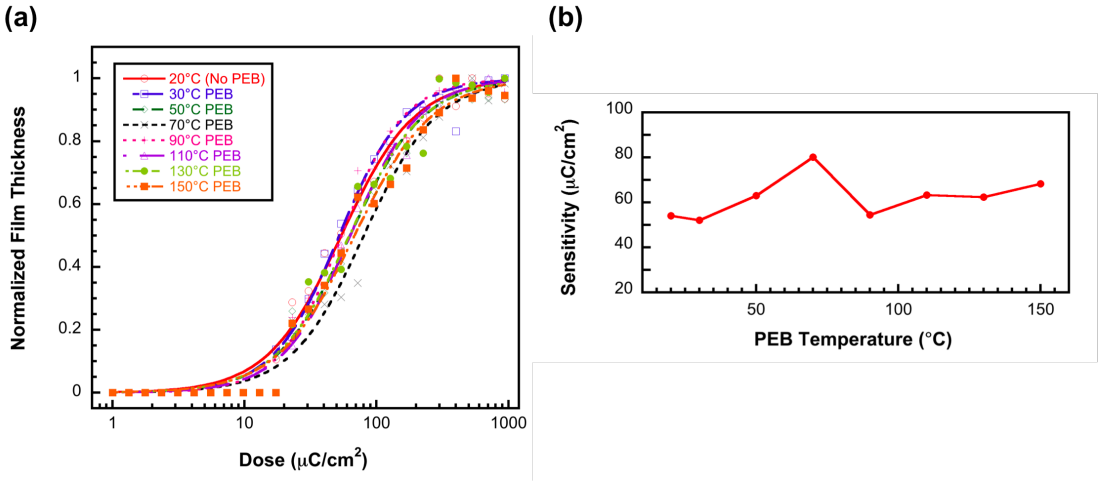

Figure 4.6 Response curves of IM-MFPT-08 with post-exposure bake (PEB) temperatures varying from 20°C to 150°C; (b) Sensitivity values from (a) against PEB temperature

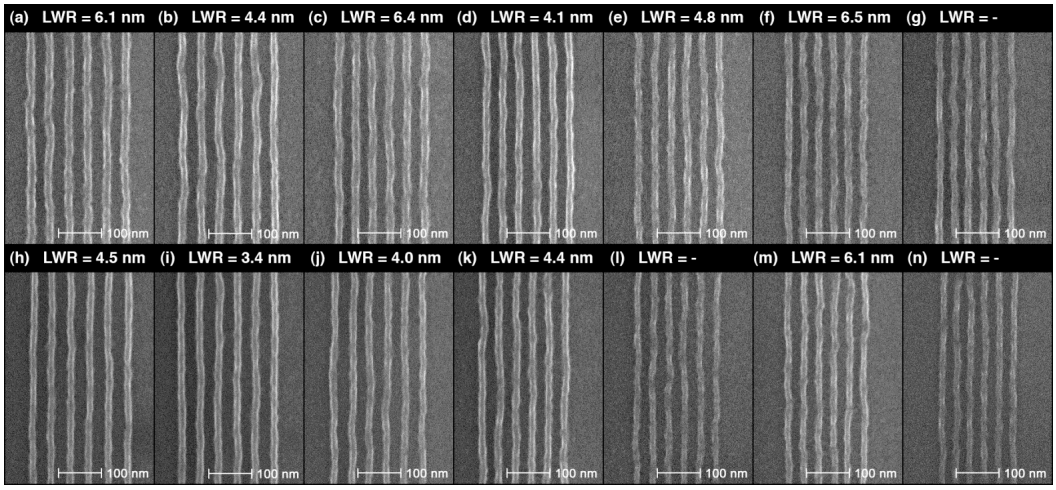

Figure 4.7 SEM images of single pixel lines written at decreasing pitches in IM-MFPT-08, without PEB (top; a–g) and with 90 °C, 1 min PEB (bottom; h–n) and, in both cases, developed in MCB–IPA [1:1]. The pitches are (from left to right) 48 nm, 46 nm, 44 nm, 42 nm, 40 nm, 38 nm, and 36 nm. Adopted from reference [4]

Dense features at pitches from 48 nm to 36 nm were patterned without PEB and with 90 °C / 1 minute PEB. Thin resist films of 20-25 nm were used in this test to avoid pattern collapse, and MCB-IPA was used as the developer. Figure 4.7 shows the SEM images of the line patterns with the measured LWR values. All of the patterns were clearly resolved. LWR was higher compared to the samples with thicker films, i.e. the samples used to test various fullerene derivatives and developers. The line dose for the sample without PEB (240-350 pC/cm) was slightly higher than the one with 90 °C / 1 minute PEB (230-300 pC/cm). LWR measurement showed that, the samples with PEB had lower LWR than those without PEB at pitch size above 42 nm. However, at 42 nm pitch and below, both two groups reached a similar LWR. The PEB process is known to help smoothen the pattern edges through an enhancement of acid diffusion.[20] On the other hand, increased acid diffusion can be disadvantageous at small pitches.[21] It was also reported that with smaller pitches, the exposure latitude tends to decrease, thus making the line width and LER/LWR more difficult to control.[22] Therefore, at the pitch size below 42 nm, the effect of LWR improvement due to the PEB process was negligible.

4.3.1.4 Combinations of the Fullerene Derivatives

Although the other two fullerene resists were either high-sensitivity but low-resolution (IM-MFP-03), or low-sensitivity with good resolution (IM-MFPT-02), a mixture of these two materials was found to have very high resolution capability with medium sensitivity. While keeping the 1:2:1 compound ratio of the fullerene derivative, CL12-01 and PAG, the fullerene part was changed to a mixture of

MFPT-02 (75 %wt.) and MFP-03 (25 %wt.). Single pixel dense lines at 32 nm and 30 nm pitch were successfully resolved with line doses of 527 pC/cm and 478 pC/cm, respectively (Figure 4.8). Due to the strong proximity effect at such a small pitch size, the feature roughness was relatively high. However, no obvious bridging or pattern collapse was observed in the dense lines. The high-resolution capability of this mixed material indicates that using a partially deprotected tBOC material in this resist system might be an option to tune and optimize the overall resist performance.

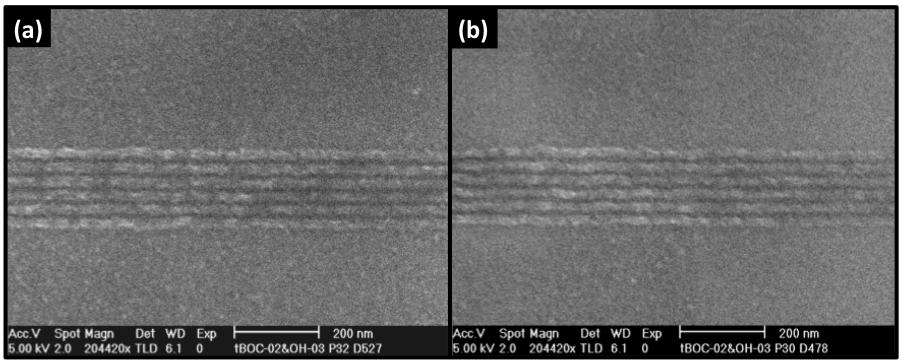

Figure 4.8 SEM images of dense lines on (a) 32 nm, and (b) 30 nm pitches in a mixed MFP-03 and MFPT-02 [1:3] CAR, adopted from reference [4]

4.3.2 Fullerene Based Resist II

In order to further analyze the MFPT-08 material and improve the lithographic performance, another scaled batch of this material was purified and separated with chromatography using silica gel. Two cuts were separated using different eluents. The first cut, MFPT-08B, was the material that came through the column with the eluent dichloromethane (DCM) / ethyl acetate (EtOAc) [1:1]. The second cut,

MFPT-08C, represented residual materials in the column from the first cut that could subsequently be washed through with the eluent DCM / EtOAc / methanol (MeOH) [2:2:1]. Chemical characterizations using mass spectroscopy and nuclear magnetic resonance (NMR) spectroscopy revealed that MFPT-08B contains the majority of the targeted fullerene compounds with adduct number between 4 and 6; and MFPT-08C has small amount of low adduct fullerene compounds (mainly bis-adduct derivatives) with other impurities which will be further discussed in Section 4.3.3. The assumed scheme of the separation is shown in Figure 4.9. The lithographic properties of MFPT-08B, MFPT-08C and blends of the two with various ratios were evaluated. Again, the corresponding three-compound CARs containing MFPT-08B and MFPT-08C are named as IM-MFPT-08B and IM-MFPT-08C, respectively.

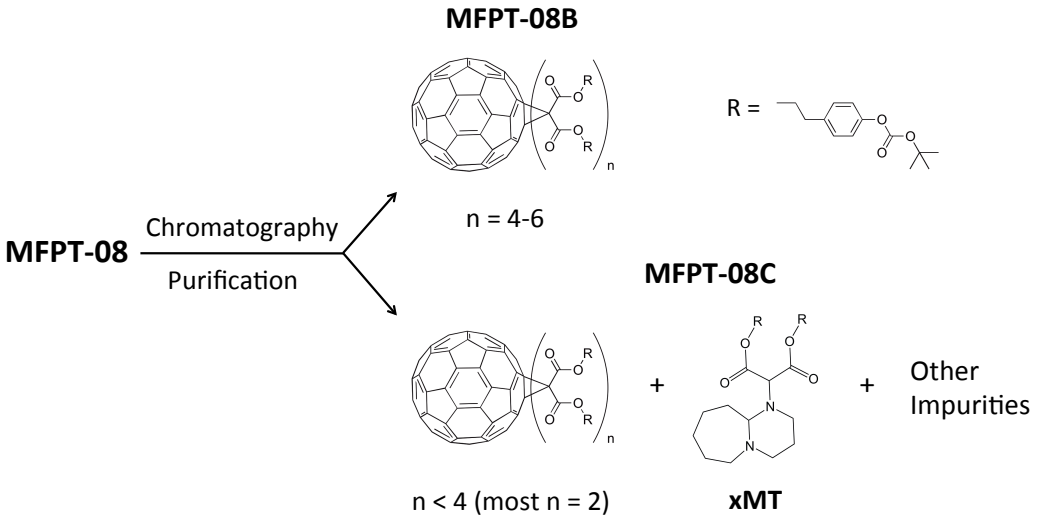

Figure 4.9 Schematics of possible molecule structures in MFPT-08B and MFPT-08C

4.3.2.1 Performance of IM-MFPT-08B and IM-MFPT-08C

Both MFPT-08B and MFPT-08C were mixed with CL12-01 and PAG at a compound ratio of 1:2:1 in ethyl lactate. The sensitivity of the two resists was evaluated using 20 keV electron beam. The samples were exposed and developed for 20 seconds in cyclohexanone. The response curves of the two resists are shown in Figure 4.10 (a). The sensitivity and contrast (in brackets) extracted from fitting were 13 $\mu C/cm^2$ (1.0) and 94 $\mu C/cm^2$ (1.7) for IM-MFPT-08B and IM-MFPT-08C, respectively. Fullerene derivatives with high adduct number and low impurity level gave a much higher sensitivity than the low adduct fullerene compounds with impurities at the same weight ratio in the resist formula. However, the contrast of IM-MFPT-08C was higher than IM-MFPT-08B. The resolutions of IM-MFPT-08B and IM-MFPT-08C were evaluated using 30 keV electron beam. Figure 4.10 (b-g) shows SEM images of line-and-space patterns on the two resists with pitch size from 48 nm down to 44 nm. The results show that IM-MFPT-08B sample had patterns resolved down to 46 nm pitch with low dose. Below 46 nm the lines started to collapse. In the case of IM-MFPT-08C, a high line dose was required (above 800 pC/cm) and the lines were wobbly, which might due to insufficient crosslinking. As the molecules in MFPT-08C have different molecular weight from MFPT-08B, the optimal compound ratio may be different as well. This will be discussed in Section 4.3.3.

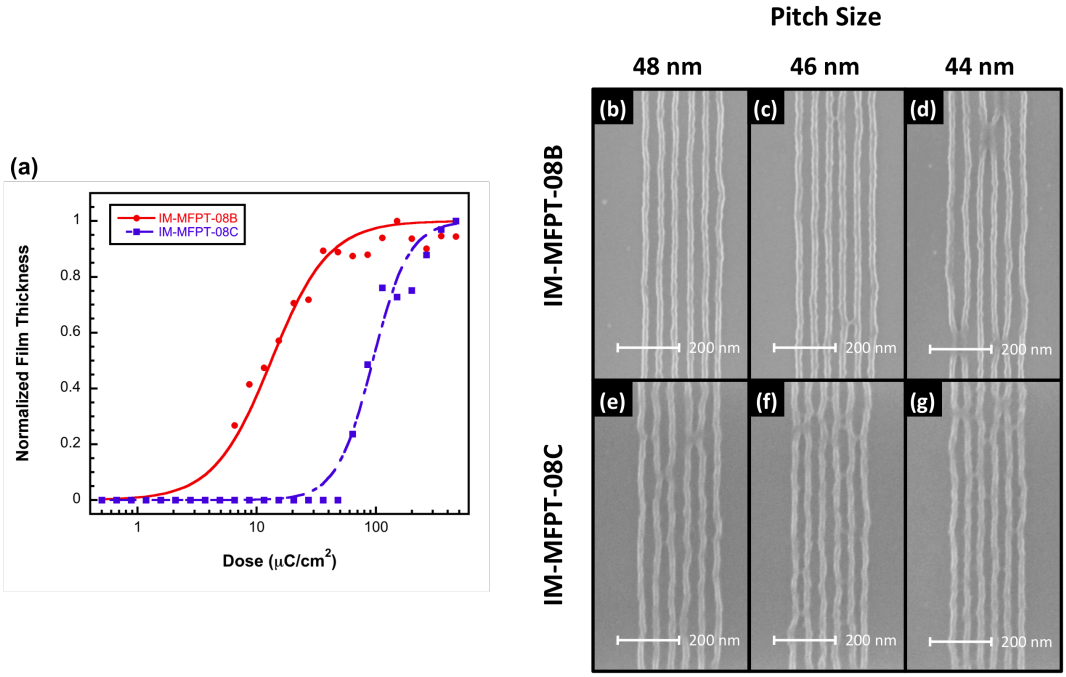

Figure 4.10 (a) The response curves of MFPT-08B and MFPT-08C mixed with CL12-01 and PAG in a [1:2:1] ratio; (b-g) SEM images of dense line patterns in IM-MFPT-08B (top, b-d) and IM-MFPT-08C (bottom, e-g) at pitch 48 nm, 46 nm and 44 nm. The line doses are: (b) 107 pC/cm, (c) 115 pC/cm, (d) 102 pC/cm, (e) 899 pC/cm, (f) 935 pC/cm, (g) 899 pC/cm

4.3.2.2 Mixture of MFPT-08B and MFPT-08C

As neither of the two cuts after separation had as good overall performance as the original IM-MFPT-08, the two materials were mixed in various ratios to optimize the resist property. While keeping the compound ratio of fullerene, CL12-01 and PAG fixed at 1:2:1, MFPT-08C was mixed into the MFPT-08B in various ratios. The response curves are shown in Figure 4.11 (a) and the calculated sensitivity and contrast against the ratio is plotted in Figure 4.11 (b). Both the dose and contrast increased linearly with the increasing ratio of MFPT-08C to 80%. The

result indicated that the mixed material with MFPT-08C ratio below 20% might have the potential of both high sensitivity and resolution.

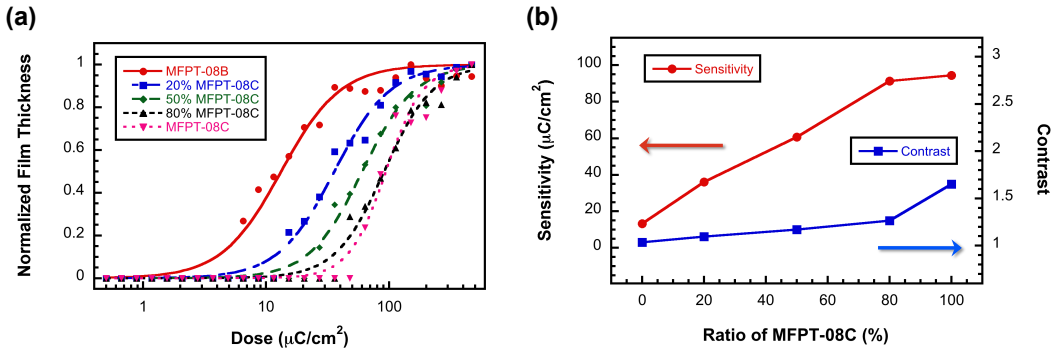

Figure 4.11 (a) The response curves of CARs containing MFPT-08B mixed with MFPT-08C in different ratios; (b) Calculated sensitivity and contrast against the MFPT-08C ratio

Based on the sensitivity results, resolution capability was tested for the blend with 5%, 10% and 15% of MFPT-08C. Line-and-space features at pitch sizes from 48 nm down to 40 nm were patterned using 30 keV electron beam. SEM images of the patterns as well as a plot of measured CD and LER values from the 48 nm pitch patterns against the MFPT-08C ratio are shown in Figure 4.12. With pitch size decreasing, samples with lower ratio of MFPT-08C were more likely to show pattern collapse. Adding MFPT-08C into the MFPT-08B improves both the resolution and LER with an increased dose from around 100 pC/cm to around 200 pC/cm. The best resolution was achieved in the material with 15% of MFPT-08C.

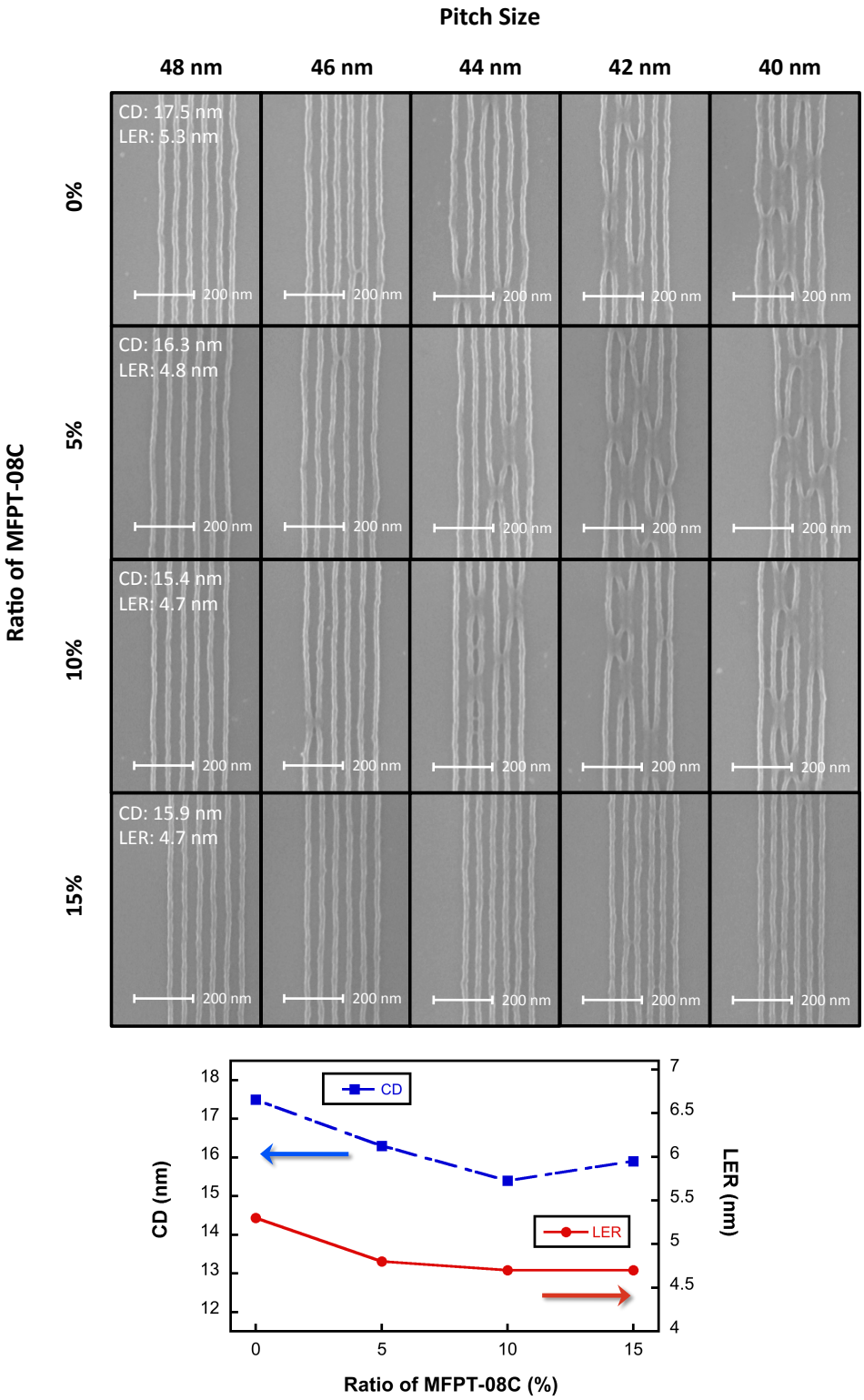

Figure 4.12 (Top) The SEM images of dense features with pitch size from 48 nm to 40 nm, in MFPT-08B mixed with 0%, 5%, 10% and 15% ratio of MFPT-08C (CAR formulation); (Bottom) The measured CD and LER from the 48 nm pitch patterns against the MFPT-08C ratio.

4.3.2.3 Post-development Processing

During the investigation of a new resist system, resist pattern analysis is often undertaken immediately after development. However, in certain situations such as large-scale patterning or, in our case, tests undertaken by collaborators in different laboratories, a delay between development and imaging is sometimes inevitable. The degradation of resist patterns after development, and the effect of a post-development bake (PDB) process on the degradation were evaluated using the MFPT-08B blended with 15% MFPT-08C. A 5-minute PDB at 90 °C and 120 °C was applied to the 50 nm pitch resist features. Figure 4.13 shows SEM images of line patterns with and without PDB. Significant improvement of line quality was observed in the sample with the 90 °C / 5 min PDB. However, PDB at 120 °C caused considerable degradation, which indicates damage of the crosslinked structures by high temperature. The CD and LER (in brackets) of the samples without PDB and with 90 °C / 5 min PDB were 19.9 nm (6.2 nm) and 18.6 nm (5.0 nm), respectively. PDB is known to help improve the LER. As the feature softens there is smoothing of the resist surface, due to the surface tension.[23] The improvement in line width might due to evaporation of organic developer which has penetrated into the crosslinked resist network, which is known to cause feature swelling.[4]

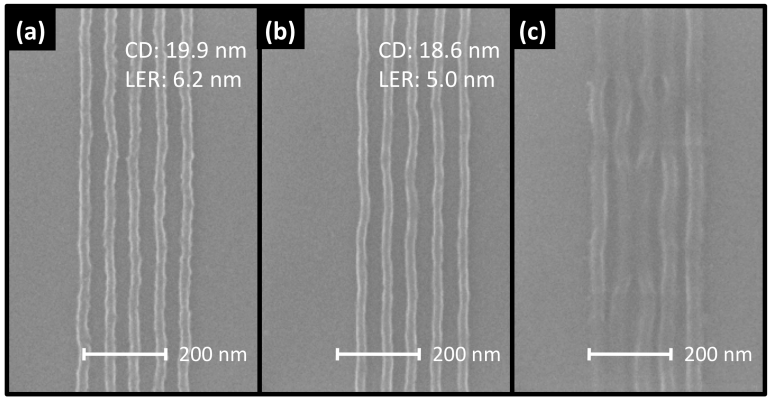

Figure 4.13 The SEM images of dense features at pitch 50 nm in MFPT-08B added with 15% ratio of MFPT-08C (CAR formulation), (a) without post-development bake (PDB), (b) 90 °C / 5 min PDB, and (c) 120 °C / 5 min PDB

The above-mentioned samples without PDB and with 90 °C / 5 min PDB were stored in air and imaged every 24 hours during the following 5 days. Figure 4.14 shows the change of line width and LER over time for the two samples. In both samples the values increased during the storage, indicating that apart from the development process, factors from the environment, such as air humidity, can also cause a swelling issue during the delay between development and imaging. The line width and LER in the PDB sample initially lower than the one without PDB. However, they reached a similar level at day 3 (for line width) and day 4 (for LER). According to the results above, imaging within 24 hours after development is suggested for this resist, even for the samples went through a PDB process. Storage in dry or vacuum condition may be necessary to reduce degradation.

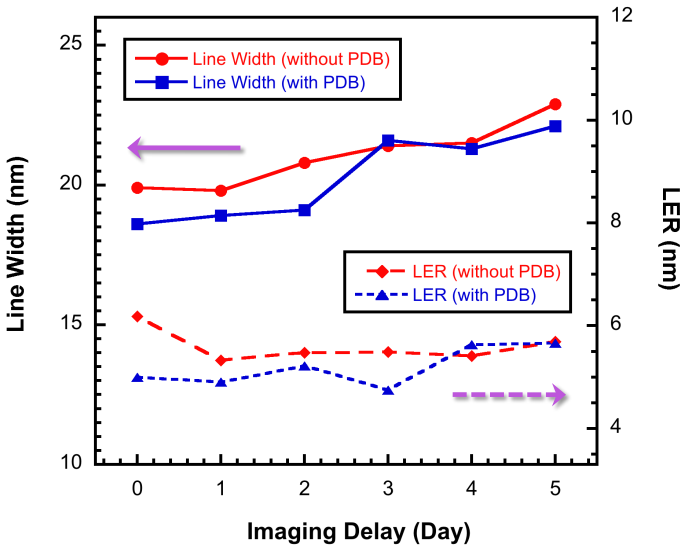

Figure 4.14 Plot of line width and LER in dense features at pitch 50 nm in MFPT-08B added with 15% ratio of MFPT-08C (CAR formulation) against time, without PDB and with 90 °C / 5 min PDB

4.3.3 IM-xMT Resist

Through using a number of different purification methods as well as compound characterizations including matrix-assisted laser desorption/ionization (MALDI) and NMR, the major "impurity" in MFPT-08C was confirmed to be a small molecule with possible structure shown in Figure 4.9 and also Figure 4.15. This molecule was a byproduct from the reaction between fullerene and the malonate precursor (3-(4-*tert*-butoxycarbonyl)phenyl-1-propyl malonate) at the presence of 1,8-diazabicycloundec-7-ene (DBU), which is added to catalyze the fullerene reaction.[4] The structures of malonate precursor and DBU are shown in Figure 4.15. Unexpectedly, a small portion of the precursor bonded to the DBU instead of fullerene during the reaction and formed these compounds.

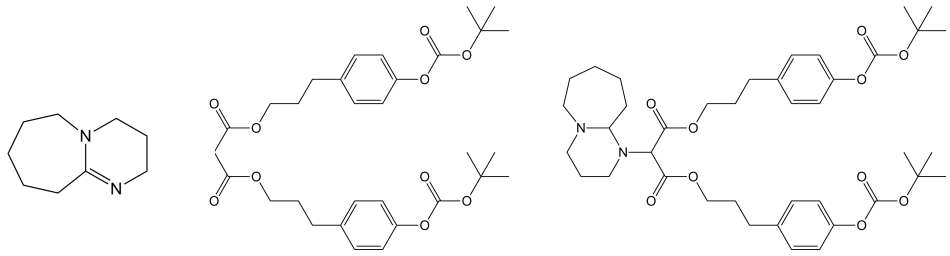

Figure 4.15 Molecule structures of (from left to right) 1,8-diazabicycloundec-7-ene (DBU), 3-(4-*tert*-butoxycarbonyl)phenyl-1-propyl malonate (precursor) and xMT molecule

As DBU itself was reported to be used as a base quencher in a similar CAR system,[24] the alkalinity of this byproduct might help suppress acid diffusion, thus improving the resolution capability in the IM-MFPT-08 type resists. In addition, this molecule has the same functional group as the main fullerene compound with even smaller molecular size, making it a potential high-performance molecular resist itself. This material, which has been named xMT, was then specifically synthesized using similar process as MFPT-08 without the addition of fullerene to the synthesis. Lithographic performance of xMT mixed with crosslinker and PAG (in ethyl lactate) as a CAR (named as IM-xMT) was evaluated and optimized.

4.3.3.1 Formulation Ratio

As the molecular weight of xMT is much smaller than the fullerene derivatives (around 1/5 of MFPT-08B), the compound ratio of the IM-xMT resist needed to be changed. Considering the difference in molecular weight, the IM-xMT resist was formulated in a weight ratio of 0.2:2:1 with xMT, crosslinker and PAG. Using cyclohexanone as a developer, sensitivity and resolution were evaluated

using this compound ratio and compared with another ratio - [1:2:1] - which was the optimal ratio in IM-MFPT-08. Figure 4.16 (a) shows the response curves of the two compound ratios and Figure 4.16 (b-g) show the SEM images of line-space patterns for the two formulations. The sensitivity and contrast (in brackets) at 20 keV are 78 μC/cm^2 (1.4) for the compound ratio [1:2:1] and 19 μC/cm^2 (1.4) for the compound ratio [0.2:2:1]. Significant sensitivity improvement was achieved in the new compound ratio without sacrificing contrast. Improvement was also obtained in the line dose and line quality in the resolution test at 30 keV. Another developer, nBA, was also tested using the same line-space pattern and similar results were achieved.

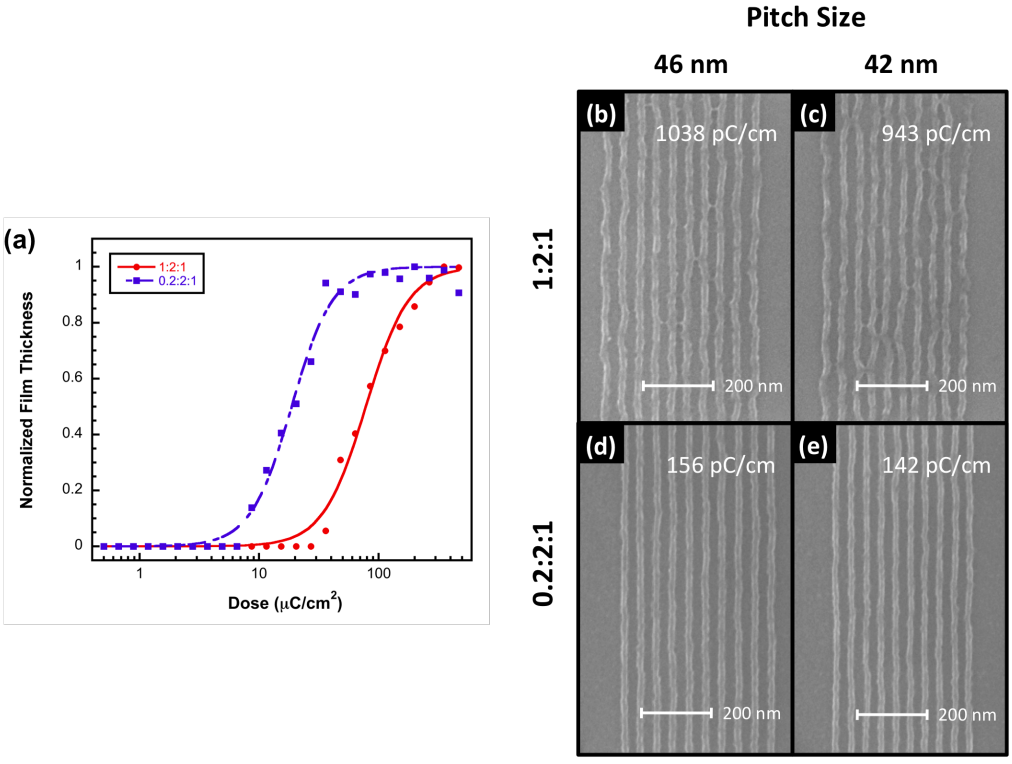

Figure 4.16 (a) The response curves of xMT mixed with CL12-01 and PAG in ratios of [1:2:1] and [0.2:2:1]; (b-e) SEM images of dense line patterns in the resists with the two formulations in (a) at pitch 46 nm and 42 nm; with dose values

4.3.3.2 Formulation Variation

A number of formulation variations were tested in the IM-xMT resist. Different crosslinkers and quenchers were tested (Figure 4.17), including the crosslinker CL08-01 (M_n = 870), which has same structure as CL12-01 (M_n = 1270) with shorter polymer chain length; another non-polymeric epoxy crosslinker, tris(4-hydroxyphenyl)methane triglycidyl ether (CL06-14); and two nucleophilic quenchers, triphenylsulfonium nonaflate (NQ-01) and triphenylsulfonium tosylate (NQ-02).

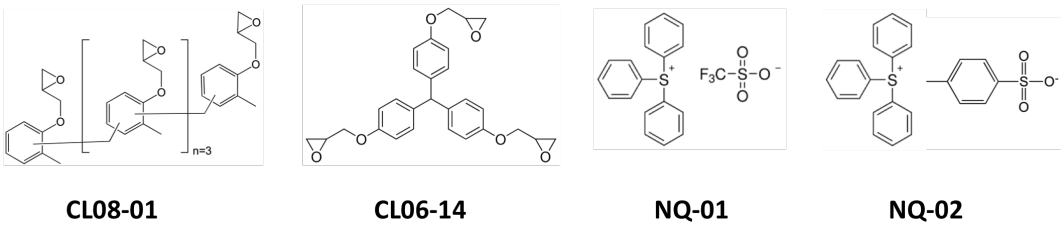

Figure 4.17 Molecule structures of (from left to right) crosslinkers: poly[(phenyl glycidyl ether)-co-formaldehyde] (CL08-01, M_n = 870) and tris(4-hydroxyphenyl)methane triglycidyl ether (CL06-14); and nucleophilic quenchers: triphenylsulfonium nonaflate (NQ-01) and triphenylsulfonium tosylate (NQ-02)

With the compound ratio of [0.2:2:1] of xMT, crosslinker and PAG, the resolution capability of IM-xMT resists with crosslinker CL08-01 and CL12-01 were compared. Figure 4.18 shows SEM images of single-pixel dense features patterned in the two formulations at various pitches. At pitch 42 nm and 40 nm, both resists resolved with CL08-01 sample having slightly better LER. However, at 38 nm pitch, the CL12-01 sample started showing bridging and the LER

increased considerably, whilst the CL08-01 sample had no obvious bridging or collapse. This result indicates that using polymer crosslinkers with smaller molecular size can improve the resolution.

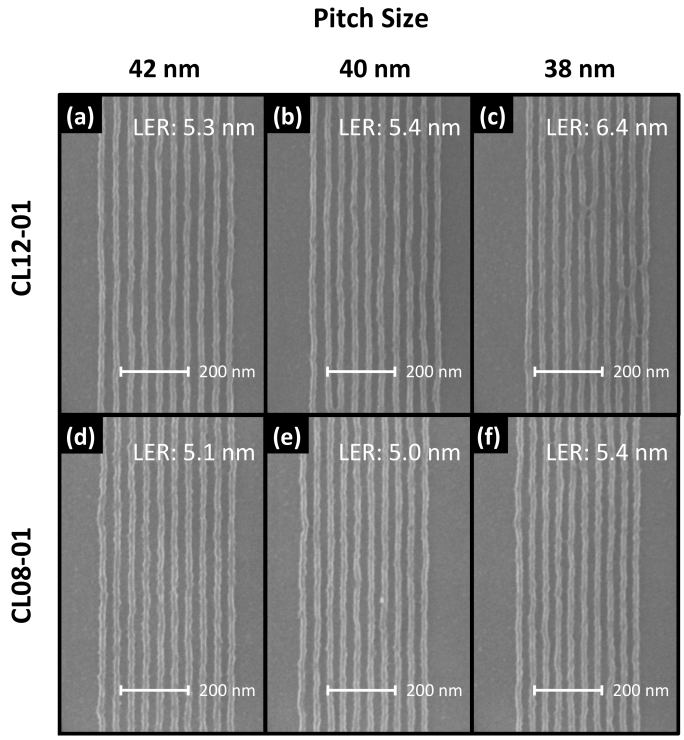

Figure 4.18 The SEM images of dense features at 42 nm, 40 nm and 38 nm pitches, in IM-xMT with CL12-01 and CL08-01 crosslinkers; with measured LER values. The line doses are: (a) 142 pC/cm (b) 156 pC/cm, (c) 142 pC/cm, (d) 107 pC/cm, (e) 117 pC/cm, (f) 107 pC/cm

Nucleophilic quenchers had been reported to be more efficient than traditional base quenchers in controlling the cationic polymerization process.[24,25] 5% of NQ-01 was added into the [0.2:2:1] formulation of IM-xMT resist with CL12-01 crosslinker. Figure 4.19 shows the SEM images of 38 nm pitch dense lines on the resists with and without quencher. The addition of nucleophilic quencher reduced

the bridging between the dense lines, thus the resolution was improved. However, the line quality in the sample with quencher was reduced and not good enough for the LER measurement, which might due to a suppressed crosslinking from the quencher.

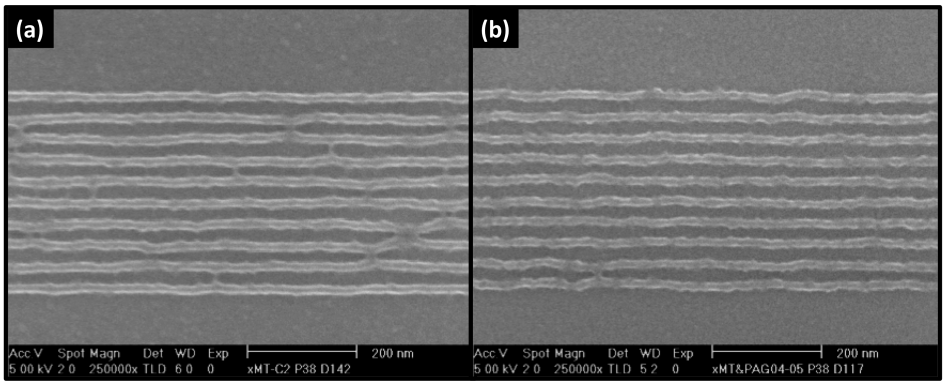

Figure 4.19 The SEM images of dense features at 38 nm pitch, in IM-xMT with CL12-01 crosslinker, without quencher (a) and with 5% NQ-01 quencher (b)

Another combination, which was optimized in the EUV tests, was a [0.2:2:1] ratio of xMT, a molecular crosslinker, CL06-14, and PAG, with an additional 5% of NQ-02. As this resist film tends to degrade on silicon substrates during baking, a fullerene based carbon underlayer was used and the PAB duration was reduced to 2 minutes instead of 5 minutes. Excellent resolution was achieved using 30 keV electron beam exposure with line dose of around twice of that for the polymer crosslinkers. Figure 4.20 shows SEM images of single pixel dense lines on this resist with pitch size from 32 nm down to 26 nm. All the lines were clearly resolved with some bridging and collapse starting from 28 nm pitch.

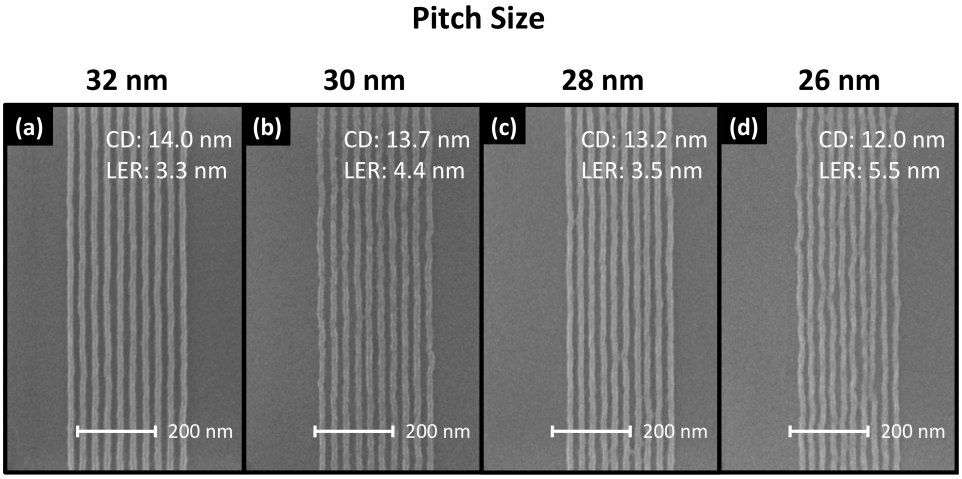

Figure 4.20 The SEM images of dense features with pitch size from 32 nm down to 26 nm, in xMT with CL06-14 crosslinker, PAG and 5% NQ-02 quencher. The line doses are: (a) 322 pC/cm (b) 311 pC/cm, (c) 377 pC/cm, (d) 283 pC/cm

4.3.3.3 Substrate Variations

To evaluate the compatibility of the IM-xMT on different substrates, resist was patterned on acetone-IPA cleaned silicon, fullerene based carbon underlayer (~20 nm) and another commercial underlayer, AL412-302, from Brewer Science (~10 nm). CL08-01 was used as the crosslinker. Single pixel dense features at 50 nm pitch were patterned using the 30 keV electron beam. Cyclohexanone was used as developer. Profile SEM images were taken together with top-down images by cleaving the chip across the resist lines. Figure 4.21 shows SEM images of patterns on the three underlayers as well as the measured CD and LER. In all the three samples the line profiles had near vertical sidewalls and no bridging between the lines, demonstrating good substrate compatibility. The line dose for the patterns on underlayers was slightly higher than those on bare silicon, which might be due to a change in backscattering in the organic underlayers.

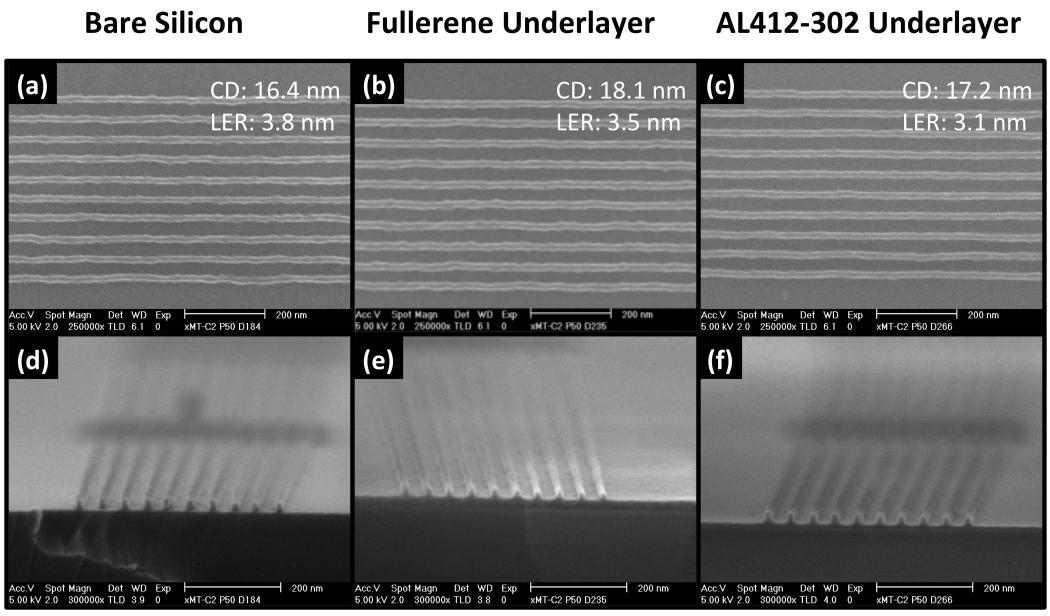

Figure 4.21 The top-down (top) and profile (bottom) images of IM-xMT dense features at 50 nm pitch, on substrates of (a)&(d) bare silicon, (b)&(e) fullerene underlayer, and (c)&(f) A412-302 underlayer

4.3.3.4 Performance at 50 keV and 100 keV

The resist tested using the 50 keV electron beam system was formulated by mixing the xMT, CL08-01 and PAG to give a ratio of [0.2:2:1]. The samples were developed in nBA and coated with 6 nm of AuPd through sputter coating after development but prior to imaging. The metal deposition was performed to improve the SEM imaging contrast, however, it potentially leads to a linewidth increase as well. Figure 4.22 shows SEM images of dense features at pitch size from 40 nm down to 30 nm. Dense lines at pitch 40 nm and 35 nm were clearly resolved with sub-14 nm line width. Lines were also resolved at 30 nm pitch with some pattern collapse. Although resist sensitivity tends to decrease with increasing acceleration voltage,[26] a relatively low dose of ~150 pC/cm was used for the patterns.*

* This indicates a potential error in the 50 keV sensitivity measurements, which should be repeated in future work.

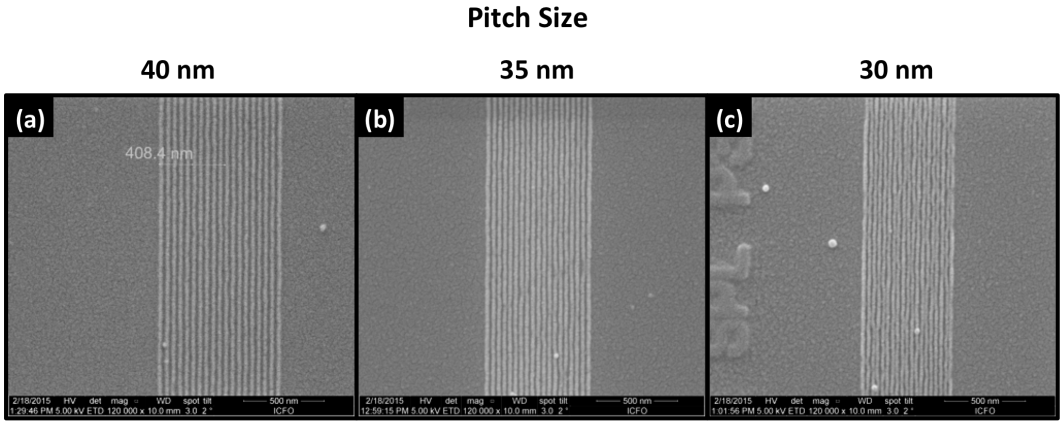

Figure 4.22 The SEM images of dense features with pitch size of 40 nm, 35 nm and 30 nm after 50 keV electron beam exposure, in IM-xMT with CL08-01 crosslinker

The lithographic performance at 100 keV electron beam exposure was evaluated using a nested square pattern with various pitches. Three resist formulations were used in this test. The first one was a [0.2:2:1] mixture of xMT, CL12-01 and PAG with 5% of NQ-01. The second was a [0.2:2:1] mixture of xMT, CL08-01 and PAG with 5% of NQ-01, and the third formulation was a [0.2:2:1] mixture of xMT, CL06-14 and PAG with 5% of NQ-02. The CL12-01 sample was developed in cyclohexanone whilst the CL08-01 and CL06-14 samples were developed in nBA. Figure 4.23 (a) and (d) show the SEM images of the patterns on CL12-01 sample at 42 nm and 36 nm pitch, respectively. The required line dose was 3-4 times higher than that for 30 keV electron beam, as expected. Dense lines were resolved at pitch 42 nm whilst some bridging was observed at pitch 36 nm. This result was similar to the resolution achieved at 30 keV. In contrast, excellent resolution down to 28 nm pitch was achieved in the CL08-01 sample. Figure 4.23 (b) and (e) show the SEM images of the patterns at 30 nm and 28 nm pitch, respectively. Lines of width ~12 nm were successfully patterned at 30 nm pitch

and, with some pattern collapse, at 28 nm pitch. Compared with the CL12-01 sample, the significant resolution improvement achieved in CL08-01 sample at 100 keV over 30 keV indicates that the polymeric crosslinkers with smaller molecular size have a higher ultimate resolution. For the CL06-14 sample, which gave the best resolution at 30 keV, there was no obvious resolution improvement at 100 keV. As shown in Figure 4.23 (c) and (f), dense features down to 30 nm pitch were resolved with a line dose around twice of those in the other two samples, which was consistent with the 30 keV results. As the CL06-14 is a non-polymeric crosslinker with even smaller molecular size than the CL08-01, the resolution for this resist formulation might be limited by other factors such as adhesion or swelling.

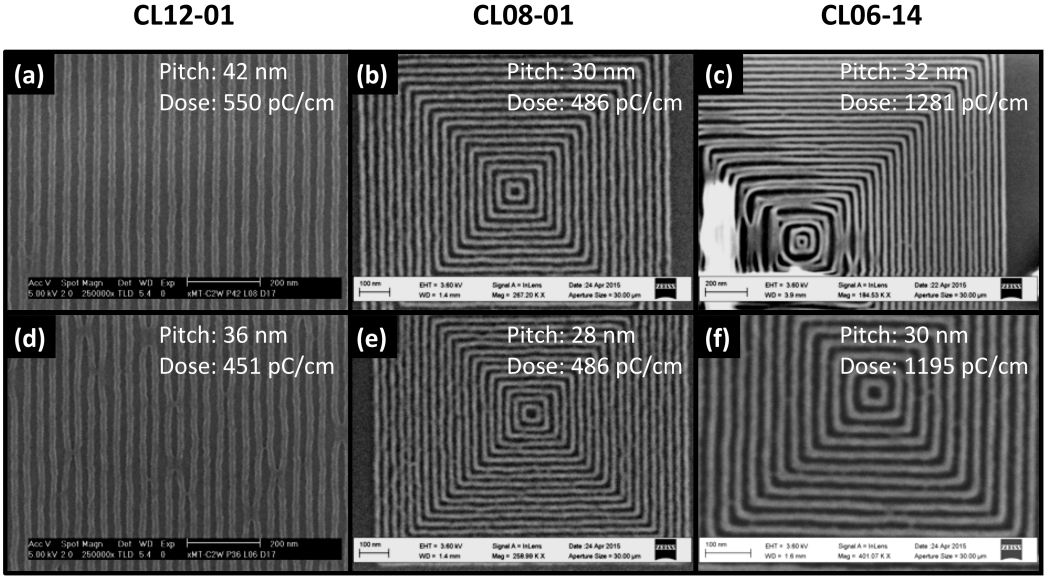

Figure 4.23 The SEM images of dense features after 100 keV electron beam exposure, in IM-xMT with (a)&(d) CL12-01 crosslinker; (b)&(e) CL08-01 crosslinker with 5% NQ-01; and (c)&(f) CL06-14 crosslinker with 5% NQ-02

4.4 Conclusions and Future Work

In this chapter a family of high-performance negative tone CARs was presented. The advantages of the "two-step" concept (introduced in Chapter 3) and small molecular materials were combined to achieve high resolution. With a *tert*-butoxycarbonyl (*t*BOC) protected phenol as the functional group, several molecular resists were developed and characterized.

First, a number of phenol-based fullerene derivatives with different side-chain length and with/without the protection group were developed. Fullerene derivatives were blended with an epoxy crosslinker CL12-01 and PAG to form chemically amplified molecular resists. Among the resist materials, a fullerene derivative with propyl side chains and *t*BOC protection, MFPT-08, showed good industrial compatibility (development in appropriate solvents), high resolution (18 nm half-pitch) in 30 keV electron beam and good sensitivity (sub-50 $\mu C/cm^2$) with 20 keV electron beam in corresponding CAR, IM-MFPT-08.

A chromatography technique was used to purify and separate a scaled batch of MFPT-08 material. Two cuts, MFPT-08B and MFPT-08C, were separated. MFPT-08B contains the most of the targeted fullerene derivative with 4-6 adducts, whilst MFPT-08C contains small amount of fullerene derivatives with low adducts (most with bis-adduct) and other impurities. Using the same formulation ratio with the crosslinker and PAG as in IM-MFPT-08 resist, IM-MFPT-08B showed very high sensitivity with relatively low resolution, whilst IM-MFPT-08C showed low sensitivity with a high contrast, but wobbly lines in

the line-space patterning. A blend of MFPT-08B (85%) and MFPT-08C (15%) was found to give a good combination of sensitivity and resolution.

Based on MFPT-08C material, another non-fullerene molecular resist, xMT, was developed. The formulation ratio with epoxy crosslinker and PAG was modified due to xMT's lower molecular weight. This resist, IM-xMT, showed resolution down to 38 nm pitch at 30 keV with the polymeric crosslinker CL12-01 and CL08-01, with a high sensitivity. Another formulation, optimized for EUV exposures using a molecular crosslinker CL06-14, has demonstrated dense features down to 26 nm pitch in 30 keV EBL albeit at a dose twice of that for the polymeric crosslinkers. These results show that the IM-xMT resists have met the requirements in both sensitivity and resolution according to the ITRS target. It also has higher overall lithographic performance as well as industrial compatibility over most commercially available negative tone electron beam resists.

Lithographic performance using 50 keV (for CL08-01 sample only) and 100 keV electron beam exposure was also evaluated. Again, high resolution with good sensitivity has been achieved in IM-xMT resists, showing considerable potential as a photo-mask patterning material. Significant resolution improvement was achieved (35 nm pitch at 50 keV and sub-30 nm pitch at 100 keV) in the resist with CL08-01 crosslinker. However, no obvious resolution improvement was obtained in the CL12-01 and CL06-14 samples at 100 keV exposure.

The results above indicate a trend that reducing the molecular size of resist compounds gives higher ultimate resolution. However, converting to small molecular materials such as xMT and CL06-14 may also change the sensitivity, film quality, adhesion, mechanical strength of the crosslinked network, etc., which can also have various influences on the resolution. Therefore, investigating the effects of molecular size and structure on the lithographic performance using novel molecular materials is suggested for future work.

References

1. International Technology Roadmap for Semiconductors, 2012 Edition, http://www.itrs.net (Accessed 29/09/2015)
2. Hu, W. W., Sarveswaran, K., Lieberman, M., Bernstein, G. H., Sub-10 nm electron beam lithography using cold development of poly (methylmethacrylate). *J. Vac. Sci. Technol. B, 22(4),* 1711 (2004)
3. Yasin, S., Hasko, D. G., Ahmed, H., Fabrication of <5 nm width lines in poly (methylmethacrylate) resist using a water : isopropyl alcohol developer and ultrasonically-assisted development. *Appl. Phys. Lett., 78(18),* 2760 (2001)
4. Yang, D. X., Frommhold, A., Xue, X., Palmer, R. E., Robinson, A. P. G., Chemically amplified phenolic fullerene electron beam resist. *J. Mater. Chem. C, 2(8),* 1505 (2014)
5. Shokouhi, B., Zhang, J., Cui, B., Very high sensitivity ZEP resist using MEK: MIBK developer. *Micro. Nano. Lett., 6(12),* 992 (2011)
6. Reinspach, J., Lindblom, M., von Hofsten, O., Bertilson, M., Hertz, H. M., Holmberg, A., Cold-developed electron-beam-patterned ZEP 7000 for fabrication of 13 nm nickel zone plates. *J. Vac. Sci. Technol. B, 27(6),* 2593 (2009)
7. Pépin, A., Studer, V., Decanini, D., Chen, Y., Exploring the high sensitivity of SU-8 resist for high resolution electron beam patterning. *Microelectron. Eng., 73,* 233 (2004)
8. Lawson, R. A., Tolbert, L. M., Younkin, T. R., Henderson, C. L., Negative-tone molecular resists based on cationic polymerization. *Proc. SPIE, 7273,* 72733E (2009)
9. Herth, E., Algre, E., Tilmant, P., Francois, M., Boyaval, C., Legrand, B., Performances of the negative tone resist AZnLOF 2020 for nanotechnology applications. *IEEE T. Nanotechnol., 11(4),* 854 (2012)
10. Yang, J. K., et al., Understanding of hydrogen silsesquioxane electron resist for sub-5-nm-half-pitch lithography. *J. Vac. Sci. Technol. B, 27(6),* 2622 (2009)

11. Kim, J., Chao, W., Griedel, B., Liang, X., Lewis, M., Hilken, D., Olynick, D., Understanding the base development mechanism of hydrogen silsesquioxane. *J. Vac. Sci. Technol. B, 27(6)*, 2628 (2009)
12. Singh, V., Satyanarayana, V. S. V., Sharma, S. K., Ghosh, S., Gonsalves, K. E., Towards novel non-chemically amplified (n-CARS) negative resists for electron beam lithography applications. *J. Mater. Chem. C, 2(12),* 2118 (2014)
13. Stowers, J. K., et al., Directly patterned inorganic hardmask for EUV lithography. *Proc. SPIE, 7969,* 796915 (2011)
14. Drygiannakis, D., et al., Stochastic simulation studies of molecular resists for the 32nm technology node. *Microelectron. Eng., 85(5),* 949 (2008)
15. Karatsu, T., Yoshimura, Y., Miura, S., Yagai, S., Kitamura, A., Ozaki, J., Okamoto, H., Functionalized Cyclohexyl methacrylate based Copolymers for Negative Resist. *J. Photopolym. Sci. Tec., 24(5),* 535 (2011)
16. Takemoto, I., et al., Tailored Glass Transition of ArF Resists for Resolution Enhancement at sub-50nm node. *J. Photopolym. Sci. Tec., 18(3),* 399 (2005)
17. Olynick, D. L., Ashby, P. D., Lewis, M. D., Jen, T., Lu, H., Liddle, J. A., Chao, W., The link between nanoscale feature development in a negative resist and the Hansen solubility sphere. *J. Polym. Sci. Pol. Phys., 47(21),* 2091 (2009)
18. Mohammad, M. A., Muhammad, M., Dew, S. K., Stepanova, M., in Directions in Nanofabrication, Dew, S. K., Stepanova, M., editors. Austria: *Springer Vienna, 2,* 11 (2012)
19. Chen, Y., Yang, H., Cui, Z., Effects of developing conditions on the contrast and sensitivity of hydrogen silsesquioxane. *Microelectron. Eng., 83(4),* 1119 (2006)
20. Hsu, D. S. H., Hsieh, W. H., Huang, C. Y., Wu, W. B., Shih, C. L., LWR reduction by photoresist formulation optimization for 193nm immersion lithography. *Proc. SPIE, 8325,* 83251M (2012)
21. Cho, K., Tarutani, S., Inoue, N., Tsubaki, H., Neisser, M., LWR study on resist formulation parameters. *Proc. SPIE, 8682,* 868217 (2013)

22. Kozawa, T., Oizumi, H., Itani, T., Tagawa, S., Analysis of dose-pitch matrices of line width and edge roughness of chemically amplified fullerene resist. *Jpn. J. Appl. Phys., 50(12R),* 126501 (2011)
23. Sho, K., Shibata, T., Shiobara, E., Ito, S., Effect of post development process for resist roughness. *Proc. SPIE, 5753,* 400 (2005)
24. Manyam, J., Novel Resist Materials for Next Generation Lithography, PhD thesis, School of Physics and Astronomy, University of Birmingham, 76 (2010), Available from: http://etheses.bham.ac.uk (Accessed 03/10/2015)
25. Lawson, R. A., Molecular resists for advanced lithography-design, synthesis, characterization, and simulation. Doctoral dissertation, Georgia Institute of Technology, 352 (2011), Available from: https://smartech.gatech.edu (Accessed 05/10/2015)
26. Takigawa, T., Kawabuchi, K., Yoshimi, M., Kato, Y., High voltage electron beam lithography. *Microelectron. Eng., 1(2),* 121 (1983)

CHAPTER 5

FULLERENE BASED NON-CHEMICALLY AMPLIFIED RESISTS

5.1 Introduction

Throughput issue has been a major concern for next-generation lithography. Due to the source power weakness in EUV lithography, and the serial nature of EBL, the importance of enhancing the resist sensitivity is high. For decades this has been solved through employing chemical amplification in organic resists.[1] However, with the minimum feature size continuously shrinking and the energy of the EUV exposure source exceeding the resist ionization threshold, the performance of conventional chemically amplified resists is approaching the limits.

In EUV and electron beam lithography, resist exposure is driven by secondary electrons. The thermalization of secondary electrons, together with the stochastic distribution of PAG, and photo-acid diffusion, causes resolution blur.[2,3] In addition, pattern collapse issue at small pitches requires substantial resist film thickness reduction, which reduces the number of photons or primary electrons absorbed, thus increasing the shot noise.[3,4] Therefore, new approaches of sensitivity enhancement other than chemically amplification need to be considered for these high-energy, low-power exposure sources. Several recent

approaches have sought to enhance the absorbance of thin films through employing materials with high absorption coefficients – such as fluoropolymers[5] or metal oxide nanoparticles[6]. It was also reported several decades ago that incorporation of heavy metals into the organic resist matrix could efficiently improve the sensitivity for X-ray lithography as the metal ions/atoms may serve as inelastic scattering centers to enhance the energy absorption at certain exposure wavelengths,[7,8] although high resolution was not achieved and work in this area was not developed to any significant extent.

In this work a number of non-chemically amplified fullerene-metal coordination complex resists have been developed (Figure 5.1). These materials have a bipyridine (Bipy) group attached to the fullerene via various addends: pyrrolidinofullerene (PF), methanofullerene (MF) and phenyl-C_{61}-butyrate (PCB). Bipyridine is a well-known bidentate chelating ligand that serves to allow facile complexation with a number of transition metals. Platinum and Rhenium were used in the Bipy-metal complex. Both the metal-containing materials and control materials (without metal) were studied and compared in this study.

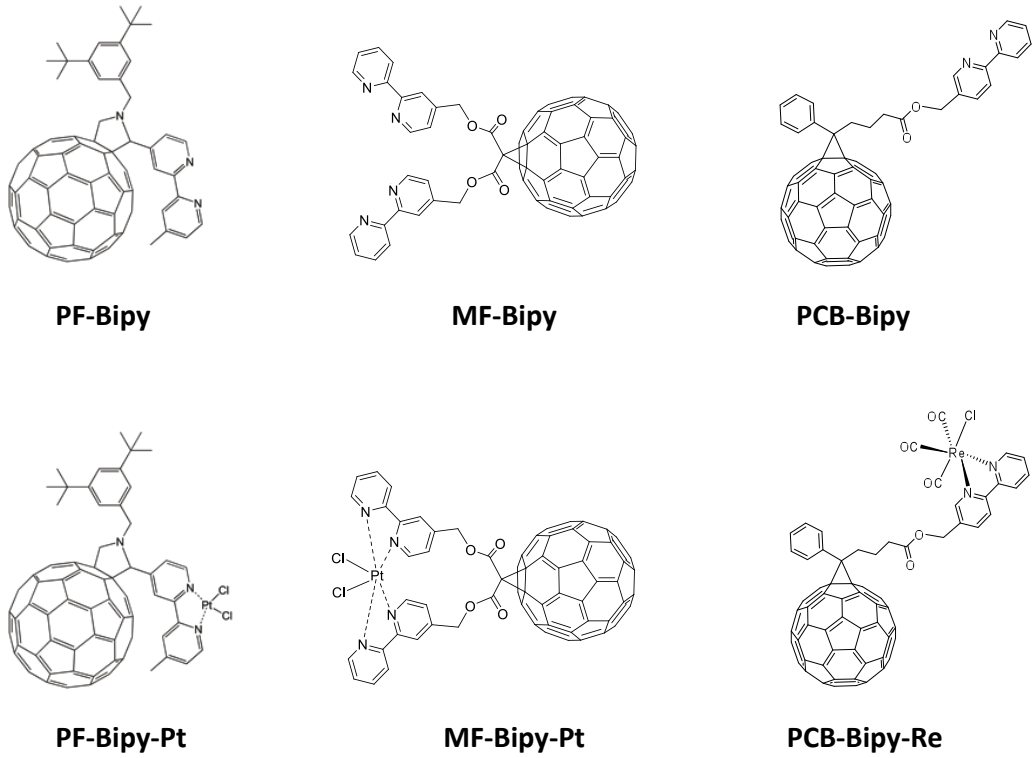

Figure 5.1 Three fullerene-metal complex resists (bottom) and the corresponding control materials without metal (top)

Fullerene was found to fragment under electron beam and re-combine to form near amorphous carbon structures.[9,10] Several fullerene derivatives have been reported to be high-resolution non-chemically amplified electron beam resists (Figure 5.2).[11] By addition of one metal atom per fullerene cage through complexation, the sensitivity at various electron beam energies can be significantly enhanced. Furthermore, the effect of metal incorporation on the resolution and sidewall quality was found to be dependent on the metal selected. The lithographic performance of these resists was also evaluated using helium ion beam lithography. An aberration corrected scanning transmission electron microscope (AC-STEM) was used to investigate the distribution of the metal

atoms before and after exposure/development and revealed a unique metal-containing carbon nano-structure.

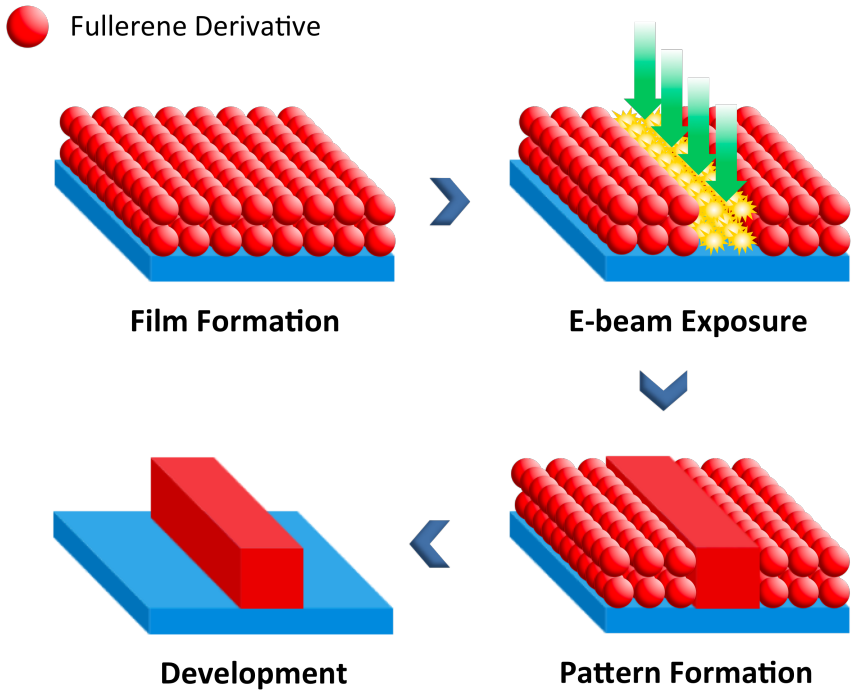

Figure 5.2 Schematic demonstration of the patterning mechanism of fullerene derivatives based on electron beam induced fragmentation

5.2 Methods

The fullerene-platinum complex PF-BP-Pt and the control material PF-BP were synthesized by Prof. Andrei Khlobystov's group from University of Nottingham. The rest of the materials were synthesized at Nano-C (USA). In the electron beam lithography tests, the materials were dissolved in chloroform or anisole and spun onto acetone-IPA cleaned silicon chips. A 70 °C / 5 min post-application bake

(PAB) was applied. No post-exposure bake was needed. The XL30 SFEG SEM was used at 30 keV for the electron beam exposure.

In some exposures a "side-by-side" method was used to compare the cross-sections between two resist patterns. In this method, two silicon chips are coated with different resists, and broken into 9 mm × 4.5 mm pieces along prescribed lines. Care is taken to ensure the resist film thickness is the same in both cases. The two pieces are then put side by side - the gap between the two chips is normally no more than 20 μm alongside the contacted edges. Best focus is achieved on sample 1 near to the gap. Then the dense lines with 100 μm length are patterned centered on the gap. The beam is then refocused near to the edge of sample 2 and the line pattern is re-exposed with a slight offset in position. As a result, each of the samples is exposed with "half" of the pattern with the same beam conditions. By exposing twice, with the beam focused on each of the samples in turn, effects of substrate and film thickness are allowed for. In addition, because the samples have been cleaved from larger samples, and thus have no edge bead, good quality cross-sections are also achieved at the edges of both samples. This method provides a direct comparison of the cross-sections between two samples and efficiently eliminates other factors such as beam calibration and damages caused by substrate cleavage after development. It additionally allows for any focal variation introduced by minor difference in the height of the two samples to be disregarded. However, the sensitivity difference between the two resists is required to be within certain range, in order to allow simultaneous exposure.

In the helium ion beam lithography (HIBL) tests, samples were prepared at the University of Birmingham before being shipped to the University of Southampton for exposure. The energy of the helium ion beam was 30 keV for both patterning and imaging. For the sensitivity tests, beam current of 1 pA was used for patterning a set of 10 μm × 5 μm rectangular features with various doses. The remaining thicknesses were measured using an AFM. For the resolution tests, the beam current was reduced to 0.4 pA. Single pixel dense lines were patterned and imaged using either the same helium ion microscope or the XL30 SFEG SEM.

In the AC-STEM characterization, both amorphous carbon coated grid and lacey formvar coated grids were used as substrates. STEM specimens were prepared by placing a few drops of material solution (1 g/L or 5 g/L in chloroform depending on the thickness required) onto the grid. The drop-coated grids were subsequently put into a vacuum desiccator and left for 2 hours before use. The STEM imaging was done by Dr. Dongsheng He from University of Birmingham. The convergence semi-angle of the electron beam and the inner collection semi-angle of the high angle annular dark field detector were 20 mrad and 62 mrad, respectively. The beam current was 35.1 pA.[12] The dwell time was 20 μs/pixel. High angle annular dark-field (HAADF) and bright field images were taken simultaneously.

5.3 Results and Discussion

5.3.1 Fullerene Derivatives as Non-chemically Amplified Resists

As the fullerene cage was found to fragment upon electron beam irradiation and perform as a negative tone resist (Figure 5.2), a number of fullerene derivatives have been studied as non-chemically amplified resists.[11,13] Those resists normally have excellent resolution but a low sensitivity. It was also found that the class of fullerene derivatives, i.e. the variation in side chains, had significant effects on their lithographic performance. Two fullerene derivatives were first found to be high-resolution negative tone resists in this work. They are the methanofullerene derivative used in the previous chapter, MFPT-08; and another common derivative, phenyl-C_{61}-butyric acid methyl ester (PCBM). MFPT-08 was dissolved in ethyl lactate whilst PCBM was dissolved in anisole. Both of the two resists used cyclohexanone as the developer. The sensitivity and contrast (in brackets) of MFPT-08 (without crosslinker and PAG) and PCBM at 20 keV were 7.3 mC/cm^2 (3.0) and 6.6 mC/cm^2 (3.8), respectively. Using 30 keV electron beam, single-pixel dense lines at 26 nm and 32 nm pitch were successfully patterned on MFPT-08 and PCBM, respectively (Figure 5.3).

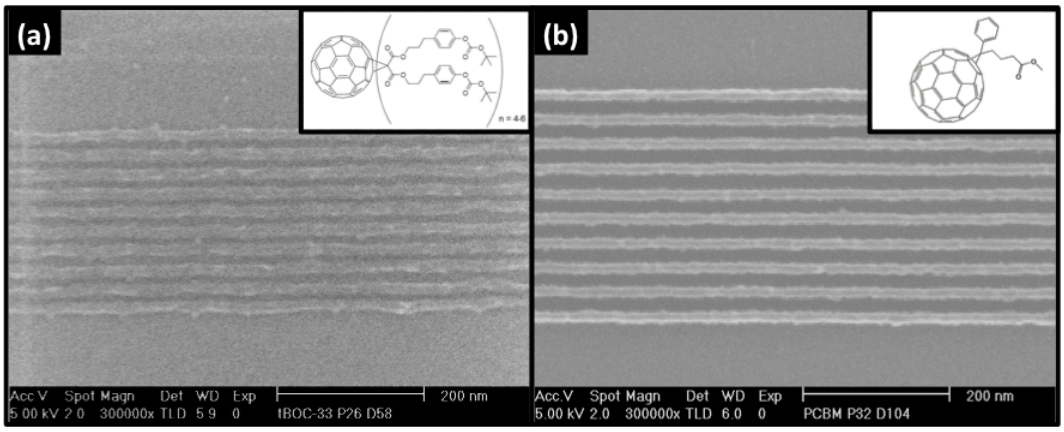

Figure 5.3 (a) Molecular structure of MFPT-08 and SEM image of 26 nm pitch dense lines in MFPT-08 with a line dose of 58 nC/cm at 30 keV; (b) Molecular structure of PCBM and SEM image of 32 nm pitch dense lines in PCBM with a line dose of 104 nC/cm at 30 keV

5.3.2 Performance of Fullerene-Metal Complex Resists

The lithographic performance of fullerene-metal coordination complex resists shown in Figure 5.1 was evaluated using electron beam and helium ion beam. PF-Bipy and PCB-Bipy material families were dissolved in chloroform whilst the MF-Bipy based materials were dissolved in anisole. The sensitivity, resolution and line profile were measured and compared between the metal coordination materials and the control materials.

5.3.2.1 EBL Evaluation on Fullerene-Platinum Complex Resists

The sensitivity and contrast of PF-Bipy and PF-Bipy-Pt were evaluated using 20 keV electron beam. The response curves of the two resists developed in MCB and cyclohexanone are shown in Figure 5.4 and the sensitivity and contrast values extracted from the fitting are shown in Table 5.1. Based on the contrasts it can be

seen that MCB is the more aggressive developer, but in both MCB and cyclohexanone development there was a significant improvement in the sensitivity for the PF-Bipy-Pt resist. Whilst slow in comparison to chemically amplified resists,[14,15] it is clear that this non-chemically amplified system has achieved a significant enhancement in secondary electron generation through the incorporation of a single platinum complex in to the derivative. A similar trend was also observed in other studies.[7,8]

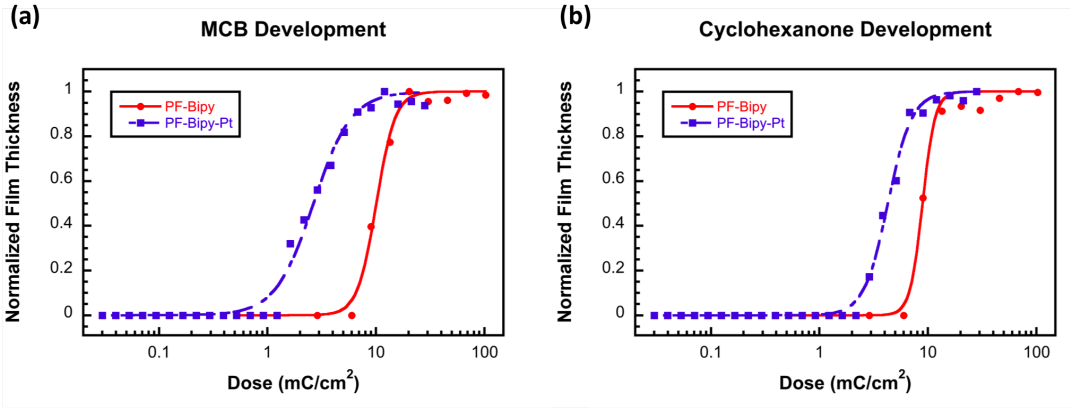

Figure 5.4 The response curves of PF-Bipy and PF-Bipy-Pt at 20 keV electron beam exposure, developed in (a) monochlorobenzene (MCB) and (b) cyclohexanone

Table 5.1 The sensitivity and contrast values for PF-Bipy and PF-Bipy-Pt at 20 keV, developed in monochlorobenzene (MCB) and cyclohexanone

	MCB Development		Cyclohexanone Development	
	Sensitivity (mC/cm²)	Contrast	Sensitivity (mC/cm²)	Contrast
PF-Bipy	10.1	2.9	8.9	4.3
PF-Bipy-Pt	2.7	1.4	4.3	2.3

A general concern is that an improvement of the resist sensitivity may come at the cost of other factors such as resolution, LER and exposure latitude due to their trade-off relationship. The resolution of PF-Bipy and PF-Bipy-Pt were evaluated through patterning sparse and dense single pixel lines at various pitches using a 30keV electron beam. Again, two developers, MCB and cyclohexanone, were used in the resolution test. For the MCB developer, ~15.5 nm sparse features and dense features at 40 nm pitch were resolved in both PF-Bipy and PF-Bipy-Pt. However, lines started to show bridging when the pitch size went below 40 nm. In contrast, using cyclohexanone developer, dense lines down to 28 nm pitch size were achieved in both PF-Bipy and PF-Bipy-Pt. Figure 5.5 shows the SEM images of sparse and dense lines from pitch 32 nm down to 28 nm for PF-Bipy and PF-Bipy-Pt resists.

Comparing the critical dimension (CD) and LER between the two materials, there was no significant difference in their resolution capability. Both materials achieved sub-14 nm features with sub-3 nm LER, showing a high resolution. Moreover, the smallest sparse feature in PF-Bipy-Pt was 12.2 nm compared with a 14.5 nm in PF-Bipy. The optimal line doses at these pitches were mostly between 50 nC/cm and 60 nC/cm for the PF-Bipy, and around 40 nC/cm for the PF-Bipy-Pt. The behavior of the two resists at larger exposure dose range was also investigated and is presented later in this section.

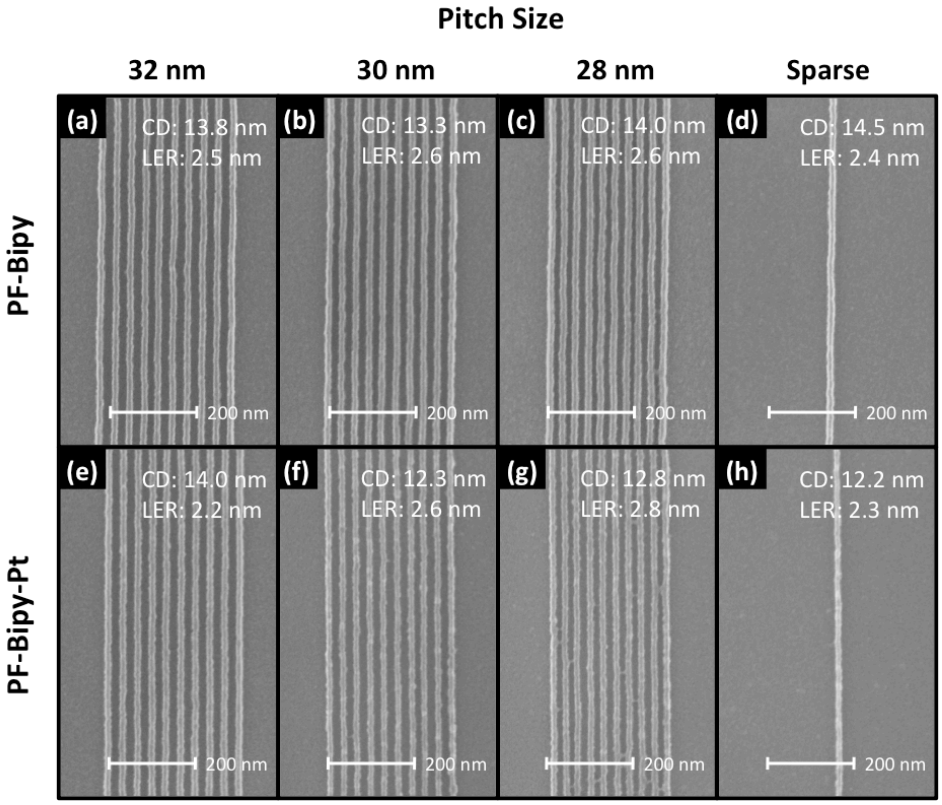

Figure 5.5 SEM images of sparse lines and dense lines in PF-Bipy and PF-Bipy-Pt, at 32 nm, 30 nm and 28 nm pitch, patterned with 30 keV electron beam, with the measured CD and LER values shown in the images. The line doses are: (a) 57 nC/cm, (b) 52 nC/cm, (c) 47 nC/cm, (d) 52 nC/cm, (e) 38 nC/cm, (f) 42 nC/cm, (g) 42 nC/cm, (h) 42 nC/cm

Similar results were obtained with the other group of fullerene derivatives, MF-Bipy and MF-Bipy-Pt. The sensitivity at 20 keV was 7.6 mC/cm^2 and 4.6 mC/cm^2 for MF-Bipy and MF-Bipy-Pt, respectively (Figure 5.6 (a)). Again the introduction of Pt complex showed certain sensitivity enhancement. Single pixel dense lines were patterned on the two materials using 30 keV electron beam. Figure 5.6 (b)-(e) show the dense features with 32 nm and 30 nm pitch. Due to a low image contrast, the CD and LER could not be measured through Summit

analysis software. However, both MF-Bipy and MF-Bipy-Pt have clearly shown resolution capability of 30 nm pitch resolution with MF-Bipy-Pt requiring lower line doses.

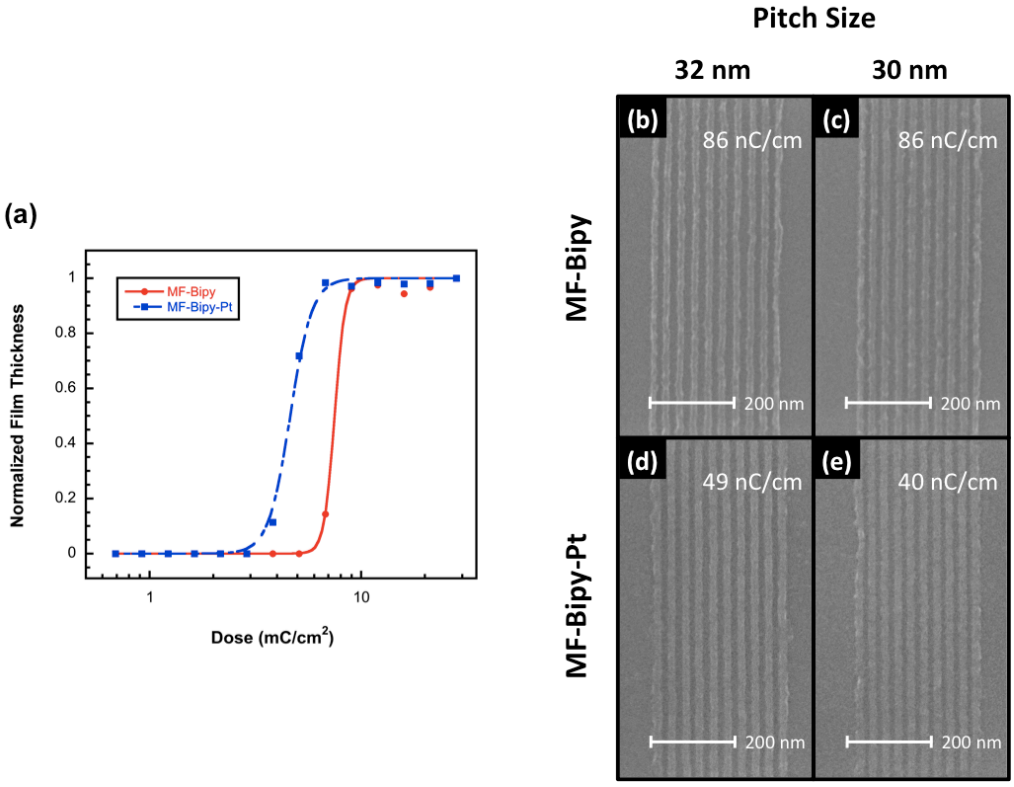

Figure 5.6 (a) The response curves of MF-Bipy and MF-Bipy-Pt at 20 keV; (b-e) SEM images of dense line patterns in MF-Bipy and MF-Bipy-Pt at 30 keV, at pitch 32 nm and 30 nm. The line doses are shown in the individual images

In order to effectively transfer resist patterns to the substrate, by etching or by other techniques, it is important that the unwanted material is effectively removed with relatively little residue and that the line patterns have near vertical sidewalls. To exam the profile of line patterns on the metal containing resists, PF-Bipy-Pt was patterned with dense lines at different pitches using 30 keV electron beam.

After development, the samples were subsequently cleaved across the lines and imaged on a tilted stage (~ 80°) to show the sidewalls. Figure 5.7 (a) and (b) show the cross-sections of 36 nm and 32 nm pitch lines, respectively. At both pitches the lines had steep sidewalls and no residual material was observed between the lines.

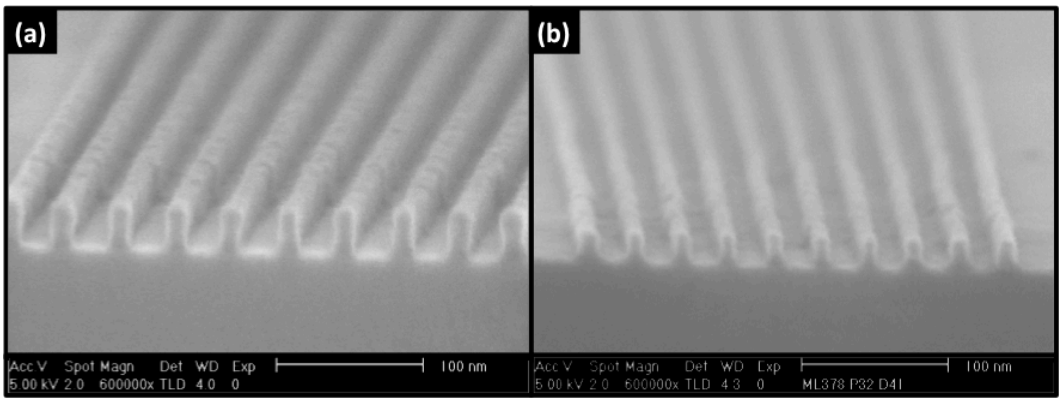

Figure 5.7 Cross-section SEM images of PF-Bipy-Pt dense features at (a) 36 nm pitch and (b) 32 nm pitch

In order to directly compare the cross-section of dense features between PF-Bipy and PF-Bipy-Pt, the previously mentioned "side-by-side" exposure method (Section 5.2) was adopted in this test. Dense features at 50 nm pitch were exposed with electron beam focused on either PF-Bipy or PF-Bipy-Pt. Figure 5.8 (a) and (b) show the cross-section images of the line patterns at different doses, with beam focused on PF-Bipy and PF-Bipy-Pt, respectively. Although the sample that was not under focus tended to have more pattern collapse at lower doses due to the height difference between the two samples, line patterns in PF-Bipy-Pt resist generally had steeper sidewall than those in PF-Bipy. The improvement in line profile is postulated to be a result of enhanced secondary electron yield, which

helps reduce the shot noise and thus improving the contrast of the latent image. In addition, whilst it shows a significantly better sensitivity, PF-Bipy-Pt can be patterned at a line dose as high as 90 nC/cm (where even PF-Bipy resist was overdosed) with reasonably good cross-section and without bridging between the lines, demonstrating improved exposure latitude after introduction of the platinum complex.

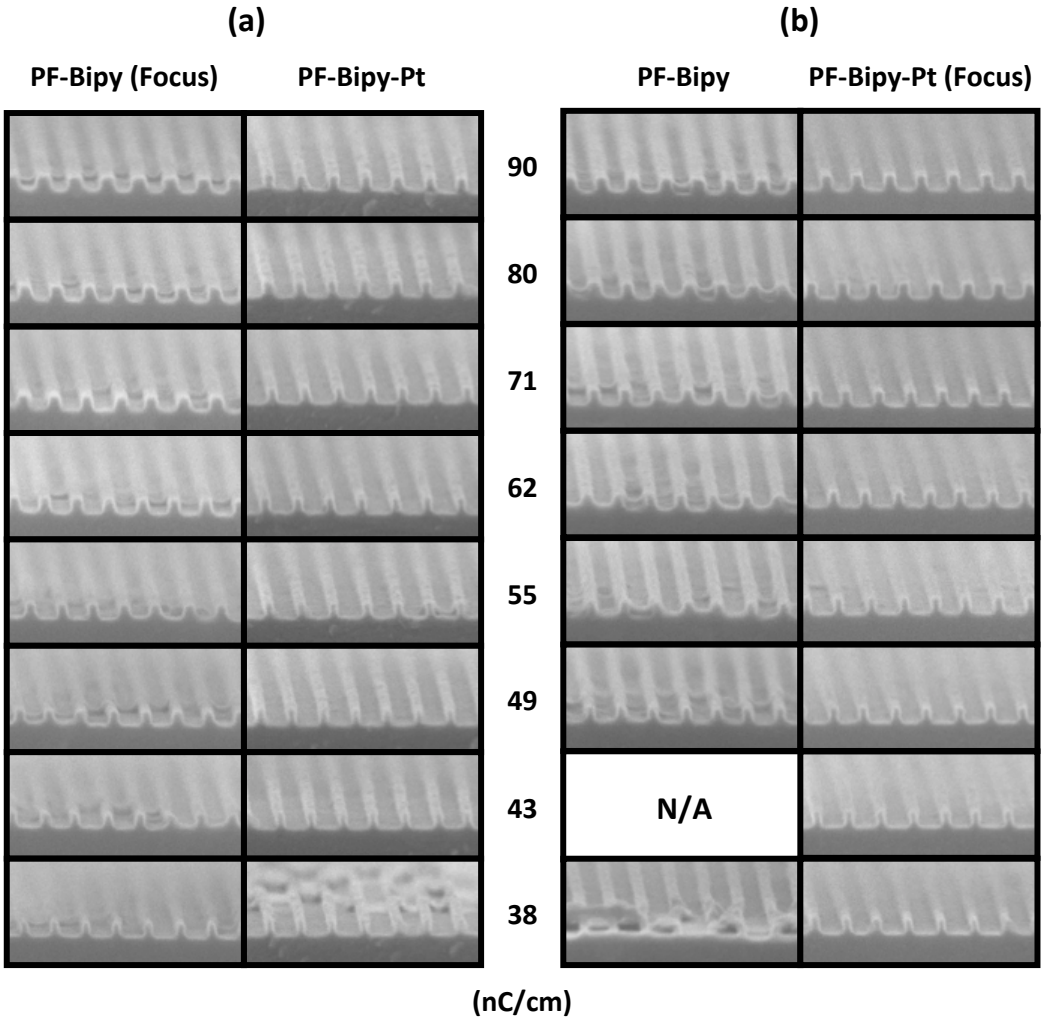

Figure 5.8 Cross-section SEM images of dense features at 50 nm pitch in PF-Bipy and PF-Bipy-Pt. The two samples were put "side-by-side" and exposed with same pattern with beam focused on (a) PF-Bipy and (b) PF-Bipy-Pt

5.3.2.2 EBL Evaluation on Fullerene-Rhenium Complex Resists

The effects of a second metal, rhenium, were also evaluated. The sensitivity and contrast of PCB-Bipy and PCB-Bipy-Re were evaluated using 20 keV electron beam. Figure 5.9 (a) shows the response curves of the two resists. The sensitivity values from the fitting were 21.5 mC/cm^2 and 6.6 mC/cm^2 for PCB-Bipy and PCB-Bipy-Re, respectively. The result shows that the introduction of rhenium can also significantly enhance the secondary electron generation. Using 30 keV beam, sub-15 nm line lines at 50 nm pitch were resolved in both resists as shown in Figure 5.9 (b) and (c).

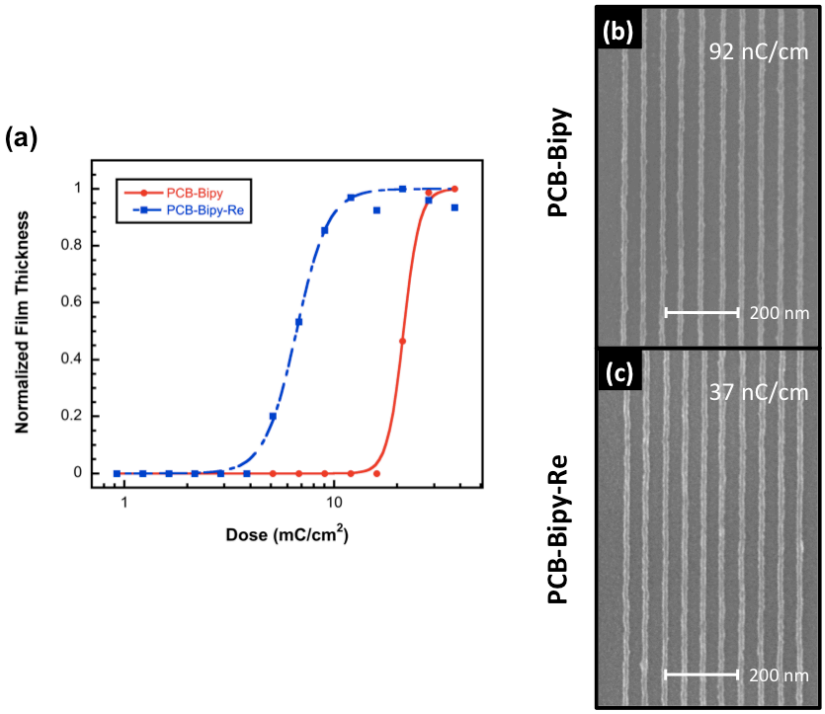

Figure 5.9 (a) The response curves of PCB-Bipy and PCB-Bipy-Re at 20 keV; (b) and (c) SEM images of 50 nm pitch dense line patterns in PCB-Bipy and PCB-Bipy-Re at 30 keV. The line doses are shown in the individual images

Due to the large difference in sensitivity between PCB-Bipy and PCB-Bipy-Re, it is difficult to do the 'side-by-side" exposure (one would be overdosed while the other is underdosed). Thus, to compare the difference in cross-section of the patterns, two samples were patterned with different dose ranges at the edge of each chip separately. Figure 5.10 shows the SEM images of line profiles for PCB-Bipy and PCB-Bipy-Re. In sharp contrast to the platinum, the rhenium-containing sample showed degraded sidewalls instead of improvements. The reason for this is still under investigation and we speculate that the difference of the two metals in electron elastic/inelastic scattering properties (especially in the low-energy range) might play an important role.

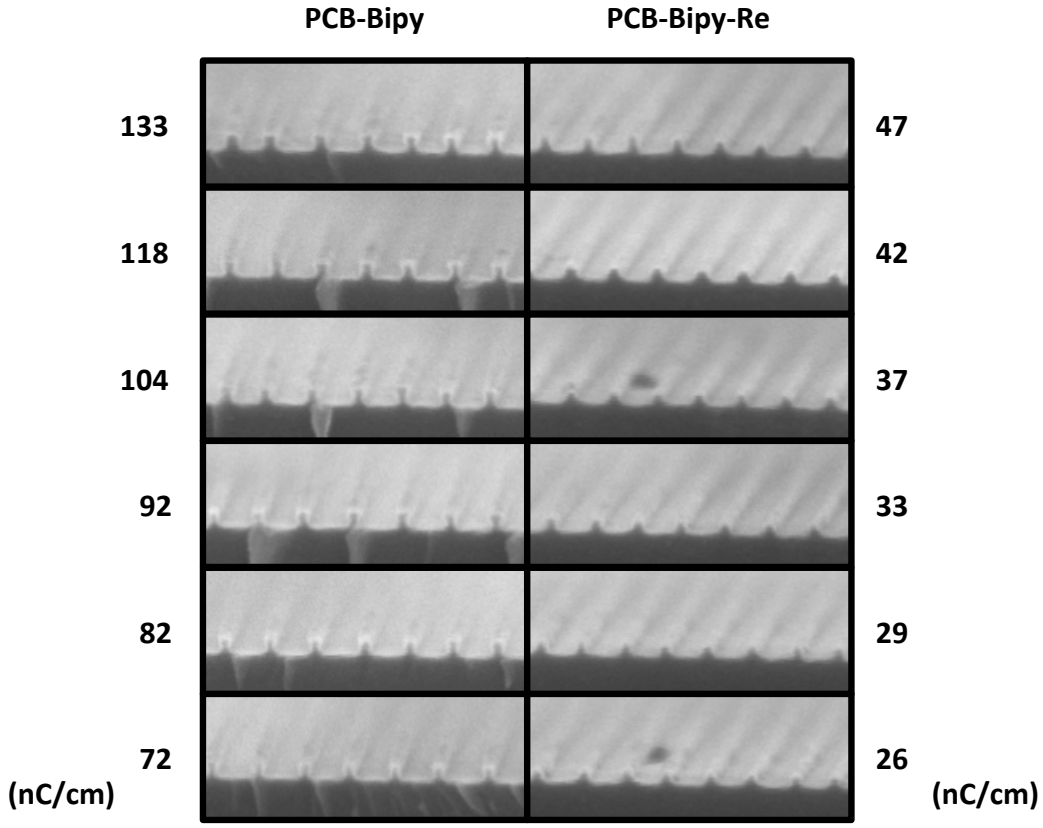

Figure 5.10 Cross-section SEM images of dense features at 50 nm pitch in PCB-Bipy and PCB-Bipy-Re with various line doses

5.3.2.3 HIBL Evaluation

The sensitivity and resolution of PF-Bipy and PF-Bipy-Pt were evaluated using 30 keV helium ion beam (HIB). Due to a higher energy deposition rate, higher secondary electron generation efficiency (~20 times larger then EBL) and negligible proximity effect, HIB has the potential for higher resist sensitivity and resolution than EBL.[16,17] However, HIBL is still relatively slow due to a low available beam current. In the sensitivity test, a number of 10 μm × 5 μm rectangles were patterned at various doses, in a 50 μm × 50 μm write field. As the pattern size was too small for the surface profiler, an AFM was used instead to measure the height of each rectangle (Figure 5.11(a)).

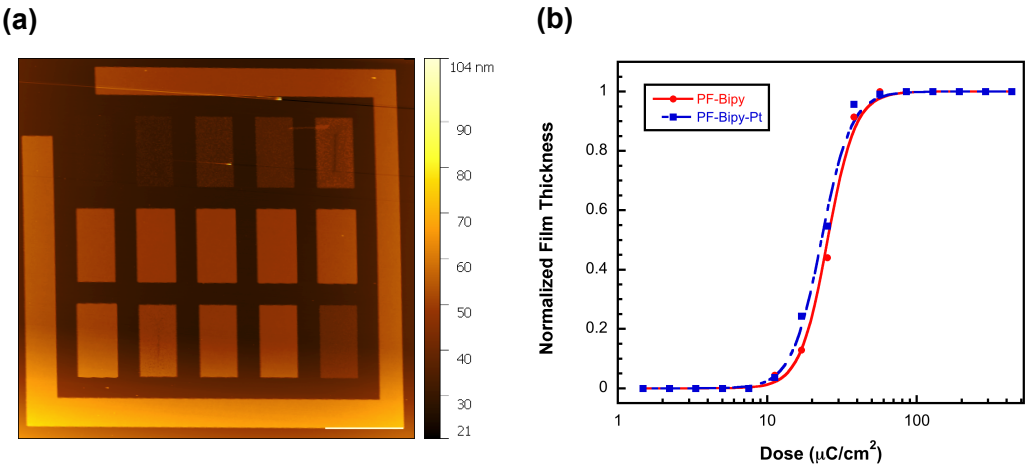

Figure 5.11 (a) AFM image of the rectangle features in a 50 μm × 50 μm write field for sensitivity measurement, patterned with 30 keV helium ion beam; (b) The response curves of PF-Bipy and PF-Bipy-Pt upon 30 keV helium ion beam exposure

The response curves of PF-Bipy and PF-Bipy-Pt resists upon 30 keV HIB exposure are shown in Figure 5.11(b). The sensitivity and contrast (in brackets) for PF-Bipy and PF-Bipy-Pt are 25.4 μC/cm^2 (2.7) and are 23.1 μC/cm^2 (2.5), respectively. Significant sensitivity improvement was achieved for both resists compared with that in EBL. However, there was little difference in sensitivity between PF-Bipy and PF-Bipy-Pt, indicating that introduction of heavy metal atoms into this resist system does not provide significant enhancement in secondary electron generation in HIBL. The reason for this is still unknown and it is postulated that in the PF-Bipy-Pt resist, the concentration of platinum is not high enough to significantly change the scattering properties of the incident ions as in the bulk platinum.[18] In addition, the high efficiency of secondary electron generation upon HIB exposure may also overwhelm the subtle contribution from the platinum atoms, making the sensitivity improvement negligible.

The resolution of PF-Bipy and PF-Bipy-Pt at 30 keV HIB was evaluated through patterning single-pixel lines with various pitches in a 10 μm × 10 μm write field. Ultra thin resist films (~15 nm) were used in this test to prevent pattern collapse and allow an estimation of the ultimate resolution. The same HIB tool and the XL30 SEM were used for sample imaging. The helium ion microscope (HIM) images of dense patterns at 20.0 nm and 18.5 nm pitch for the two resists are shown in Figure 5.12.

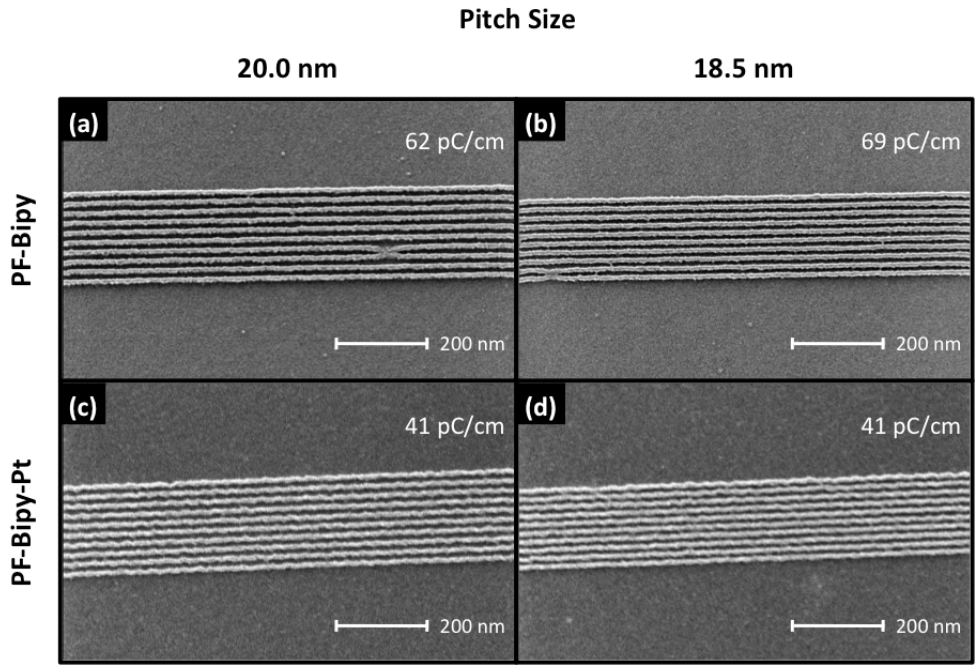

Figure 5.12 Helium ion microscope (HIM) images of dense lines in PF-Bipy and PF-Bipy-Pt, at 20.0 nm and 18.5 nm pitch, patterned with 30 keV helium ion beam. The line doses are shown in the individual images

The SEM images of lines with pitch from 20.0 nm down to 15.0 nm are shown in Figure 5.13. Compared with SEM, HIM had higher image resolution and surface sensitivity due to the narrow distribution of the generated secondary electrons.[19,20] PF-Bipy demonstrated excellent resolution down to 15 nm pitch. Although with some wobbling in the 15 nm pitch features, the space between dense lines was cleared without obvious residue or bridging. On the other hand, the wobbling issue was more serious in PF-Bipy-Pt patterns and dense features at 18.5 nm pitch could just be resolved. For 15 nm pitch lines there was considerable amount of microbridging and collapse observed. It may be necessary to further thin the resist film. The wobbly lines might be a result of swelling and insufficient adhesion, which have increased effect in ultra-thin films and at ultra-small pitch

sizes. Similar effects were observed in another study in which 5 nm wide lines at 10 nm pitch were patterned by HIB in a 5 nm HSQ resist layer.[20]

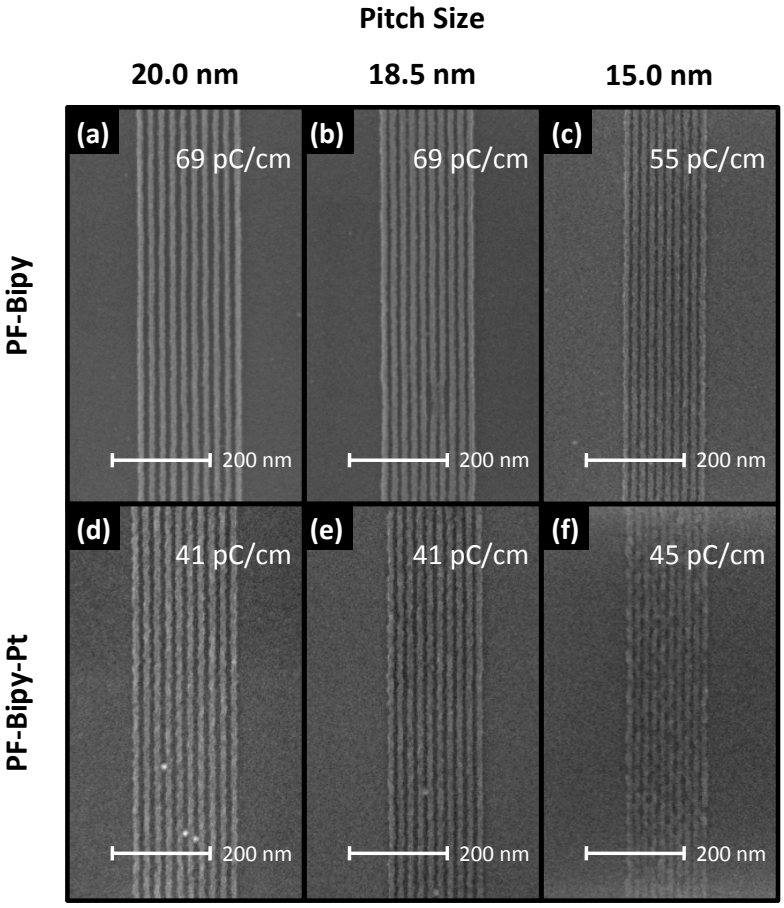

Figure 5.13 SEM images of dense lines in PF-Bipy and PF-Bipy-Pt, at 20.0 nm, 18.5 nm and 15.0 nm pitch, patterned with 30 keV helium ion beam. The line doses are shown in the individual images

5.3.3 AC-STEM Characterization

In order to investigate the behavior of metal atoms during the lithography process including film casting, exposure and development, characterizations at molecular or even atomic level is necessary. AC-STEM and EDX characterization of PF-

Bipy-Pt was undertaken to monitor the material's performance at various patterning steps.

First, powders of dry material were dispensed onto a lacey carbon TEM grid and characterized by the AC-STEM. To find areas that were thin enough for the atomic level imaging, the majority of images were taken at the edges of small grains as shown in Figure 5.14 (a). With a HAADF detector, the dark field (DF) images, together with the bright field (BF) images, were taken simultaneously. Figure 5.14 (b) and (c) show a DF image and the corresponding BF image of PF-Bipy-Pt, respectively. The Pt signal shows as bright dots in the DF image due to platinum's high atomic number (Z_{Pt}=78) in relation to other light elements in the molecule (Z_C=6, Z_N=7, Z_{Cl}=17). As can be seen from Figure 5.14 (b), the platinum was well dispersed in the material without obvious aggregation. From the size (~0.2 nm) and brightness, those "dots" were estimated to be individual atoms. A HAADF image intensity/size distribution of the Pt atoms based on statistical analysis is necessary to confirm the postulated single-atom distribution. However, this is difficult to realize in these samples due to the background noise, which mainly comes from the material thickness variation. Carbon structures can also be observed in the BF image (Figure 5.14 (c)). However, no fullerene structure could be identified due to the noise and thickness (material overlapping). In addition to the dry material, PF-Bipy-Pt was also dissolved in chloroform (in a concentration of 1g/L) and dispensed onto the grids through drop coating. A similar distribution of Pt atoms was obtained.

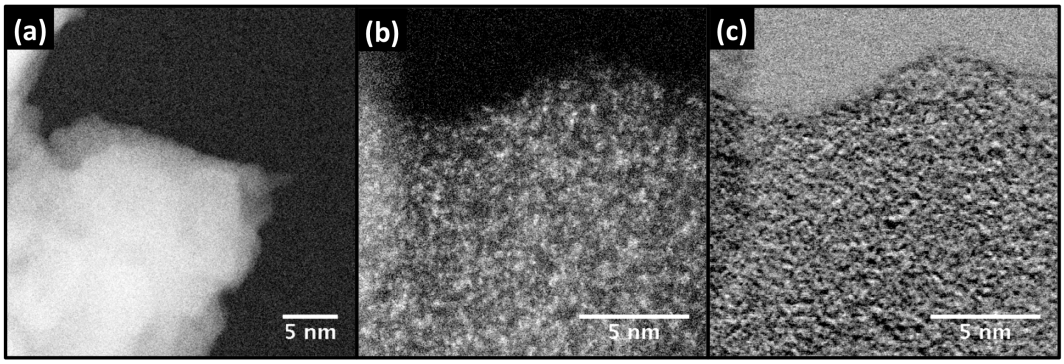

Figure 5.14 (a) HAADF STEM image of PF-Bipy-Pt material in powder; (b) Dark field image of PF-Bipy-Pt in atomic resolution, showing Pt as bright spots; and (c) corresponding Bright field image of PF-Bipy-Pt in atomic resolution

To test the stability of this structure, a continuous scan with a focused 200 keV electron beam (35.1 pA beam current and 5.24 s/frame (20 μs/pixel) scan rate) was applied to the sample. Figure 5.15 (a) and (b) show the DF images at the beginning and after 30 minutes' scan (equivalent to a dose of 5788 C/cm^2), respectively. There was no obvious change in the distribution of Pt atoms. The high stability of the well-dispersed Pt atoms upon electron beam exposure might be due to two factors. First is the chelation bonding between the bipyridine and platinum that prevents the individual Pt atoms from moving and aggregating. The second is fragmentation and re-combination of the fullerenes upon high-dose radiation,[21] which forms an amorphous carbon structure with the Pt atoms to be stably embedded inside. However, the change in the carbon structure during electron beam exposure was not observed in the BF images again due to the noise and material thickness.

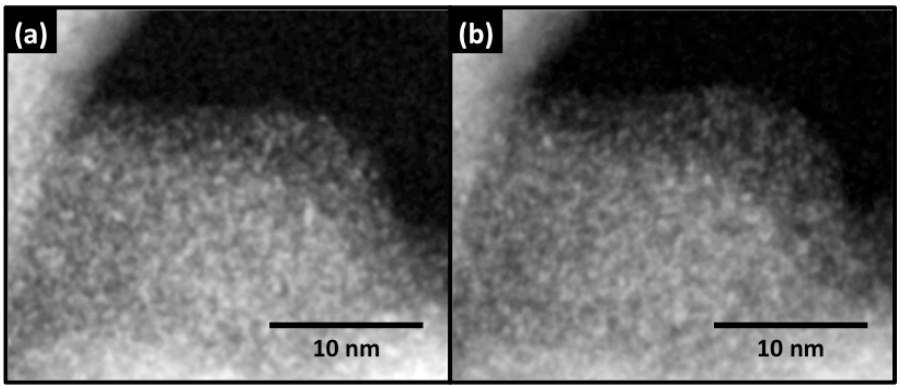

Figure 5.15 HAADF STEM images of PF-Bipy-Pt after the 200 keV electron beam (a) initial scan and (b) 30 minutes' continuous scan

In order to monitor the change of Pt distribution during the normal 20 keV and 30 keV electron beam exposure followed by the development process, the lithography process was undertaken on PF-Bipy-Pt films (drop-coated with 5 g/L solution in chloroform) on holey carbon grids. Isolated lines were patterned using a 30 keV electron beam, and MCB was used to remove the unexposed areas. Figure 5.16 (a) shows a small area of unexposed resist film on the holey carbon membrane and Figure 5.16 (c) shows a portion of the exposed and developed line pattern. As the contrast of the image is associated with the atomic number (Z-contrast), the high brightness of the line indicates that it most likely contains heavy metal atoms. The incontinuity of the line is ascribed to the surface roughness of the carbon coated TEM grid used as substrate. An EDX Pt mapping was performed with the samples in Figures 5.16 (a) and (c), and the distributions of Pt signals are shown in Figures 5.16 (b) and (d), respectively. For the unexposed sample, the distribution of Pt signals matches the distribution of the film. For the developed line feature, there was a strong Pt signal within the line,

indicating that the Pt atoms in the exposed regions tended to stay in the patterned structures rather than being removed by the developer. In comparison, the relatively weak Pt signal outside of the patterned region might be either due to a small amount of PF-Bipy-Pt trapped on the amorphous carbon substrate, or background noise.

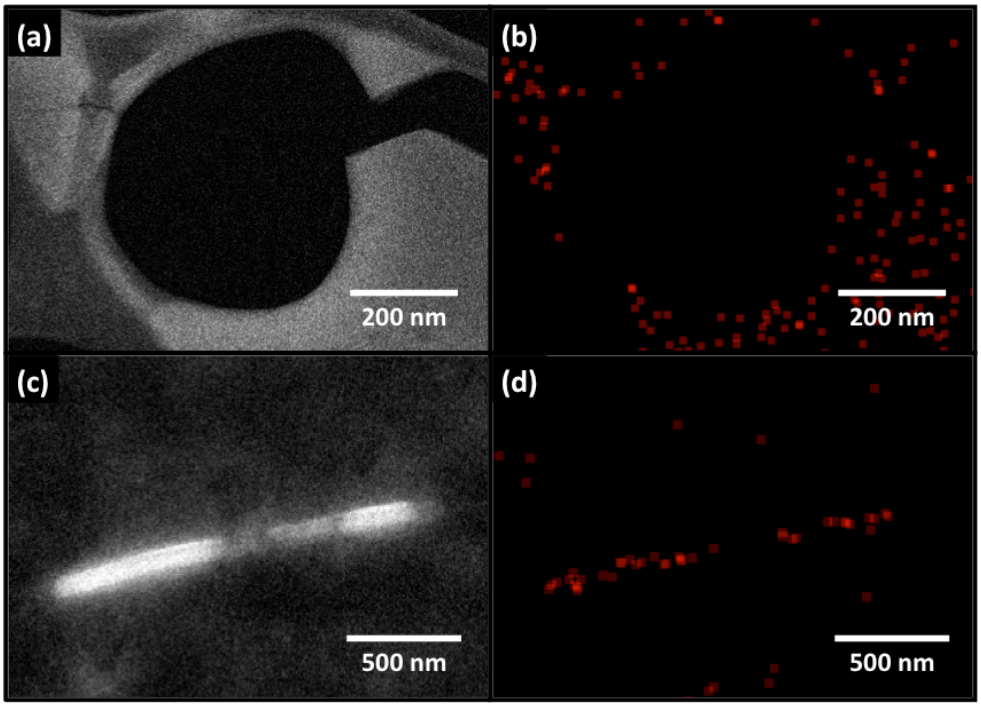

Figure 5.16 (a) HAADF STEM image of PF-Bipy-Pt film on a holey carbon TEM grid and (b) the EDX Pt mapping of the area in (a); (c) HAADF STEM image of a sparse line pattern in PF-Bipy-Pt and (d) the EDX Pt mapping of the area in (c)

The patterned lines shown in Figure 5.16 (c) were too thick to be viewed in atomic resolution (a thick film was required for patterning due to the roughness of the substrate). In order to further investigate the effect of the lithography process

on the distribution of Pt atoms in the subsequently formed carbon structures, thinner films of PF-Bipy-Pt on two carbon grids (drop-coated with 1 g/L solution in chloroform) were prepared and an area exposure was performed on each at 20 keV. One sample was then developed using MCB, whilst the other was not processed further. Figures 5.17 (b) and (c) show the DF images of the samples without and with 30 seconds' MCB development, respectively. Well-dispersed Pt atoms were observed after 20 keV exposure and remained so after subsequent development process, forming an unique Pt containing carbon nano-structure as illustrated in Figure 5.17 (a).

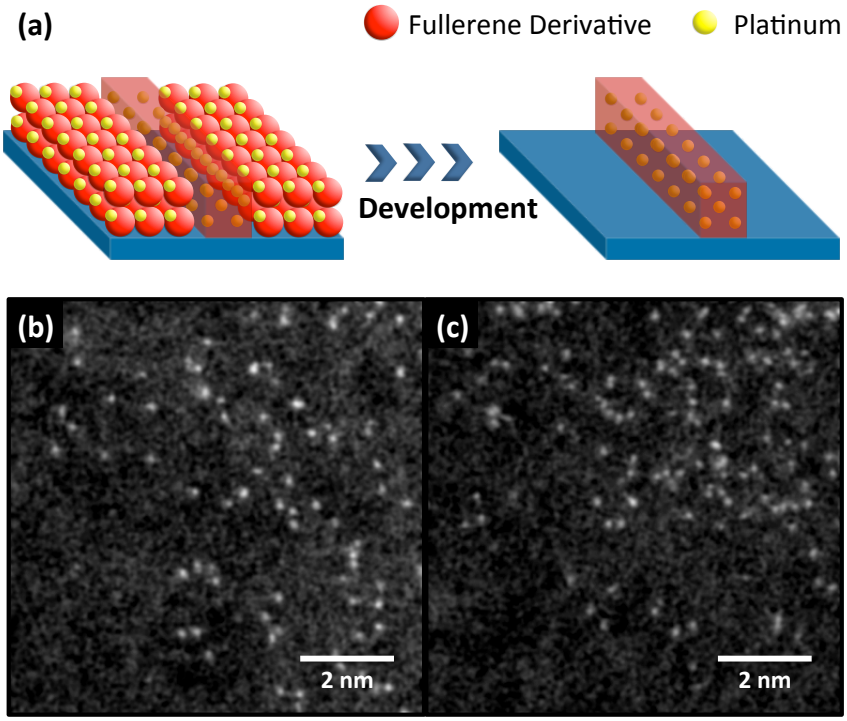

Figure 5.17 (a) Schematic diagram of the Pt distribution in PF-Bipy-Pt film during lithography process; (b) & (c) HAADF STEM images for 20 keV exposed PF-Bipy-Pt films (b) before and (c) after MCB development

5.4 Conclusions and Future Works

Several non-chemically amplified fullerene-metal coordination complex resists have been developed in this work. It has been found that the heavy metal incorporation leads to a significant enhancement in the sensitivity in EBL without obvious reduction in the high-resolution patterning capability. However, a cross-section study of the patterned line features reveals that the choice of metal can affect the line profile. Fullerene-platinum complex resists had improved line profile whilst the fullerene-rhenium complex resists gave a degraded profile. The reason for this is still unknown and it is speculated that the difference of the electron elastic/inelastic scattering properties of the two materials (especially in the low-energy range) might play an important role. In the HIBL, both the fullerene-platinum complex resist and the control material showed much higher sensitivity and resolution compared with EBL. However, the sensitivity difference between the two materials became negligible in HIBL. HAADF STEM imaging shows that platinum is well-dispersed in the film of the fullerene-platinum complex resist and stable during 200 keV STEM beam scanning, and 20 keV lithography electron beam exposure, as well as the subsequent development process. The combination of these features makes this material capable of fabricating unique carbon nanostructures with well-dispersed Pt atoms embedded.

The sensitivity improvement through incorporation of heavy metal atoms into organic resists provides a novel way to solve the sensitivity requirement for next generation lithography. Although the sensitivity of the materials developed in this work is still far too slow compared to most commercial resists for industrial

production, the concept of this sensitivity enhancement method could potentially be a good alternative to the chemically amplified resists, which generally suffer from a trade-off between sensitivity and resolution. In addition, this resist provides a novel patternable Pt-containing carbon nano-structure, which might be useful in other areas such as catalysis. Future work is suggested in four areas: First, lithographic evaluation of various types of metal-complex resists is needed to understand the effects of different metals on lithographic performance and the relation to the electron scattering properties. Second, a similar method of metal incorporation could also be applied to one or more compounds in the chemically amplified resists such as IM-MFPT-08 and IM-xMT to see if similar improvements in lithographic performance can be obtained. Further characterization and analysis are necessary to confirm the individual dispersion of Pt atoms in the film. Finally the modification of the carbon structures upon radiation requires further investigation.

References

1. Ito, H., Chemical amplification resists for microlithography. *Adv. Polym. Sci., 172,* 37 (2005)
2. Kozawa, T., Tagawa, S., Radiation chemistry in chemically amplified resists. *Jpn. J. Appl. Phys., 49(3R),* 030001 (2010)
3. Mack, C. A., Thackeray, J. W., Biafore, J. J., Smith, M. D., Stochastic exposure kinetics of extreme ultraviolet photoresists: simulation study. *J. Micro-nanolith. MEM., 10(3),* 033019 (2011)
4. Tanaka, T., Morigami, M., Atoda, N., Mechanism of resist pattern collapse during development process. *Jpn. J. Appl. Phys., 32(12S),* 6059 (1993)
5. Yamamoto, H., Kozawa, T., Tagawa, S., Yukawa, H., Sato, M., Onodera, J., Enhancement of acid production in chemically amplified resist for extreme ultraviolet lithography. *Appl. Phys. Express, 1(4),* 047001 (2008)
6. Stowers, J. K., et al., Directly patterned inorganic hardmask for EUV lithography. *Proc. SPIE, 7969,* 796915 (2011)
7. Thompson, L. F., Feit, E. D., Bowden, M. J. Lenzo, P. V., Spencer, E. G., Polymeric resists for x-ray lithography. *J. Electrochem. Soc., 121,* 100 (1974)
8. Haller, I., Feder, R., Hatzakis, M., Spiller, E., Copolymers of methyl methacrylate and methacrylic acid and their metal salts as radiation sensitive resists. *J. Electrochem. Soc., 126,* 154 (1979)
9. Hunt, M. R., Schmidt, J., Palmer, R. E., Electron-beam damage of C_{60} films on hydrogen-passivated Si (100). *Appl. Phys. Lett., 72,* 323 (1998)
10. Lu, J., Yeo, P. S. E., Gan, C. K., Wu, P., Loh, K. P., Transforming C_{60} molecules into graphene quantum dots. *Nat. Nanotechnol., 6(4),* 247 (2011)
11. Robinson, A. P. G., Palmer, R. E., Tada, T., Kanayama, T., Preece, J. A., Philp, D., Jonas, U., Deiderich, F., Electron beam induced fragmentation of fullerene derivatives. *Chem. Phys. Lett., 289(5),* 586 (1998)
12. He, D. S., Li, Z. Y., A practical approach to quantify the ADF detector in STEM. *J. Phys. Conf. Ser., 522,* 1, 012017 (2014)

13. Manyam, J., Novel Resist Materials for Next Generation Lithography, PhD thesis, School of Physics and Astronomy, University of Birmingham, 45 (2010), Available from: http://etheses.bham.ac.uk (Accessed 09/10/2015)
14. Manyam, J., Gibbons, F. P., Diegoli, S., Manickam, M., Preece, J. A., Palmer, R. E., Robinson, A. P., Chemically amplified fullerene resists for e-beam lithography. *Proc. SPIE, 6923,* 69230M (2008)
15. Gibbons, F. P., Robinson, A. P., Palmer, R. E., Diegoli, S., Manickam, M., Preece, J. A., Fullerene resist materials for the 32 nm node and beyond. *Adv. Funct. Mater., 18(13),* 1977 (2008)
16. Joshi-Imre, A., Bauerdick, S., Direct-Write Ion Beam Lithography. *J. Nanotechnol., 2014,* 1 (2014)
17. Stepanova, M., Dew, S., Nanofabrication: Techniques and Principles. Germany: *Springer Berlin,* 103 (2011)
18. Utke, I., Moshkalev, S., Russell, P., Nanofabrication using focused ion and electron beams: principles and applications. New York: *Oxford University Press,* 770 (2012)
19. Hlawacek, G., Veligura, V., van Gastel, R., Poelsema, B., Helium ion microscopy. *J. Vac. Sci. Technol. B, 32(2),* 020801 (2014)
20. Stepanova, M., Dew, S., Nanofabrication: Techniques and Principles. Germany: *Springer Berlin,* 94 (2011)
21. Robinson, A. P. G., Palmer, R. E., Tada, T., Kanayama, T., Shelley, E. J., Philp, D., Preece, J. A., Exposure mechanism of fullerene derivative electron beam resists. *Chem. Phys. Lett., 312(5),* 469 (1999)

CHAPTER 6

CONCLUSIONS AND FUTURE OUTLOOKS

6.1 Conclusions

The work presented in this thesis focuses on developing new resist systems for next generation lithography. Studies on three novel resist systems have been undertaken, including a polymer based chemically amplified resist system, a chemically amplified molecular resist system, and a fullerene non-chemically amplified resist system.

In the first, a new method to control the catalytic chain reaction in chemically amplified resists was proposed and applied to a model polymer resist system. After the demonstration of this method, it was further applied to the second molecular resist system. Finally, another route to resist sensitivity improvement via metal addition was investigated in the non-chemically amplified system, and a family of fullerene-metal complex resists has been developed.

In the polymer resist study, poly(4-hydroxystyrene) (PHOST) and poly(4-tert-butoxycarbonyloxystyrene) (PBOCST), were investigated by blending the polymer with a crosslinker and a photo-acid generator as a three-compound negative tone resist. Two types of crosslinkers were tested in this system and in both cases, PBOCST showed better overall performance compared with PHOST.

Through controlling the post-exposure bake (PEB) conditions, PBOCST resists demonstrated higher resolution capability with similar sensitivity to that in PHOST. The improvement of PBOCST is postulated to be from a "two-step" reaction, in which the *tert*-butoxycarbonyl (*t*BOC) group is first removed through an acid-catalysed deprotection reaction, and then the released phenolic hydroxyl group takes part in the crosslinking reactions. This "two-step" process might provide better control of the catalytic reaction chain length and increase the chemical contrast, thus improving the resolution capability. This method also has the potential to be employed in a variety of base materials with different types of protection groups.

In the following work, a family of fullerene derivatives was developed on the basis of the "two-step" concept. Among them, a fullerene derivative with propyl side chain and *t*BOC protection, MFPT-08, showed a combination of good industrial compatibility, high resolution and good sensitivity. A chromatography technique was used to separate a scaled batch of MFPT-08 material and each of the separated components was individually characterized. It was found that the high performance of MFPT-08 actually comes from a mixture of the targeted fullerene compound and a small portion of "impurities". The major compound in the "impurity" was found to be a small molecule with same functional group as the main compound, named as xMT. Blended with different epoxy crosslinkers and PAG in an appropriate compound ratio, xMT showed resolution down to 38 nm pitch with a polymeric crosslinker and 26 nm pitch with a molecular crosslinker at 30 keV. Electron beam exposures with higher energy at 50 keV and

100 keV showed considerable improvements in resolution for the polymeric crosslinker. However, there was no improvement achieved for the molecular crosslinker, indicating that the resolution is not limited to the molecular size of the crosslinker in this system at sub-30 nm pitch. The film quality, adhesion and mechanical strength of the crosslinked network may affect the ultimate resolution.

In addition to the chemically amplified resist systems, several non-chemically amplified fullerene-metal coordination complex resists have been developed. It has been found that the heavy metal incorporation leads to a significant enhancement in the sensitivity in EBL without obvious reduction in resolution. With an enhanced secondary electron generation that contributes to the improved sensitivity, the type of metal atom was also found to have an effect on the pattern sidewall quality. This is postulated to be due to the difference in electron elastic/inelastic scattering properties (especially in the low-energy range) of different metals. A fullerene-platinum complex resist was characterized using an AC-STEM with atomic resolution. The results show that platinum is well dispersed in film of the fullerene-platinum complex resist and stable during the 200 keV STEM beam scanning, the EBL patterning and the development process. This property makes this material capable of fabricating novel carbon nanostructures with well-dispersed Pt atoms embedded.

In summary, the chemically amplified resist system developed in this work has shown excellent lithography performance and demonstrated potential as a candidate for next generation lithography. Although another fullerene-metal

complex resist system requires a relatively high dose that is significantly in excess of industrial targets, the method of metal incorporation provides a new approach to sensitivity enhancement, which may also be possible to apply to chemically amplified systems.

6.2 Future Work Suggestions

A number of future work directions are suggested. In the development of negative tone chemically amplified resists, further understanding of the reaction mechanism is necessary. This can be carried out via two approaches. Firstly, more lithographic measurements on both the model polymer resist system and the molecular resist system are suggested, including more systematic comparisons between protected and unprotected resists in various process conditions, and evaluation of the effects of different protection groups, crosslinker types and molecular sizes. Secondly, other characterization techniques such as infrared (IR) spectroscopy and nuclear magnetic resonance (NMR) spectroscopy may be useful to understand the crosslinking chemistry by tracking functional groups before, during and after the crosslinking reactions. In addition to the reaction mechanism studies, the effects of resist compounds with smaller molecular size are also worth investigating.

In the development of metal-containing resists, the preliminary results presented in this thesis have revealed a variety of possible areas for future work. Firstly, evaluations on various types of metal-complex resists are necessary to understand

the effect of different metals on lithographic performance and its relation to the electron scattering properties. Both experimental and simulation work may be needed due to possible difficulties in synthesizing some of the target materials. In addition, similar methods of metal incorporation could also be applied to one or more compounds in the chemically amplified resists such as IM-MFPT-08 and IM-xMT to see if similar improvements in lithographic performance can be obtained. Moreover, further characterization and analysis at the atomic level is suggested to further understand the distribution of metal atoms in the film as well as the change of carbon structures upon radiation. Finally, due to the novel structures that the fullerene-metal complex resists can form, these materials may also have potential applications in the area of catalysis. Some initial electron-chemistry tests (through collaboration with other groups) have indicated certain catalytic behavior of the fullerene-platinum complex material, showing the potential for patternable ultra low metal content catalysts.